University of Stavanger

Faculty of Science and Technology

MASTER'S THESIS

Study program/Specialization: Petroleum Technology – Reservoir	Spring semester, 2016 Open
Writer: Jørgen Durum Gjestvang	…… (Writer's signature)
Faculty supervisor: Karl Audun Lehne External supervisor(s): Karl Audun Lehne	
Thesis title: Reservoir characterization of the Snorre Field	
Credits (ECTS): 30	
Key words: Reservoir characterization, Snorre, Lunde, Statfjord, fluvial, petrophysics	Pages: 92 + enclosure: 0 Stavanger, 10th June/2016 Date/year

Abstract

The fluvial sandstone in the Snorre field consists of braided to meander streams deposited in arid and in humid climate that show a clear differences in the sedimentology and reservoir properties, especially the silt content in large part of the reservoir which decrease the reservoir properties and water saturation. The heterogeneity of these fluvial formations combined with the faulting history makes this reservoir highly complex with many local and regional barriers. In addition erosion up to 1000m in some part of the reservoir subdividing the reservoir into six different fluvial assemblages with separate reservoir properties. These six fluvial assemblages are evaluated from conventional core analysis consisting of porosity, permeability and grain density and results from SCAL reports including capillary pressure curves, grain size distribution and determination of factors such as; Formation factor, cementation factor, lithology factor and saturation factor applied in determination of the water saturation. The reservoir results are compared with drill stem tests for evaluation of the zone properties compared to the petrophysical properties. The reservoir is segmented based faults interpretation, pressure data, fluid analysis and results from the drill stem tests.

Acknowledgement

I would like to thank my supervisor Karl Audun Lehne for his guidance through this thesis. Without help and guidance with Interactive Petrophysics and his general knowledge in petrophysics this thesis would not be possible.

I would also like to thank Leif Larsen for his guidance to evaluate drill stem test from the field, the test would not have been possible without his input.

Table of content

List of figures

List of tables

1 Introduction

This reservoir characterization is based on the initial exploration data from the 1980's and the data are collected from the Norwegian Petroleum Directorate (NPD). Before the logs are interpreted in Interactive petrophysics (IP) a thorough formation evaluation based on the sedimentology, palaeosols and mineralogy is conducted. Vertical trend and regional correlation suggest that change in the properties of the formation is caused by change in the depositional environment and not burial diagenesis. The sedimentology divides the reservoir into six different fluvial sandstone assemblages that will be evaluated throughout this thesis.

The petrophysical evaluation interprets the reservoir properties such as porosity, permeability and grain density from the conventional core analysis. Trends in porosity and permeability are used to fully evaluate the rest of the well without any core data. The grain density is used to evaluate trends in heavy minerals and to estimate the ρ_{ma} used when calculating the porosity. The lithology and volume of clay of the formations is found from the well-known crossplot between bulk density/neutron density and the gamma ray. Results from the SCAL reports are mostly used to calculate water saturation using three methods: Indonesia, Waxman Smith and capillary pressure. Further are grain size distribution and mudlogs evaluated to identify silt content in the reservoir, which decrease the reservoir properties and the water saturation. The average reservoir properties are calculated with the net to gross (N/G) are correlated through the field, and different fluvial sandstones are showing different properties related to their depositional system. A CPI plot is constructed and consists of the initial log data and the evaluated reservoir properties

The results from the petrophysical evaluation can be interpreted with the results from the drill stem tests, which gives the zone permeability and are used to evaluate heterogeneity or boundary effects. The OWC contacts are calculated from the pressure data, and consists of both good and some bad data and in some cases the results are unreliable. In addition to local barrier the Snorre area is heavily faulted and eroded resulting in rotated fault blocks that are gradually eroded from the south to the north resulting in a segmentation of the reservoir. This segmentation is important because the reservoir properties changes significantly within each depositional system.

2 The Snorre Field

2.1 General

Snorre was discovered in 1979 by Saga Petroleum AS and are located in the northern part of the North Sea, block 34/4 and 34/7, in the Tampen Spur area. Today Statoil operates the field and the area is about 100 square km and water depth at 300-350m. The field is located on the western margin of the Viking Graben and the Neighbour fields are Statfjord, Vigdis, Tordis and Gullfaks. The field is one of the major fields in the North Sea and has a huge potential in IOR [3].

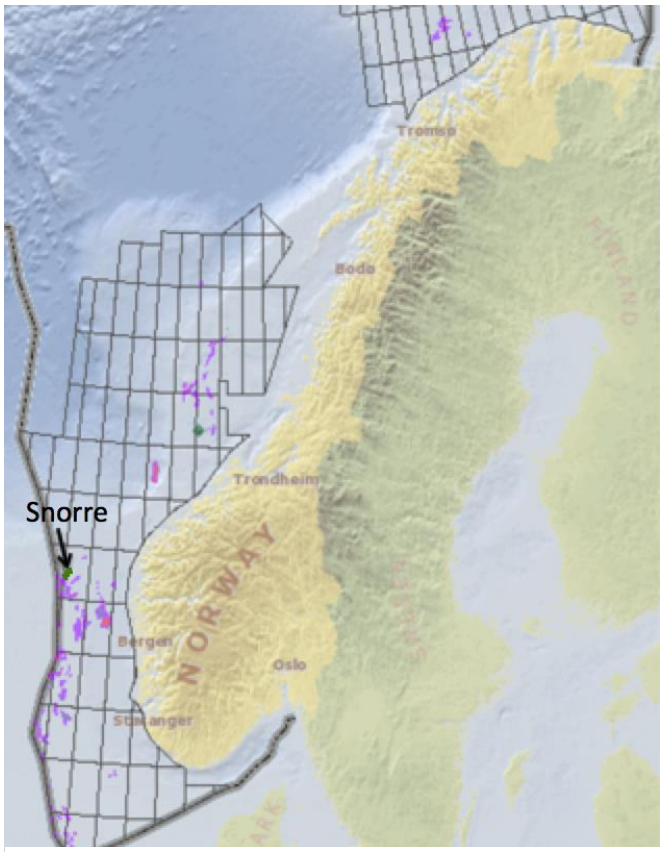

Figure 1: Location of the Snorre Field (NPD)

2.2 Reservoir and recovery strategy

The reservoir depths are 2400-2700m and are fluvial deposition from the late Triassic and early Jurassic period. The reservoirs are highly complex due to several faulting periods and the heterogeneity causes by deposition of fluvial system. It contains many fluvial channels and internal flow barriers. The field has been produced from pressure maintenance, water injection, water alternating gas injection (WAG) and surfactant in parts of the reservoir (NPD).

Ownership			**Resources in place**	
	Statoil Petroleum AS	33,27556 %	Oil	556,00 mill Sm3
	Petoro AS	30,00000 %	Gas	59,50 mrd. Sm3
	Exxon Mobile AS	17,44596 %	**Reserves**	
	Idemitsu Petroleum AS	9,60000 %	Oil	259,50 mill Sm3
	DEA Norge AS	8,57108 %	Gas	6,60 mrd. Sm3
	Core Energy AS	1,10740 %	NGL	4,80 tonn
			Remaining reserves	
			Oil	63,50 mill Sm3
			Gas	0,30 mrd. Sm3
			NGL	0,10 tonn

Figure 2: Ownership, resources and reserves of The Snorre Field (NPD)

2.3 Production history and development

Snorre has two platforms, Snorre A and B, and a subsea installation Snorre UPA. The field has been producing from Snorre A, located south in the field, since 1992 and the oil and gas are sent to Statfjord for final processing and export. Subsea installation Snorre UPA is located in the middle of the field and is connected to Snorre A. The PDO (plan for development and operation) was changed in 1994 after the Vigdis field was tied back to Snorre A (NPD).

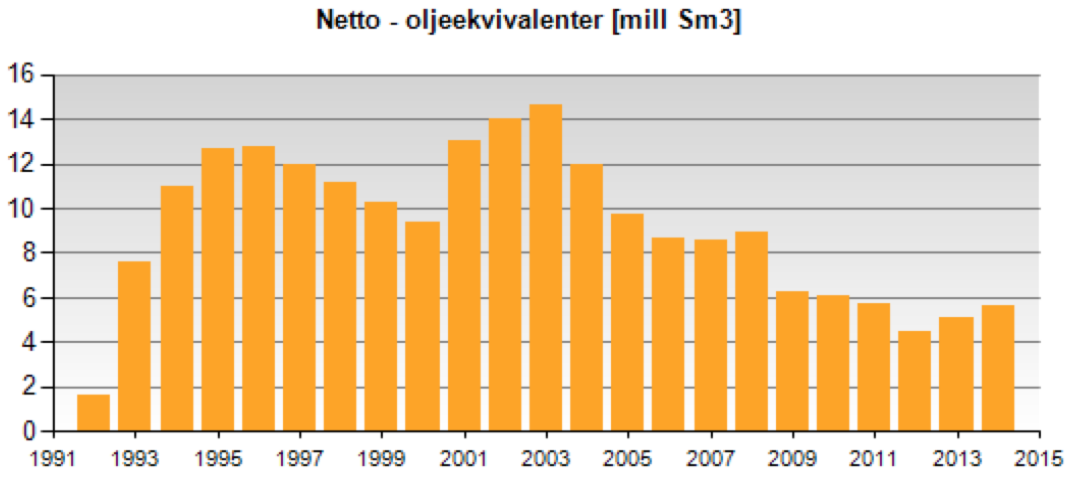

Figure 3: Production history (NPD)

Snorre B was approved in PDO approved in 1998 and started producing in 2001. Snorre B is a semi-submersible production, drilling and quarters (PDQ) unit. A third platform, Snorre C, is planned to be PDO approved in 2017 to extend production until 2040 (NPD).

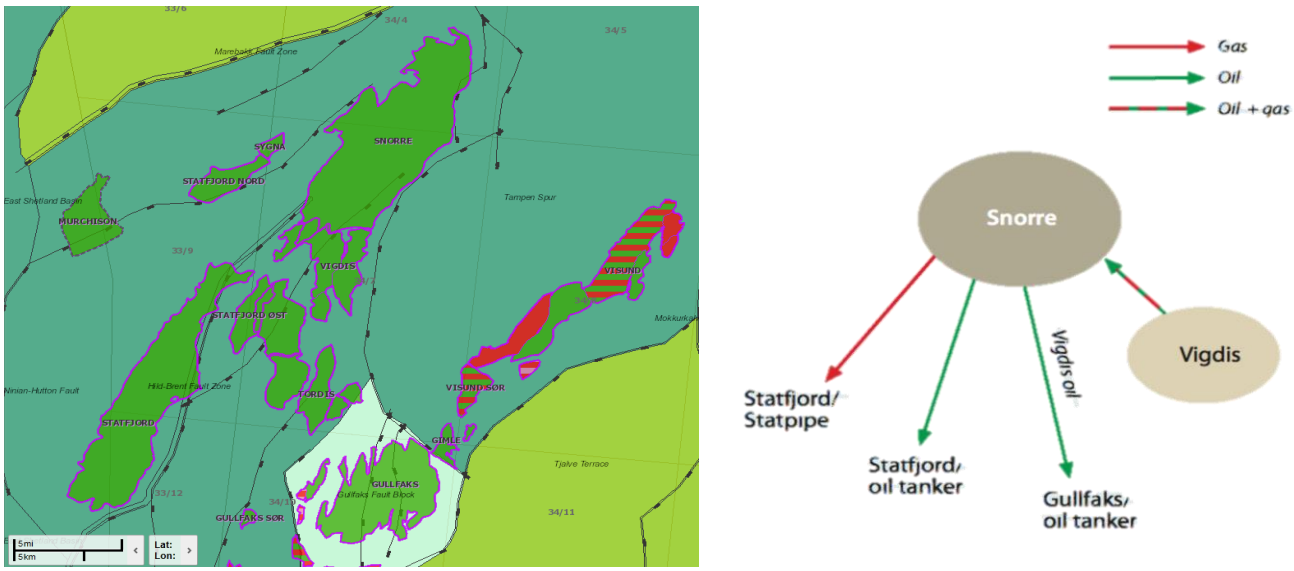

Figure 4: Location of nearby fields and transportation of oil/gas connected to Snorre Field [1]

2.4 Structural evolution

The reservoirs of the Snorre field consist of 25% Statfjord Fm and 75% of Lunde formation, respectively from early Jurassic and late Triassic period. In the structural evolution of the Snorre field, there are two episodes of rifting followed by post-rift subsidence. The first rifting occurs from late Permian until early Triassic, followed by rapid subsidence in the Triassic basin. This deposition is fluvial deposition, Lunde Formation, with wide alluvial plains of rivers flowing towards a seaway located to the north. In the early Jurassic, the Statfjord Formation was deposited as braided streams on alluvial plains.

After deposition of the Dunlin group and Brent group the first rifting reaches a thermal equilibrium, and in the late Jurassic the second rifting occurs. This rifting creates the Viking Graben, east of the Snorre Field. Under these conditions, the Viking Group were deposited as marine shales. This second rift reactivated the perm-trias faults and created new fault with the same strike, but opposite dip direction. In this period, the Snorre area was at a topographic high causing erosion of newly sediments. The whole area was also south-westly rotated due to the rifting.

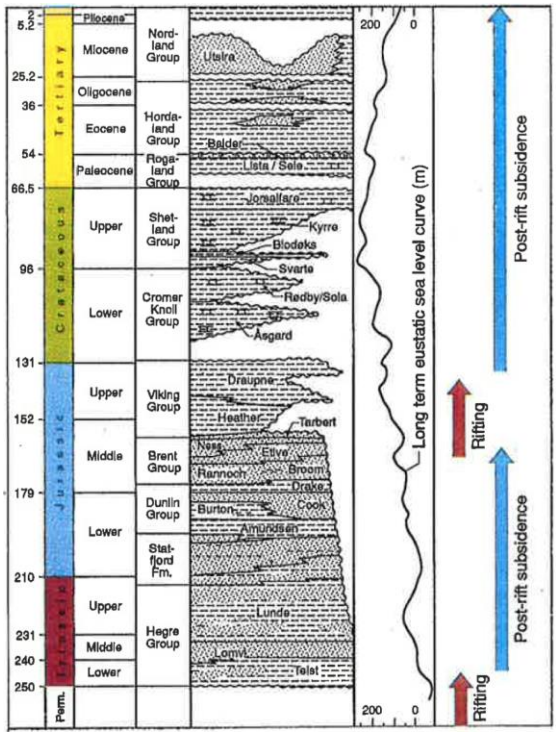

Figure 5: Stratigraphic chart [2]

The erosion continued in the Cretaceous period caused by uplift and sea level drop, called the Base Cretaceous Unconformity (BCU). After the period with erosion carbonate sediments were deposited of the Cromer Knoll Group. At the end of the cretaceous period the topography of the Snorre block was filled [2].

2.5 Future development - Snorre 2040

The Snorre project 2040 involves installation of a new platform, Snorre C, between the current platform Snorre A and C. The purpose of this project is to extend the life of the field until 2040. The project has been postponed several times due to the complexity of the project, and to select the most profitable solution to maximize the recovery. The current recovery factor is estimate to increase from 47% to 54% from the Snorre 2040 project [Statoil]

3 Formation Evaluation

The Lunde formation is from the age of Norian to early Rhaetian from the late Triassic, and the thickness is about 800-850m. The Lunde was originally defined in the Cormorant Formation by Deegan & Scull (1977), but later redefined as the Hegre Group by Vollset & Dore (1984) and subdivided the Lunde formation into three parts; Lower, middle and upper. Final definition is by Lervik (2006), which compromise only the upper member as the Lunde formation and established the Alke Formation by the middle and lower member. The Statfjord formation were defined by Deegan & Scull (1977) and subdivided into; Raude, Eiriksson and Nansen. The Statfjord formation was raised to group and subdivided into the three mentioned formations [7]

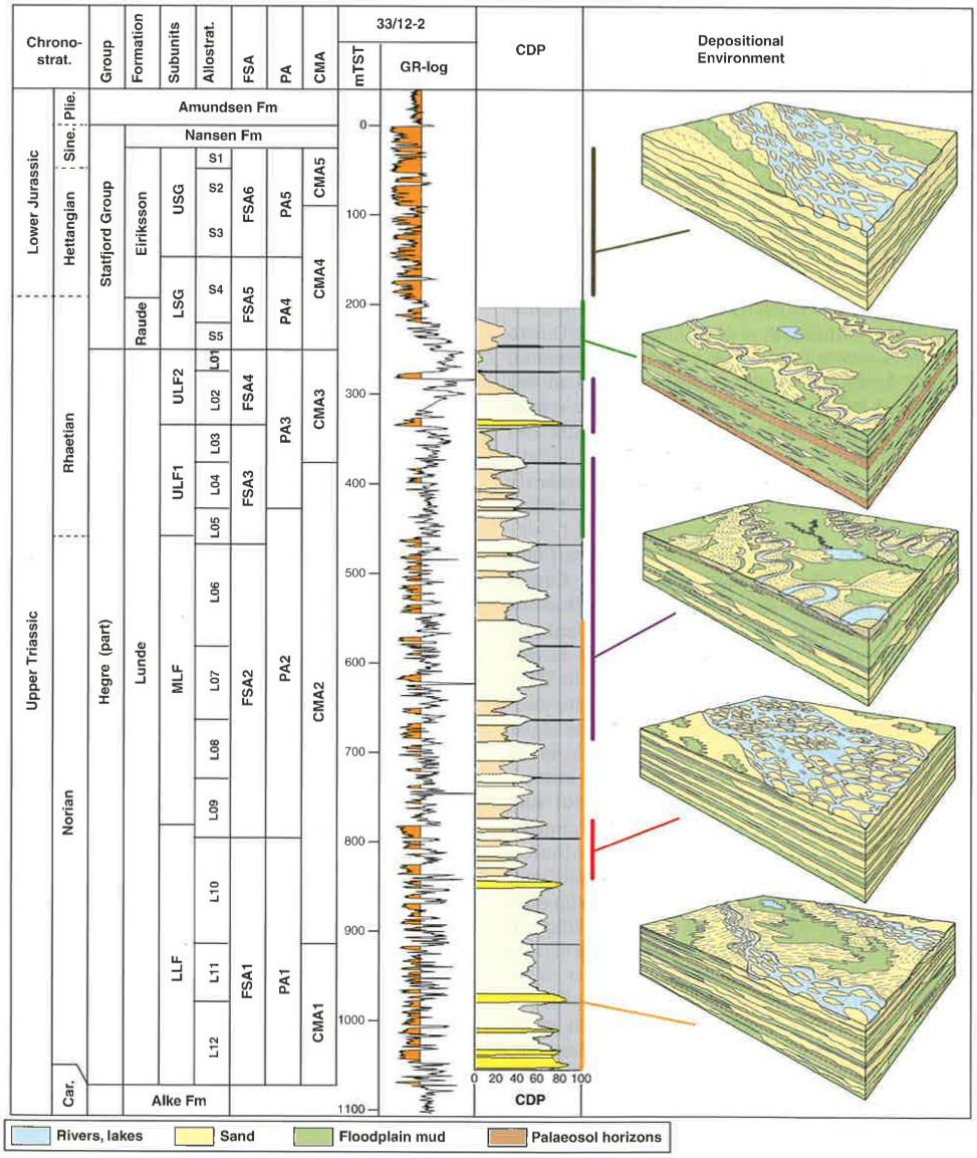

Figure 6: Stratigraphic of Lunde formation and Statfjord group with gamma ray log channel deposition proportion (CDP), depositional environment with true stratigraphic thickness. Statfjord and Lunde subdivided into the allostratigraphic units, fluvial sandstone assemblages (FSA), palaeosol assemblages (PA) and clay mineral assemblages (CMA) [4]

The Lunde formation is most commonly subdivided into a lower, middle and upper part, but can also be subdivided into 12 allostratigraphic units, L01-L12. Similar the Statfjord GP can be subdivided into S01-S05. A study from 2014 by J. P. Nystuen et al. has evaluated data from 36 wells from the Lunde formation and Statfjord group from the Snorre field and adjacent field in the Tampen Spur. This study comprises 3500 m of core from 22 selected wells, which has been studied in detail with respect to fluvial deposition using standard sedimentological logging techniques. Based on the result of this study the formation can also be subdivided based on different fluvial sandstone assembly (FSA), palaeosol assembly (PA) and clay mineral assembly (CMA), see Figure 6 [4].

The CDP is defined by the proportion of channel deposits relative to the bulk volume and is highest in the lower Lunde, and decreasing up through the Lunde formation reaches a minimum at the transition between the Lunde formation and Statfjord group. In the Statfjord the CDP is increasing again [4].

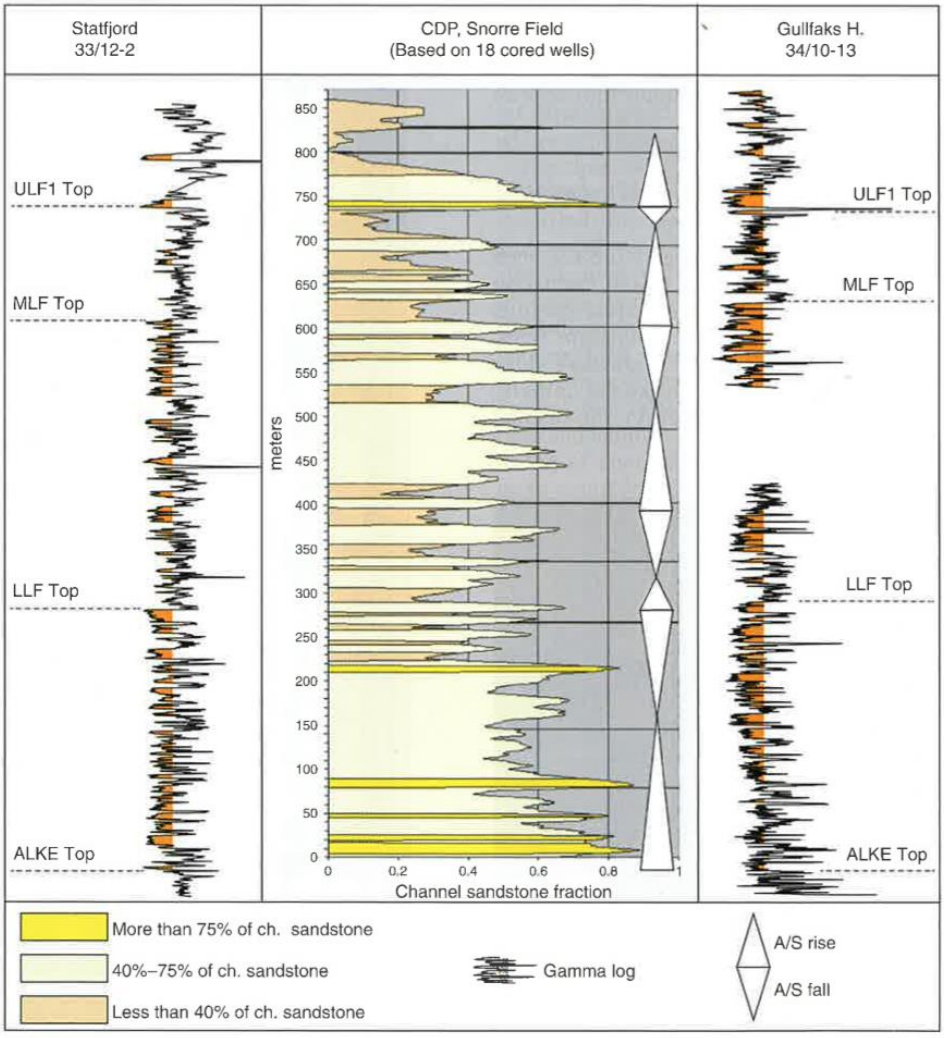

Figure 7: Channel deposition proportion (CDP) of Lunde formation. A/S rise represent the relation between rate of accommodation and rate of sedimentation [4]

3.1 Sedimentology – Fluvial Sandstone Assemblies (FSA)

The Lunde Formation is deposited by alternating sandstone and mudstone from a fluvial depositional system, and the time span is about 15 million years, with a roughly sedimentation rate of 0.055 mm/years. The lower part was deposited in an arid to semi-arid climate during the age of Norian, and is dominated by braided stream deposits. The underlying formation, Alke Fm, is dominated by lacustrine/thermal basins and the mark between the two formations are a fluvial sandstone body in the lower part of the Lunde formation. From the lower to the middle Lunde Formation the depositional system is changing to wide alluvial fans and plain, slightly shifting into a meandering fluvial system. In the transition from the Middle to the Upper member of Lunde Formation, during the late Norian and early Rhaetian, the climate is changing to semi humid climate and the fluvial system is meandering streams. The upper part of the Lunde formation and the lower of the Stat is interpreted to be single isolated sinuous to straight stream deposits. In the upper Statfjord formation the climate is humid and consists of braided stream deposits [4].

The Lunde formation and Statfjord group consist of repeated succession of channelized sandstone bodies interbedded with overbank facies (levee and crevasse-splay sandstones) and distal overbank and floodplain mudrocks with beds of sandy to silty sheet-flood deposits. The fluvial sandstone assemblages is characterised by particular fluvial facies and facies associations, CDPs and inferred channel types. [4]

3.1.1 FSA1: Mobile braided stream channel belts

This assemblage compromises L12-L10 and the fluvial sandstones are associated with low-angle or plane-parallel cross-stratified beds. There is no change in vertical grain size except at the top of individual channel infill succession. This sandstone bodies has been interpreted to form in mobile braided stream channel belts, forming large sheet-like multi-storey and multi-lateral composite sandstones, which can extend for several kilometres. An individual channel infill ranges in thickness from 6 to 9m and can be single or form multi storey sandbodies up to 40m. These have mainly box-shaped vertical grain size with a slightly upward fining at the uppermost part of the top. The CDPs is varying from 66% in L12 to 53% in L10. On average the floodplain fines are

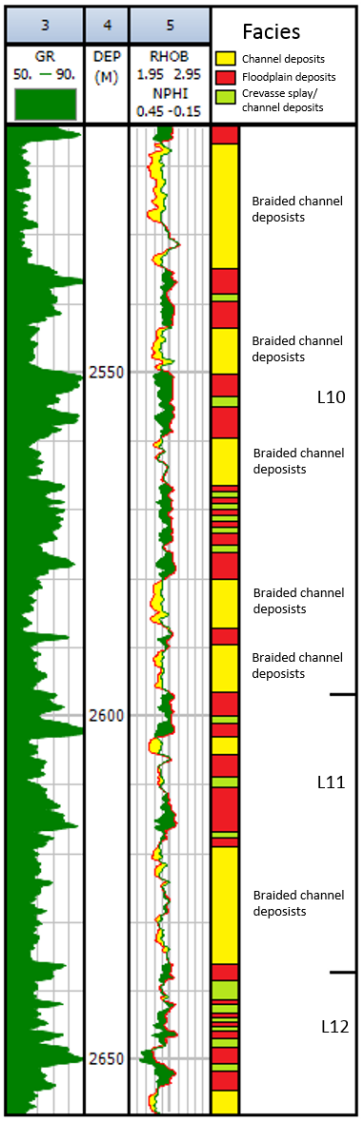

Figure 8: Sedimentation of FSA1 with gamma ray, neutron/density log from well 34/4-7

occupying about 35 % and fine-grained overbank sandstone 10%. The reddish-brown mudstones indicate an arid to semi-arid climate [4].

3.1.2 FSA2: Braided to meandering streams

This assemblage comprises L09-L06 and shows equal amount of CDPs and flood plain fines (40%), and crevasse splay sandstones approximately 20% to 25%. The CDP is evenly distributed, separated by flood plain, compared to the upward fining in FSA1. The sandstones are mainly structureless or plane-parallel stratified. Thin mudstone beds can be found interbedded in the sandstones, and are increasing from L09 to L06. The sandstone bodies are 7 to 9m thick and are individually upward fining and bioturbated floodplain are separating them. The lower part, L08 and L09, are interpreted as braided streams, deposited during ephemeral floods. The interval L07 has mixed braided to sinuous character and the interval above, L06, has upward fining sinuous to meandering channel deposited as point bars. Also found in L06 is crevasse channel and crevasse splay deposits [4].

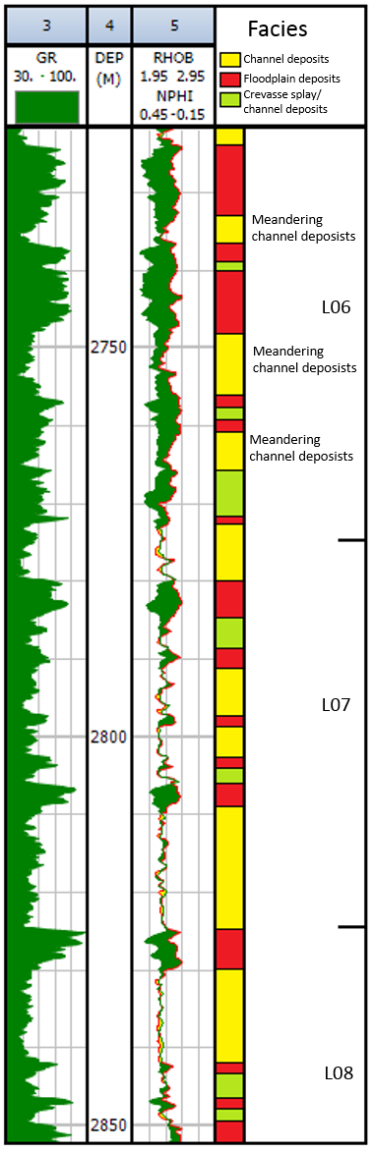

Figure 9: Sedimentation of FSA2 with gamma ray, neutron/density log from well 34/7-3

3.1.3 FSA3: Isolated meandering or straight streams

This assemblage comprises L05-L03 in the Upper Lunde Formation. General trend is increasing flood plains facies, with the CDP ranges from 36% in L04 and 24% in L03. The sandstone bodies are fining upwards and can be up to 7m thick, and have distinct erosional lower boundaries toward underlying floodplain. The upper boundary is transitional into overbank facies or flood plain. This section is interpreted as isolated single storey channel formed by fluvial incision in floodplain mud. Coarse grained sandstone are found in the lower part of FSA 3 and fining upwards into medium grained to fine grained trough cross-stratified beds, and fine to very fine grained sandstone that are parallel laminated or structureless or strongly bioturbated [4].

3.1.4 FSA4: Meandering streams

This assemblage compromises L02 and L01 and differ significantly from FSA 3, with a CDP ranging from 48.2% to 4.1%. The sandstone in unit L02 varies from 5 to 15m and multi storey bodies can occur up to 40m in thickness. The multi-storey sandstones in L02 are thought to represent large compound bed-forms of superimposed 3D sand dunes, overlain by levée and overbank to floodplain fines. The sandstone bodies in L01 occur as single storey channel infill successions. Both L02 and L01 have individual upward fining trend, dominated by cross stratificated beds and are interpreted as meandering river deposits. These beds pass into current-ripple laminated fine grained and very fined grained sandstone. Thin beds of bioturbated mudstone are alternated in the sandstones. The single storey sandbodies in L01 are interpreted as isolated sinuous or straight channels with mud-dominated flood plains [4].

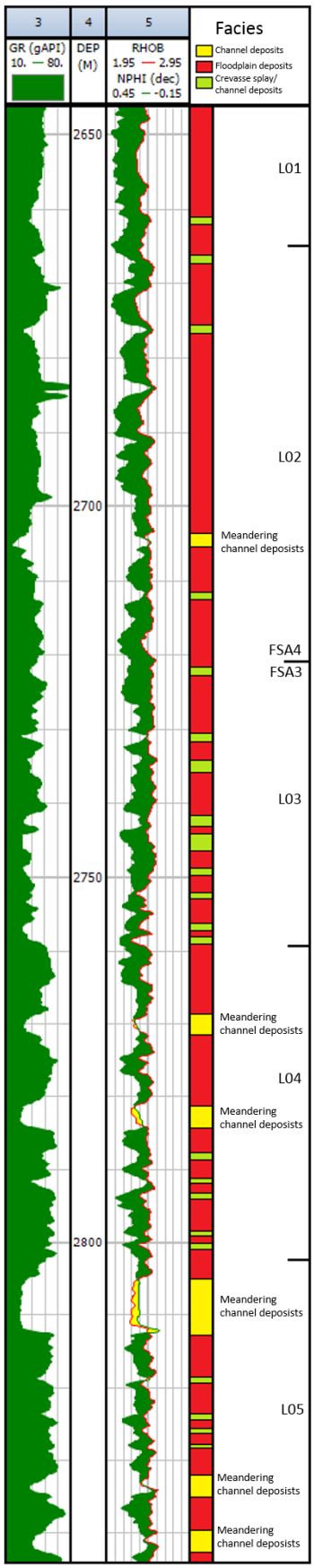

Figure 10: Sedimentation of FSA3-FSA4 with gamma ray, neutron/density log from well 34/7-4

3.1.5 FSA5: Sand sheets and single floodplain channels

This sandstone bodies in this assemblage varies from a few decimetres up to 3-4m and occurs in the allostratigraphic units S5 and S4. The sandstone are underlain erosional channel floor surfaces. The lower part of Statfjord, S5 and lower S4, together with the L01 from Lunde represent a change in the sandstone architecture. From this point, the sandstone changes from fining upwards to coarsening upwards. The figure to the right show a fining upwards meandering deposits at the bottom of the Statfjord, unlike S1-S3 that have coarsening upward sandstones. This fluvial system in this assemblage is interpreted as single and narrow, low sinuosity or meandering streams. The CDP is very low, constant below 20% [4].

3.1.6 FSA6: Mobile braided stream channels

This assemblage include the top 3 allostratigraphic units in the Statfjord Group and is dominated by multi-storey sandstone with medium to coarse grained and generally quartz rich. The beds are parallel or cross stratified forming blocky or coarsening upward trends. The erosional channel base is covered by pepples of quartz, quartzite, metamorphic crystalline rock, intrabasinal mudstone clasts and coalified plant fragments. Some sandstone bodies appear as red due to the content of the iron oxide goethite. The high energy braided stream is most likely triggered by an influx coarse-clastic debris (cf. Schumm, 1981). Low accommodation space, high precipitation and river discharge could have enhanced the streams leading to a braided fluvial system [4].

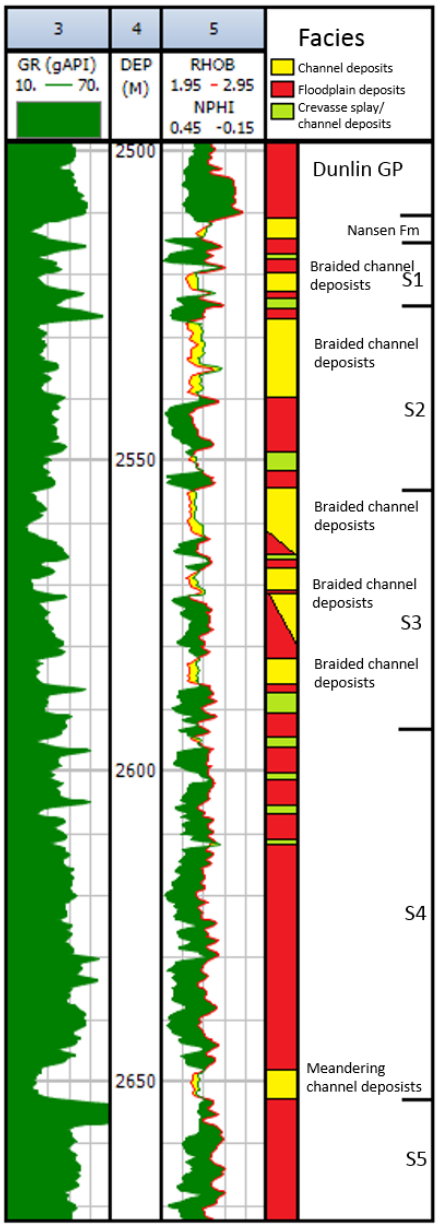

Figure 11: Sedimentation of FSA5-FSA6 with gamma ray, neutron/density log from well 34/7-6

3.2 Palaeosols and mudrock facies

Throughout the Lunde formation there is presence of palaeosols mudrocks due to pedogenic processes that occurred. These processes happen when there is a break in the sedimentation and erosion, and are mostly developed in floodplain mudstone and to little extend in fine grained sandstone. The properties of the rocks are dependent of the intensity and duration of the pedogenic processes, and are referred to as pedocomplexes and are subdivided into compound, composition and cumulative. The different processes create mudrock characteristics and can be divided into 5 different mudrock facies. Many of the processes give colour to the rocks making them good for correlation between wells [4].

Table 1: Mudrock facies and characteristics of the Lunde formation and lower Statfjord group [4]

Mudrock facies	Mudrock characteristics
MF1: Laminated mudrock	• Variable content of clay, silt, sand and mud aggregates • Plane parallel lamination • Red-brown colour, small isolated rhizocretions, up to 10cm-deep desiccation sand filled cracks • Interpretation: Deposited in small temporal ponds or shallow lakes on floodplain.
MF2: Unstratified and structureless	• Clay/sand ratio relative low, and lower than in MF3 and MF4 • Red-brown colour, discrete and isolated carbonates nodules, isolated rhizocretions, burrows, 10 to 60cm deep sand-filled desiccation cracks. • No mud aggregates, peds or pedogenic slickensided surfaces • Interpretation: Mud altered by pedogenic processes to entisols/Inceptisols
MF3: Mudrock with slickensided fault surfaces	• Clay/sand ratio higher than in MF2. • Brownish-red colour, frequent arcuate (curved) and smooth randomly orientated slickensided surfaces, spheroidal and angular peds (soil particle), ptygmatic folds, rhizocretions, isolated carbonate nodules. • Interpretation: Mud altered by pedogenic processes to high chroma vertisols
MF4: Greyish and mottled mudrocks	• Generally higher content of clays, some mudrocks with high contents of fine-grained to medium-grained sand. • Greenish-grey and mottling red-greenish mud aggregates. Slickenside horizons, spheroidal peds, mud aggregates, 0.1 to 1.5 m-deep sand-filled desiccation cracks, complex mottling patterns. • Interpretation: Mud with colour formed by reduction of pedogenic processes of iron oxides due to fluctuating groundwater level of waterlogging
MF5: Reworked mudrock	• Texturally varied reworked pedogenic mud aggregates (0.1mm to 5mm) and carbonate rip-up clasts (1cm to 6cm). • Brownish-red colour, some places mottled green-red. • Interpretation: Reworked mud and calcrete nodules deposited as infill of shallow channels in crevasses splay and sheet floods.
Definition of palaeosols: **Gleyed soil and palaeosols**: Soil or palaeosols with blueish grey and greenish grey colour, accumulation of organic matter common, root structure may be preserved in top of gleyed beds **Vertisols:** Calcrete-rich soils with wide desiccation cracks and peds formed by repeated seasonal dry-wet cycles, calcrete nodules common, no remains of primary sedimentary features. **Inceptisols:** Relicts of primary sedimentary features may be present. May have calcrete nodules. **Entisols:** Slight degree of soil formation. Primary sedimentary features little altered. **Rhizocretions:** Root system created through chemical weathering, decomposition, reprecipitation and cementation. (Modified from Retallack, 2001)	

3.2.1 Palaeosol Assemblage 1 (PA1)

This assemblage correlates entirely to the FSA1 and it is compromised by reddish-brownish mudrocks with 50-60% of sand and silt. The flood plain consists of laminated mudrocks (MF1) and unstratified, structureless mudrocks (MF2). The clay (<2μm) content is relatively low. Intervals of with thin entisols and inceptisols mixed with laminated beds and capped by laminated mudrocks or sheet flood sandstones. Carbonate nodules are commonly with 20-30% of the total mudrock volume and also occur in a few horizons up to 0.2 – 0.4m. PA1 also contains small-scale sand filled desiccation, which occurs sporadically. Scattered calcrete nodules, vertically stacked calcrete nodules, rhizocretions, root structure and burrows are common [4].

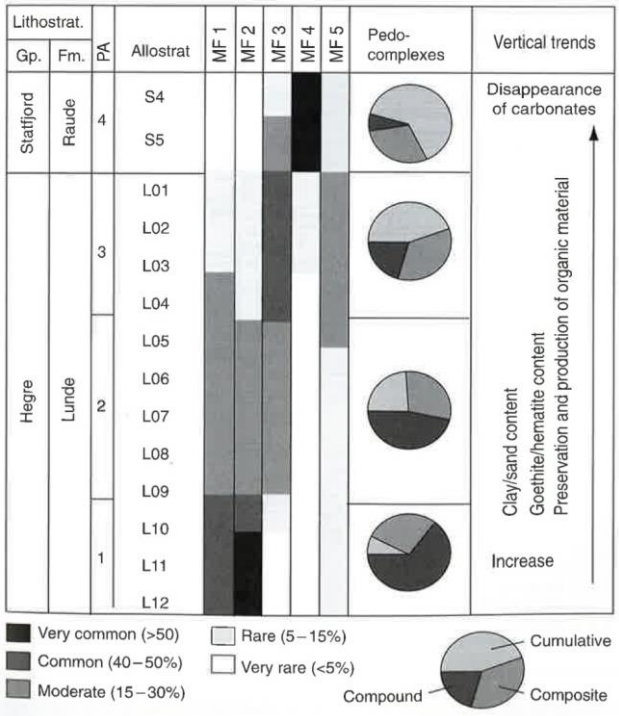

Figure 12: Stratigraphic of mudrock facies and pedocomplexes [4]

3.2.2 Palaeosol Assemblage 2 (PA2)

PA2 through L09-L05 compromises FSA2 and the lower part of FSA3. PA2 consists of 45-50% of the total rock volume in this assemblage and correlates to red and reddish-brown laminated mudrocks (MF1) and entisols/inceptisols (MF2). Also high chroma vertisols from MF3 are common. Reworked mudrock (MF5) are present as reworked mud aggregates and reworked carbonate nodules. Reworked carbonate is a sign of alluvial mud with calcrete has been eroded. This assemblage also contains scattered small calcrete nodules, nodular carbonate horizons, vertically stacked carbonate nodules, rhizocretions, root structures and burrows [4].

3.2.3 Palaeosol Assemblage 3 (PA3)

This assemblage consist of the rest of FSA3 and FSA4 (L05-L01). The mudstones are red and reddish-brown and dominated from mudrock facies MF3 with a high chroma vertisols. Entisols/inceptisols from MF2 and reworked mudrocks MF5 are common. Induvial vertisols can be up to 6-7m thick and are commonly overlain by reworked mudrocks, sheet flood sandstones or laminated mudrocks. Thin layer with carbonate horizons or nearly coalesced carbonate occurs. Vertically stacked calcrete nodules, carbonate box-work structures, rhizocretions, root structure, burrows, soil peds (Müller et al. 2004) and deep and wide sand filled desiccation cracks are all abundant in PA3. Overlaying sandstone bodies are typically laminated MF1overlain by entisols/ inceptisols MF2 and vertisols MF3. All of the mudrock facies have

relatively high clay/sand ratios and percentages of very fine-grained material are dominated by cumulative pedocomplexes [4].

3.2.4 Palaeosol Assemblage 4 (PA4)

This assemblage compromises S5 and S4, dominant reddish-brown in S5 and increasing mottled and green to grey upwards in S4. Commonly found mudstone mottled with low chroma vertisols (MF4), replacing the reddish entisols/inceptisols from the underlying PA3. Palaeosols horizons can be up to 5-7m thick and the mottling pattern are gleying or oxidation along cracks or ped margins. Coalified plant debris are common and a content of goethite up to 10% can occur [4].

3.2.5 Palaeosol Assemblage 5 (PA5)

Consist of the upper Statfjord, S3-S1 and are dominated by grey to grey-greenish palaeosols. Slickenside are present but not common. More common are caolified plant debris (wood) at the base of fluvial channels. Carbonate nodules, rhizocretions and soil peds are absent in this section. This assemblage is characteristics by inceptisols, entisols and low chroma vertisols. A high content of goethite are present and are characterised by greenish-grey with high organic content formed from gleying processes. This type only occurs in S1 and S2 [4].

3.3 Mineralogy

The general mineral interpretation of the channelled sandstone of the Lunde Formation is a feldspathic with an average feldspar/quartz ratio of 0.56, from Table 2. The Statfjord Group sandstones are quartz arenite with an average feldspar/quartz ratio of 0.18 (Table 2) [4].

Table 2: Average content of major minerals in Fluvial Sandstone Assemblage in the Lunde Formation and Statfjord group [4]

Units	Number of samples	Quartz	K-feldspar	Plagioclase	Kaolinite	Mica
S1-S2	13	69	6,3	7,1	12,6	5
S3-S4	5	70,4	8,3	8,9	10,4	2
L01-S5	2	51,3	9,2	17,1	14,5	7,9
L05-L02	12	54	10,1	19,4	12,2	4,3
L08-L06	11	50,4	11	21,3	11,8	5,5
L09	11	52,3	12,3	25,4	4,6	5,4
L12-L10	11	50,4	13	14,4	6,9	5,3

Table 3: Average content of non-clay mineral in % of bulk composition in mudrocks with palaeosols in the Lunde Formation and Statfjord group [4]

Unit	Number of samples	Quartz	K-feldspar	Plagioclase	Calcite	Dolomite	Siderite
S1	5	46,6	3,8	2,0	0,1	0,0	3,7
S2	4	26,6	5,9	10,4	0,3	0,2	0,2
S3	13	45,6	8,9	8,8	0,4	1,4	1,1
S4	6	33,4	8,5	25,3	1,1	9,2	0,1
S5	3	31,6	2,4	0,4	0,1	0,2	0,3
L01	2	13,3	2,2	18,5	0,8	0,2	0,6
L02	23	28,4	6,6	19,4	1,5	5,5	0,1
L03	12	20,8	5,4	22,2	21,4	1,9	0,3
L04	14	18,5	6,6	34,2	8,6	6,2	0,6
L05	6	23,1	7,8	19,5	0,7	5,8	0,1
L06	7	23,6	7,2	19,8	5,1	5,3	0,1
L07	31	21,8	10,1	20,5	1,2	2,4	0,0
L08	17	21,1	5,9	18,8	22,8	2,4	1,1
L09	12	14,6	12,1	25,0	17,4	1,0	1,8
L10	15	14,5	6,3	18,2	28,9	11,0	1,4
L11	7	20,2	7,1	22,4	1,8	0,7	0,0
L12	5	18,9	8,3	19,5	3,0	0,0	0,0

Clay mineral such as illite, smectite, kaolinite and chlorite occurs throughout the formation, and the formation can be divided into 3 clay mineral assemblage (CMA) based on the total amount and relative occurrence of these minerals in the mudrocks (Table 3). The clay minerals are

formed from clastic grains or diagenetic products from feldspar and mica, while calcite fills the pore spaces. The clay minerals recorded variation in mineral content is mainly related to the sediment source and depositional environment factors and not burial diagenesis. This is based that there is no significant trend in the mineral composition with the burial depth in the formation. The stratigraphic trend is however eminent, see tables below. [4]

Table 4: Average content of clay minerals and iron oxides in mudrocks within the CMAs [4]

CMA	Units	Smectite	Swelling Mix Layer [ML]	Chlorite	Illite	Kaolinite	Goethite	Hematite
5	S1	8	4	0	2	75	11	0
4	S5-S3	82	1	0	3	11	2	2
3	L03-L01	29	13	8	15	18	3	15
2	L10-L05	33	2	9	23	11	1	22
1	L12-L11	1	13	15	36	22	1	13

3.3.1 Clay Mineral Assemblage 1 (CMA1)

In this assemblage there is no or very little smectite, compared to CMA2 and CMA3 where smectite is the dominant mineral. Illite is the most abundant mineral with an average of 41% of the clay minerals compared to kaolinite which has 26%. Hematite is the most abundant iron oxide in this assemblage [4].

3.3.2 Clay Mineral Assemblage 2 (CMA2)

The most significantly change from the first to the second assemblage is the abundance of smectite, which is practically 0 in the first and about 90% of all the clay minerals in the L10 unit (not visible in the table). From L10 to L05 to content of smectite is decreasing to almost zero at the top of L05, and has an average of 42% of the clay minerals. The upward decrease of smectite is accommodated with an increase illite from very little in L10 unit to about 80% in the L05 unit. The amount of chlorite varies greatly through this assemblage with a slightly upward–decreasing trend. Kaolinite shows no significantly trend throughout this assemblage, and the amounts are relatively low. Hematite is the dominant iron oxide, showing an abundance of 40% at the upper part of L05 and decreasing to the uppermost part to the transition to CMA3. The amount of the swelling minerals is practically 0 in this assemblage [4].

3.3.3 Clay Mineral Assemblage 3 (CMA3)

The content of smectite is varying from 0 to 80% at the most of the clay mineral and has an upward-decreasing trend. The swelling mineral is also varying, and as a contrast to the smectite, the swelling mineral is upward-increasing until the uppermost part of L01 where it is reduced to 0. The content of illite varies from 80% of the clays at the L03 to 15% in the L02 and L01. The content of kaolinite varies significantly, with no specific trends and has peaks at the upper part

of L02 and L03 separated by a low in the L02. The abundance of goethite is recorded increases in a floodplain mudstone in the middle of the L02 unit [4].

3.3.4 Clay Mineral Assemblage 4 (CMA4)

This assemblage consists of the lower Statfjord group, S5-S4, and consists of the most significant change in the mineralogy in the whole Lunde-Statfjord succession. From the uppermost allostratigraphic in Lunde, L01, and the lowermost in Statfjord, S5, the content of smectite is increasing abrupt from around 5% to 80-90% at the boundary between the units. The content of smectite is high throughout the assemblage, until it drops to 0 at the top of the unit S3 at the transition to CMA5. Illite is relatively low, under 10% and chlorite is totally absent. The same goes for goethite and hematite. There is a sharp increase in the content of kaolinite in S3, approximately around where the increase of channelized sandstone [4].

3.3.5 Clay Mineral Assemblage 5 (CMA5)

This assemblage consists of S2 and S1and are dominated by a high content of kaolinite, between 60-100%, and almost 0 content of smectite except at the uppermost of S1. Swelling minerals, chlorite and illite are practically 0 and the only iron oxide are goethite [4].

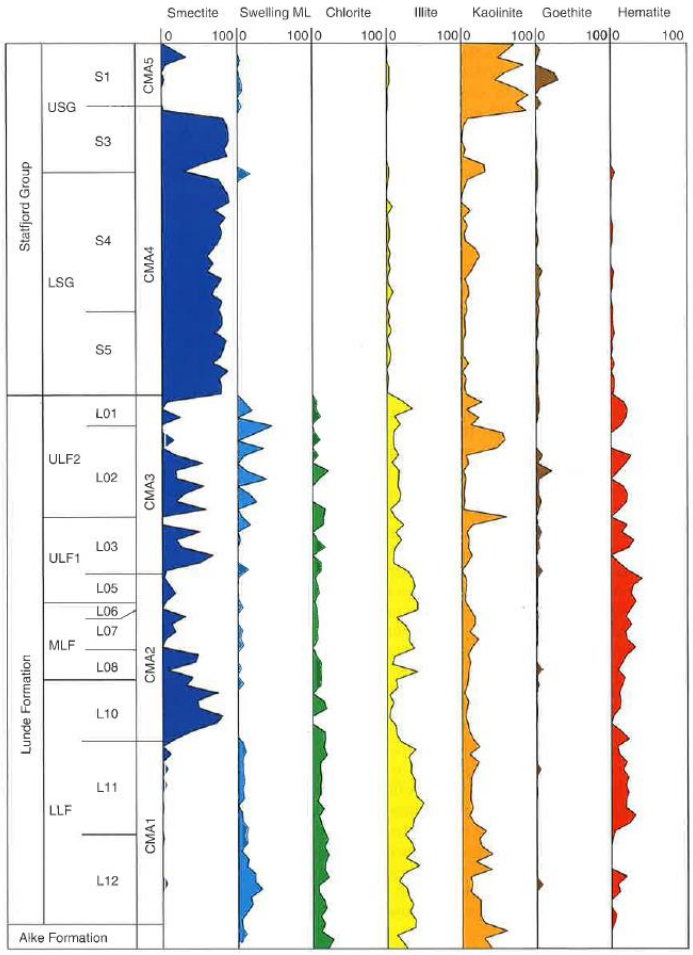

Figure 13: Stratigraphic of the clay minerals and the clay mineral assemblages 1-6 through the Lunde and Statfjord group [4]

3.4 Vertical trends in alluvial, pedogenic and mudrock features

The general trend through the Lunde Formation is upward-fining successions as the climate is changing from a semi-arid to a semi-humid. From the allostratigraphic unit L01-S05 the succession are changing to coarsening-upward successions and this where applied as the lithostratigraphic boundary between the formations by Deegan and Scull (1977). The lower and partly into the middle Lunde member is dominated by ephemeral braided streams and throughout the middle and into the upper member the system is changing to small and large meandering fluvial system. The meander streams are dominating through the upper Lunde formation and the uppermost part is characterized by floodplain and single-storey sandbodies. The upper Lunde formation is dominated by floodplain and single-storey channelized sandstone, compared to the middle/lower, which contains both single and multi-storey sandbodies. This is well represented in the channel deposition proportion (CDP) plot in Figure 7, where the channel deposits reaches its lowest at the uppermost part of the Lunde formation. Compare this to the lower part of Lunde formation, the CDP reaches very high values indicating that the environment is very different through this unit [4].

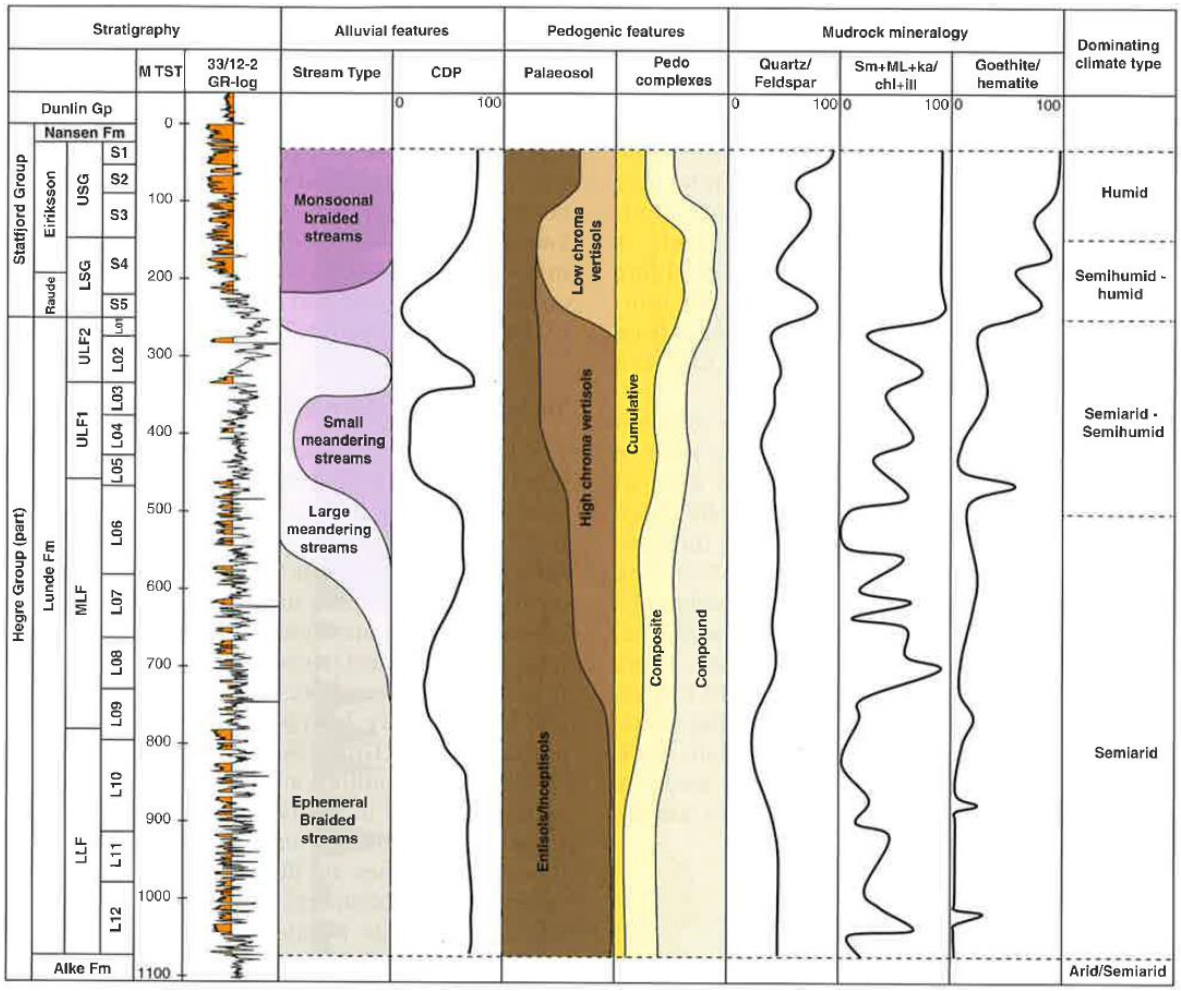

Figure 14: Stratigraphic vertical trend in the Lunde formation and Statfjord group with alluvial features, pedogenic features, mudrock mineralogy and dominating climate type [4]

The lower Statfjord is dominated by small floodplain streams, and some occasionally single-storey channelized sandstones. In the Statfjord formation the climate is changing to a more semi humid climate and the upper Statfjord the climate is considered to be humid. The upper Statfjord is interpreted as monsoonal braided streams with a very high CPD, although the CPD does not cover all of the Statfjord. The palaeosols are changing from entisols/inceptisols in the LLF to higher chroma vertisols in the MLM and this being dominating through the ULF. In addition to these changes in the mudrock facies, there is an upward increasing content of clay fraction in the mudstones through the Lunde formation. The formation contains a selection of minerals which is varying through the formation and is mainly related to the depositional environment. Further the alluvial features, pedogenic features and mudrock mineralogy show a strong correspondence to the stratigraphic positions of changes in the formation [4].

4 Petrophysical evaluation

One of the most important objectives for a reservoir petro physicists is to be able to evaluate given log data from the well, incorporate this data in context to the geology and the reservoir to give the best possible complete picture of the reservoir. This involves evaluating important properties like porosity, permeability and water saturation. In particular how the pores are connected are very important and are greatly affected by the grain geometry, hence the porosity and flow through reservoir.

Due to erosion in the Snorre area in the Triassic-Jurassic the reservoir is segmented into the six described fluvial assemblages. These are evaluated separately to establish comparable reservoir units based on the sedimentology of the units.

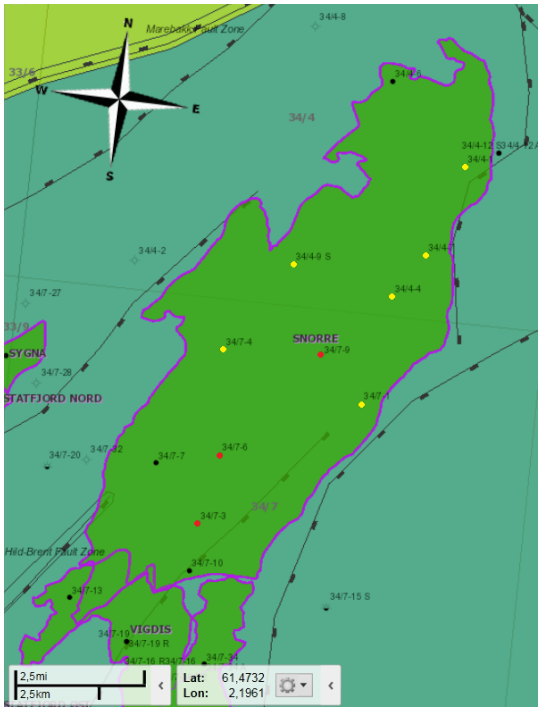

Figure 15: Location of the wells in the Snorre Field

4.1 Wells

In this reservoir characterization the exploration wells from the Snorre Field are evaluated to give the best possible picture of the reservoir and its properties. All of the data available are from when the field was discovered in the 1980's. There are a total of 12 wells evaluated, where 3 of them are key wells and contain SCAL reports and available drill stem test. Some of the wells are only used for pressure data and estimating oil-water-contact.

*Table 5: Available data from the wells. * Data not conclusive or not sufficient amount of data:*

	Block 34/7							Block 34/4				
	3	6	9	4	1	7	10	9S	4	7	1	6
RFT	x	x	x	x*	x	x	x		x	x	x*	x
Conventional Core Data	x	x	x						x	x		
DST	x		x									
SCAL	x	x	x									
Log data	x	x	x	x				x	x	x	x	

4.1 Lithology and Volume of clay

To describe the lithology of the reservoir one of the most used plot are the crossplots between RHOB (density) and the NPHI (neutron density). This is a very good indicator to identify if the reservoir is homogeneous or more heterogeneous, if there is gas present, chlorite coating or bad hole. The figures in this chapter shows the crossplots of the three key wells with zonation, and even though the reservoir is very heterogeneous, there are still able to see different trends in the reservoir.

4.1.1 Lunde formation

In well 34/7-3 the different FSAs (fluvial sandstone assemblages) is clearer than in the other two. The uppermost, FSA4, consists of almost only clay/little content sand, this is very clear from the NPHI histogram and the clay volume lines. The underlying FSA3 is becoming sandier, and the two lowest assemblies consist of a mix of sandstone and mudstone. The clay/sand content can be seen very clearly from the NPHI histogram. Comparing the two lower formations, there are some distinct differences in the RHOB. FSA2 seems to have a much lower RHOB than FSA1, hence higher porosity than FSA1. This can also be proven by extrapolating the point on to the sand-line. This can be seen in the histogram for RHOB, the highest frequency for FSA2 lies around 2,3g/cm^3, and is much more clustered than FSA1 and might indicating a more homogeneous unit.

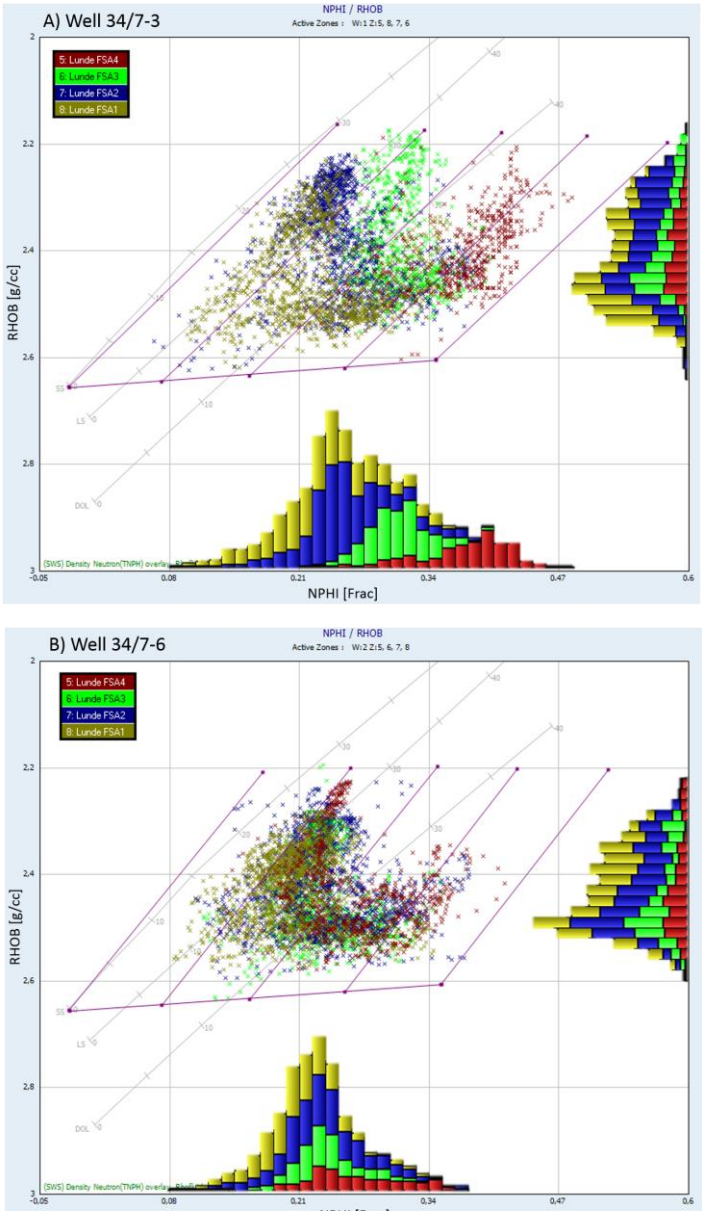

Figure 16: Crossplot of neutron/density from well 34/7-3 and 34/7-6 with zonation and Vcl lines from Lunde formation

The next well, 34/7-6, is completely different from the first well. The assemblages are much less clustered compared to the first well, however combined they might appear more clustered than the first well. The reason is that the values in the NPHI in the two upper assemblies have a much lower

values, see histogram, and they look more like the two bottom layers, hence mixed layers of sandstone and mudstone. All though the two lowest assemblies most likely contains more channelized sandstone, based on the formation evaluation.

The last well, 34/7-9, is probably the most heterogeneous well out of the three. It contain big variations in the density (RHOB), and there is some erosion of the uppermost assemblage FSA4. The green cluster of points highest up in the crossplot represents a very good and clean channelized sandstone bodies. This show very high porosity, from the SS-line, and the log show large separation between RHOB and NPHI indicating low/zero content of silt.

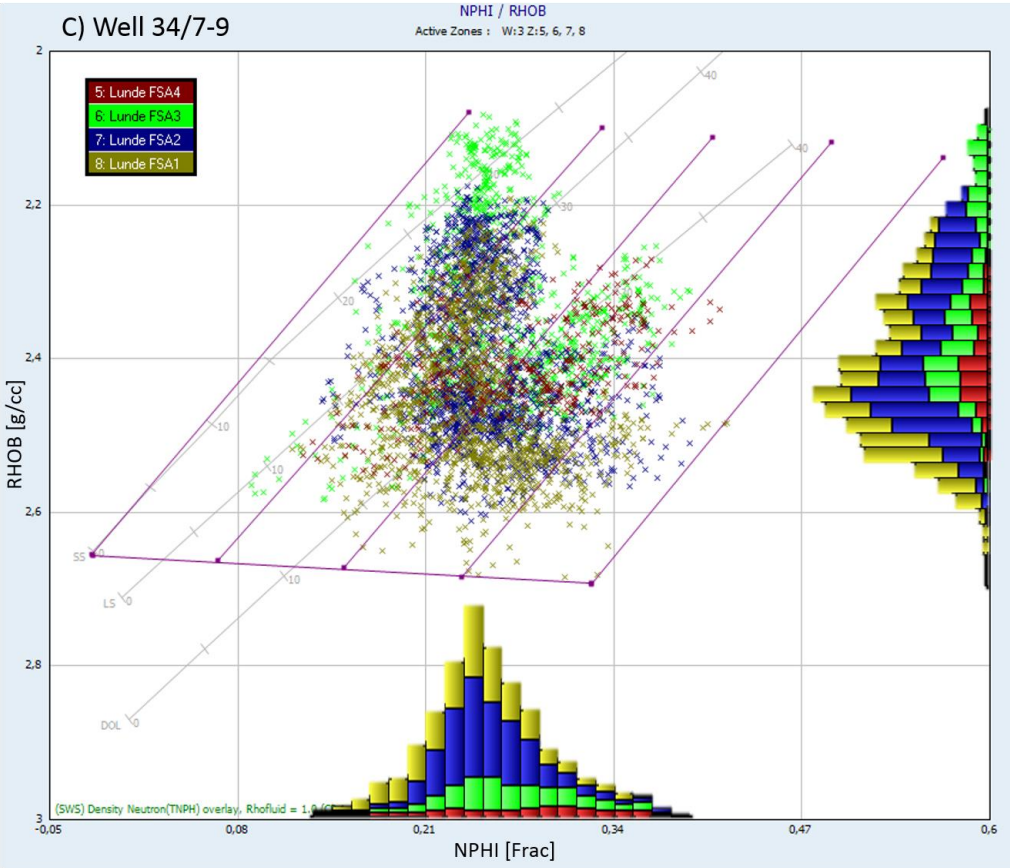

Figure 17: Crossplot of neutron/density from well 34/7-9 with zonation and Vcl lines from Lunde formation

The lithology of Lunde is very heterogeneous, and correlation between wells is difficult. However the lower and the middle (FSA1 and FSA2) assemblages tend to show higher content of channelized sandstone compared to the upper FSA.

4.1.2 Statfjord Group

The lowermost assemblage in the Statfjord group, FSA5, has almost the same sedimentology as FSA4 and are dominated by mudstone with single channelized sandstone. FSA5 in 34/7-3 consist of both mud plains and sandstone, compared to almost completely mudstones in 34/7-6. FSA6 is dominated by multi-storey channelized sandstone and are clearly clustered close to the sand line in the crossplot. The crossplot from the two key wells look similar at first, but the sandstone in well 34/7-6 closer to the sand-line indicating cleaner sandstone with less silt/clay content than in 34/7-3. However the porosity seems a bit higher in well 34/7-3 than in 34/7-6.

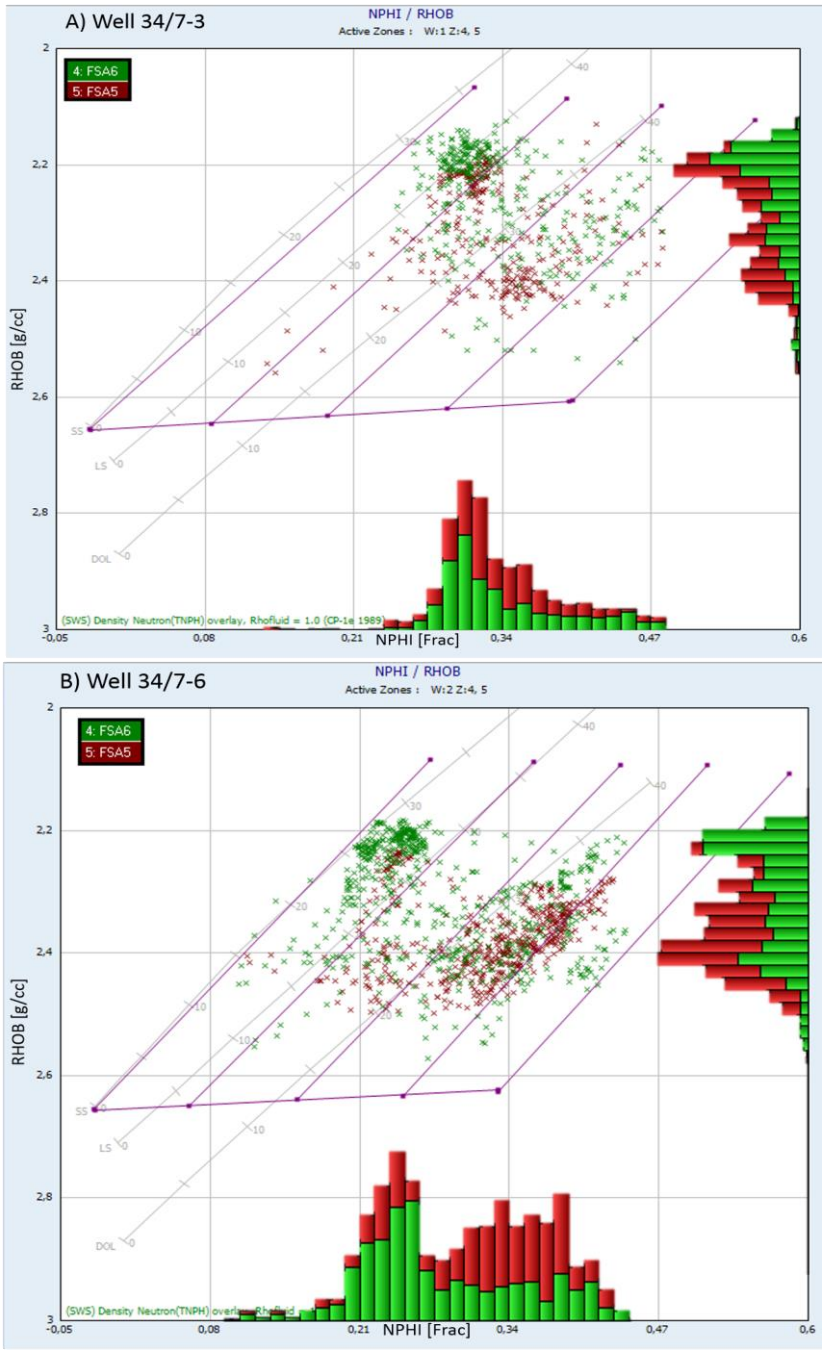

Figure 18: Crossplot of neutron/density from well 34/7-3 and 34/7-6 with zonation and Vcl lines from Statfjord group

4.1.3 Volume of clay, Vcl

The volume of clay is part of the net to gross calculation and therefore an important parameter to calculate correctly. The fraction can be calculated from the clay and sand baseline, marked red and green in the Figure 19. A single indicator (GR) and a double indicator (neutron/density) are used to calculate the V_{cl}. The aim is to match the two V_{cl} from these two indicators as best possible. The two V_{cl} are plotted to the right and shows god match through the whole section. The gamma ray is blowing out of proportion some parts of the reservoir and are not taken into account, probably noise from the equipment of some small layers that have very high content of radioactive minerals. The neutron and density can be plotted in a crossplot with the GR on the z-axis, Figure 20. By putting the GR on the z-axis, the relation between GR and the volume of clay becomes clearer. Lower GR values are located close to the sand line and high GR values towards the clay line.

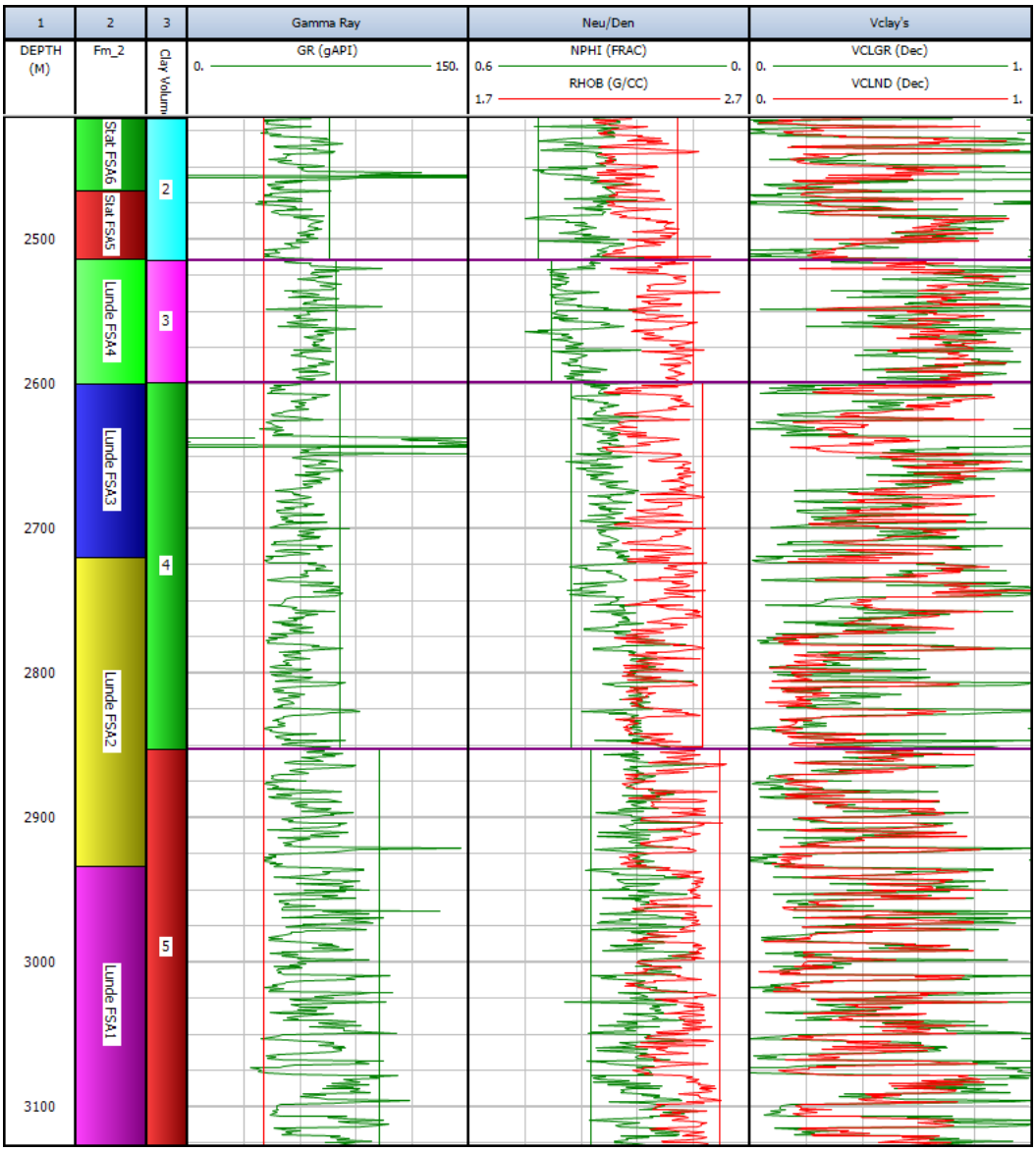

Figure 19: Show Vcl calculation with single gamma ray and double neutron/density indicator from well 34/7-3

Normally the formations are divided into different clay volume zones because the logs are changing through the reservoir, and can often be correlated to subdivision of the formation. This is the case in this well, except for the FSA2 where the clay zone is divided in the middle of the subdivided unit. This correlates well to the sedimentology and the change of depositional system from braided streams to meandering streams.

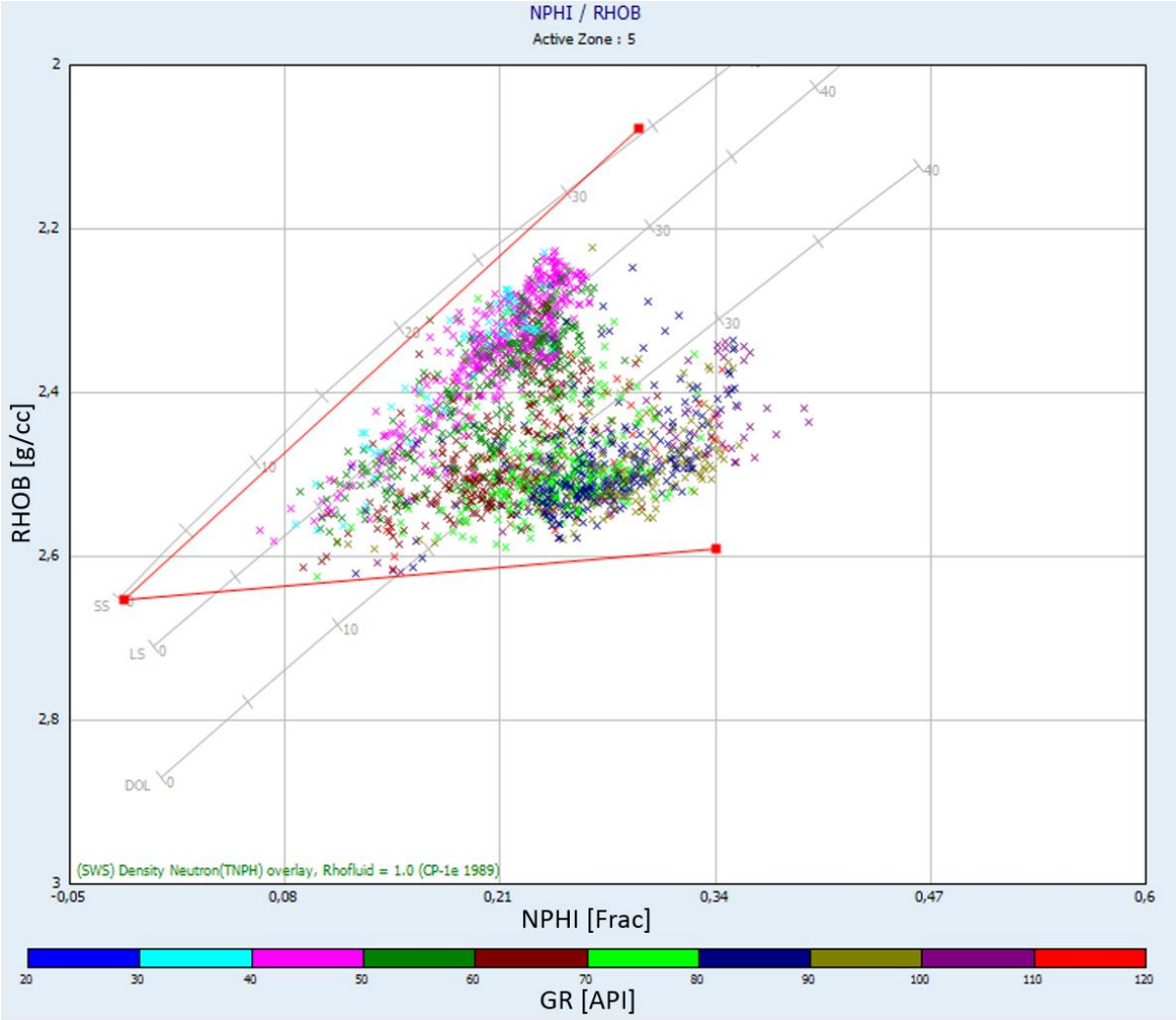

Figure 20: Crossplot between NPHI and RHOB with GR on the z-axis from clay volume zone 5 well 34/7-3. See Figure 19.

4.2 Conventional core analysis

Conventional core data covers porosity, permeability and grain density. These are important factors regarding the quality and have a direct impact on other calculation such as net to gross (N/G) and water saturation. Porosity and permeability is evaluated from both logs and conventional core data. The conventional core section have measurement every 0.25m and vary in length due to length of the reservoir/or desired zone. The evaluation from the logs and the conventional cores should match well, however in such a heterogeneous reservoir the permeability must be calculated with caution.

4.2.1 Overburden correction

The data from the core analysis is corrected before the values can be used for calculation in Interactive Petrophysics (IP). The correction used is for Triassic reservoir from 2500-3000m depth:

$$\phi_{res} = 0.94 * \phi_{lab}$$

$$k_{res} = 0.65 * k_{lab} \ , \qquad k > 10\ mD$$

$$k_{res} = 0{,}50 * k_{lab} \ , \qquad k < 10\ mD$$

Both porosity and permeability need to be depth corrected in order to get the core data to match the calculated porosity and permeability curves. This is done by using the tool "Interactive Depth Shift" in IP. Normally they are 1-5 m offset.

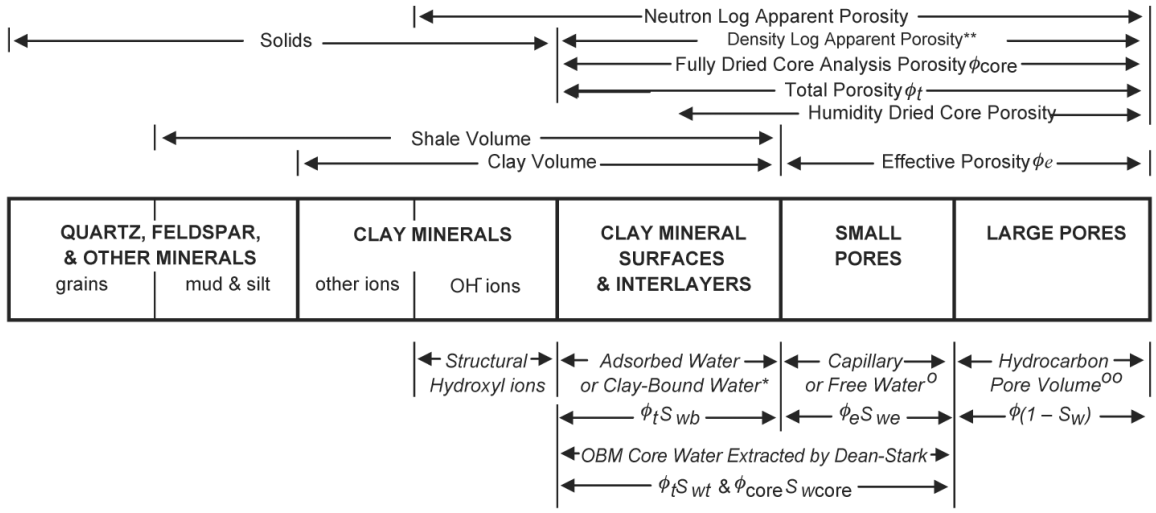

** Density log apparent porosity using the grain density of dried core and correct invaded-zone fluid density.
* Smectite clays have a large capacity to adsorb water, whereas most other clay minerals have little or no adsorbed (or bound) water.
°° This model has no mobile water, and the model sandstone will produce water-free hydrocarbons during its initial production phase.
° As height above the hydrocarbon-water contact increases, capillary water volume decreases and hydrocarbons displace capillary water. Humidity dried core analysis porosity is shown as including some of the clay-bound water.
Box sizes are schematic.

Figure 21: Total, effective, and core porosities and their associated water saturations in shaly sands (after Woodhouse and Warner) [6]

4.2.2 Porosity Evaluation

The porosity can be evaluated with and without taking the volume of clay into account. If not taking Vcl (volume clay) into account the porosity can be simply calculated by only considering the matrix and the pore space, called the total porosity

$$\phi_T = \frac{\rho_{ma} - \rho_b}{\rho_{ma} - \rho_f} = \phi_D$$

Where ρ_b is the RHOB log and $\rho_f = 1$ g/cm^3. ρ_{ma} is normally chosen to be 2.65 or 2.66 g/cm^3, but in some wells the value is even higher, see chapter 4.2.4. If volume of clay is considered the formula for effective porosity is

$$\phi_E = \frac{7\phi_{DC} + 2\phi_{NC}}{9}$$

Where ϕ_{DC} and ϕ_{NC} is the corrected values for the clay volume, and can be calculated from the formulas

$$\phi_{DC} = \phi_D - V_{cl} * \phi_{D_{cl}} \quad , \qquad \phi_{D_{cl}} = \frac{\rho_{ma} - \rho_{cl}}{\rho_{ma} - \rho_f}$$

$$\phi_{NC} = \phi_N - V_{cl} * \phi_{NC_{cl}}$$

The values for $\phi_{D_{cl}}$, $\phi_{N_{cl}}$, ρ_{cl} are found or calculated from the clay zone in the logs. The neutron value used in the calculation also has to be corrected for lithology, which in this case is 0.04 for sandstone:

$$\phi_{NC} = (\phi_N + 0.04) - V_{cl} * (\phi_{NC_{cl}} + 0.04)$$

In clean sandstone the effective porosity is equal to the total porosity. The value used in calculating the effective porosity is listed in Table 6 for the three key wells. Big differences in the total and effective porosity for Statfjord is observed due to high values of PHID$_{cl}$ ($\phi_{D_{cl}}$) and NPHI$_{cl}$ ($\phi_{NC_{cl}}$) compared to the Lunde formation

Table 6: Clay correction values used in effective porosity

	Well 34/7-3			Well 34/7-6			Well 34/7-9		
Unit	RHOBcl [g/cm3]	NPHIcl [frac]	PHIDcl [frac]	RHOBcl [g/cm3]	NPHIcl [frac]	PHIDcl [frac]	RHOBcl [g/cm3]	NPHIcl [frac]	PHIDcl [frac]
FSA5-6	2,39	0,40	0,16	2,43	0,37	0,13			
FSA 4	2,48	0,35	0,10	2,50	0,33	0,09	2,45	0,35	0,12
FSA 3	2,46	0,31	0,12	2,51	0,30	0,08	2,47	0,31	0,11
FSA 2	2,46	0,28	0,12	2,52	0,30	0,08	2,51	0,29	0,08
FSA 1	2,47	0,23	0,11	2,52	0,25	0,08	2,52	0,29	0,08

4.2.3 Evaluation of porosity and permeability

The permeability of the cores are measured by putting the cores in a respectively cell and let the flow of air go through and increasing the confining pressure and measure the permeability at each pressure. This has to be corrected from air to fluid before imported into the software and it

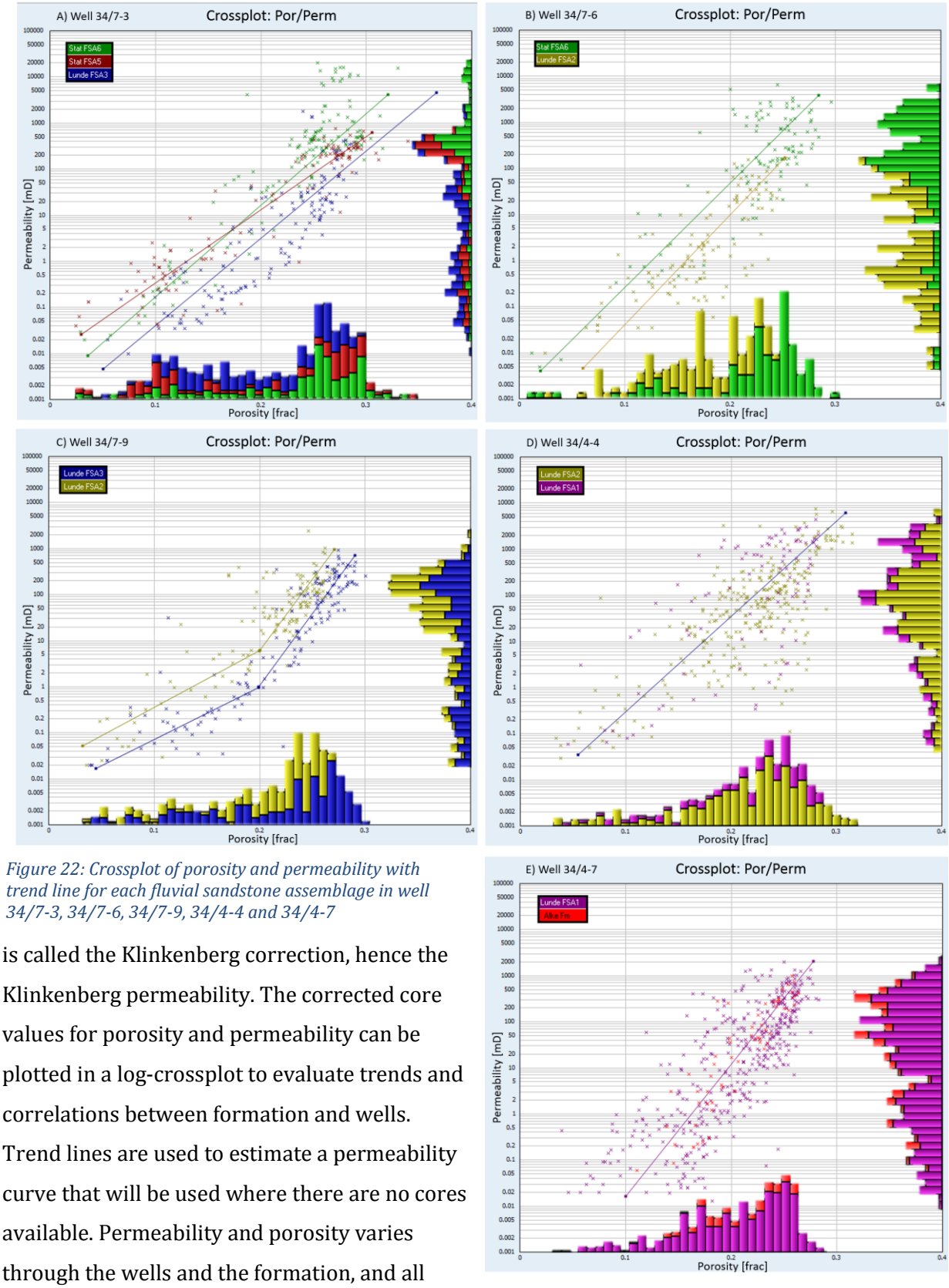

Figure 22: Crossplot of porosity and permeability with trend line for each fluvial sandstone assemblage in well 34/7-3, 34/7-6, 34/7-9, 34/4-4 and 34/4-7

is called the Klinkenberg correction, hence the Klinkenberg permeability. The corrected core values for porosity and permeability can be plotted in a log-crossplot to evaluate trends and correlations between formation and wells. Trend lines are used to estimate a permeability curve that will be used where there are no cores available. Permeability and porosity varies through the wells and the formation, and all tough the sedimentology changes trends can be evaluated accordingly to their FSA. The top FSA of the Statfjord group, FSA6, shows a higher permeability at the same porosity than the underlying assemblages (Figure 22A and B). FSA6 has the highest permeability, especially this

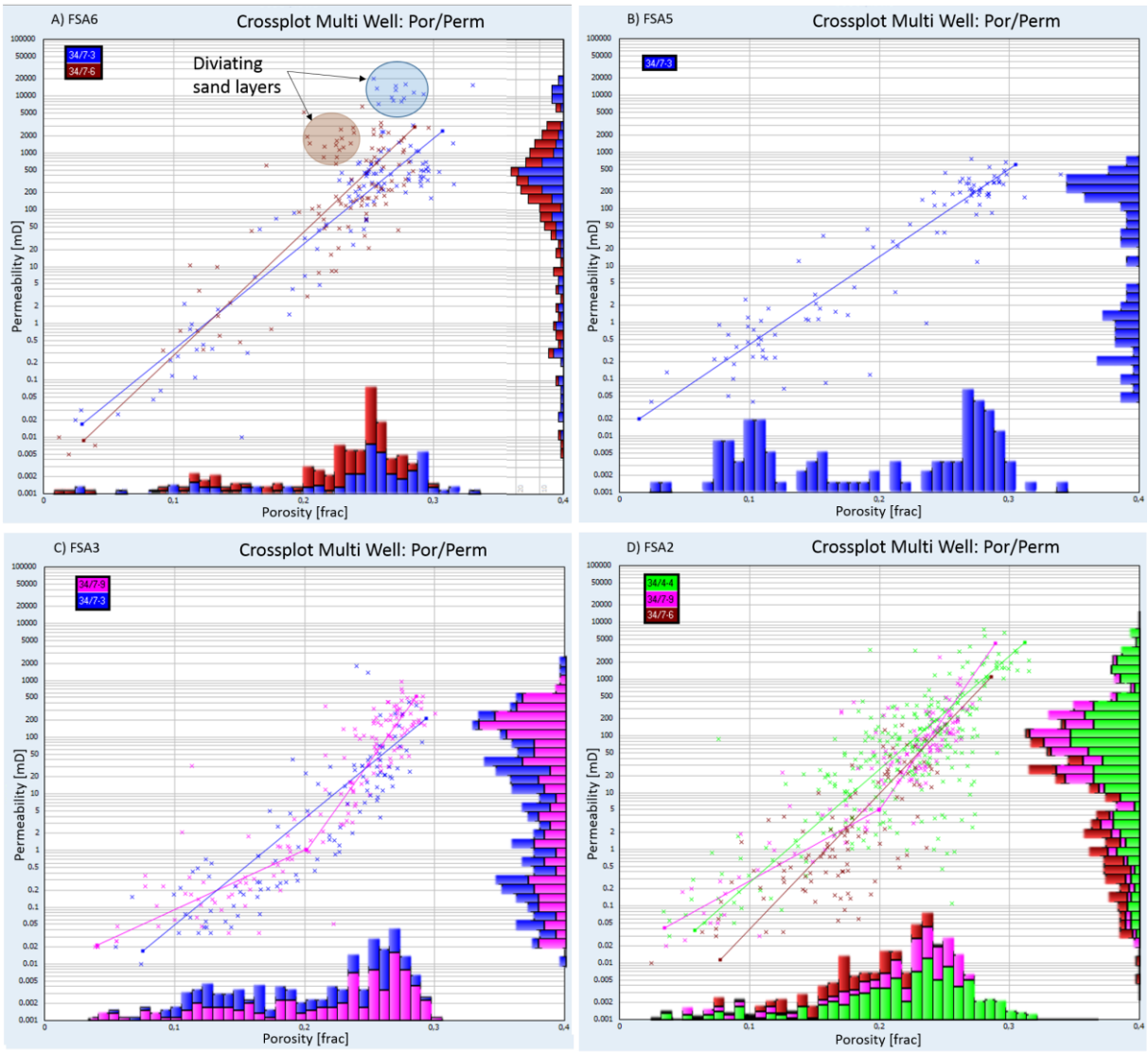

Figure 23: Crossplot for porosity and permeability for each fluvial sandstone assemblages

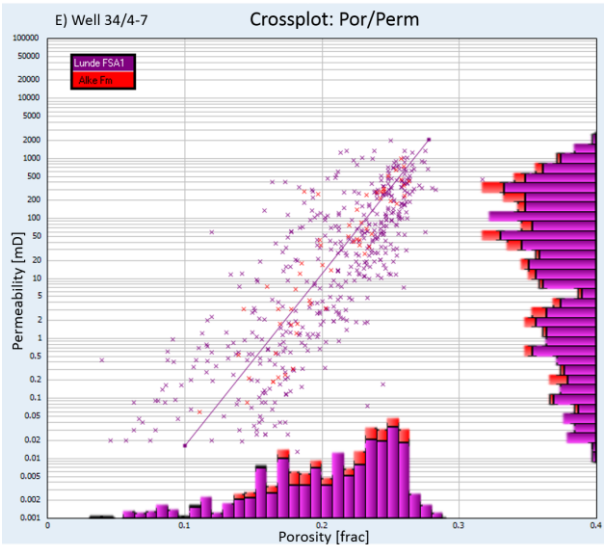

formation has some sandstone layers which can reach 20000mD in from the conventional core data, see Figure 22a. These are found at the uppermost part of the Statfjord and FSA6 and are not considered when applying trend line, to avoid overestimating the permeability in the rest of the assemblage. The lower assemblage in Statfjord, FSA5, show a lower permeability trend than FSA6 and can be interpreted as different depositional environment causing lower permeability

The uppermost fluvial assemblage of the Lunde formation, FSA4, has no core data available, and contains mainly floodplains with some single storey sandstones. FSA 3 show a lower permeability trend than both the Statfjord formation and the underlying fluvial assemblies, FSA2 and FSA1 (Figure 22A and B). It is noticeable that even though the porosity is higher for FSA3 than for FSA2 in well 34/7-9 the permeability are the same, which indicate that FSA2 should have better reservoir quality than the overlying formation FSA3 (Figure 22C). In well 34/7-9 the trend is deviating from the other wells and are separated into two parts, for porosity lower and higher than 0.20, to be able to get a good match between the trend lines and the data points.

The FSA2 and FSA1, middle and lower Lunde formation, show several similarities. In well 34/4-4 and well 34/4-7 one trend line fits all the data in the well, also containing the underlying Alke formation in well 34/4-7. The data in these two wells are also more scattered and shows great variation in permeability for same porosity. The reason for this can be bad/good sorting of the grains, silt content or mineralogical effect. Different mineralogical effects such as pore-bridging, pore lining and pore filling caused respectively by illite, chlorite and kaolinite can occur, but at this reasonable shallow depth this may not be the case (depth 2400-2600m). The trend line in well 34/4-7 are steeper than in well 34/4-4, which indicate that permeability is increasing more in well 34/4-7 compared to 34/4-4. Table 7 contains all the formula used to evaluate sections or wells without core data.

Table 7: Results from the porosity/permeability evaluation on the different fluvial assemblages

Well	FSA	Porosity	k = 10^(a+bϕ)
Well 34/7-3			
	FSA6		10^(-2.205240 + 18.548620 * ϕ)
	FSA5		10^(-2.057600 + 15.882180 * ϕ)
	FSA3		10^(-3.294689 + 18.966240 * ϕ)
Well 34/7-6			
	Stat:		10^(-2.854246 + 22.684620 * ϕ)
	FSA2		10^(-2.915425 + 18.802270 * ϕ)
Well 34/7-9			
	FSA3	ϕ > 0.2	10^(-6.206480 + 31.225550 * ϕ)
	FSA3	ϕ < 0.2	10^(-2.294338 + 11.492270 * ϕ)
	FSA2	ϕ > 0.2	10^(-5.354239 + 30.761100 * ϕ)
	FSA2	ϕ < 0.2	10^(-1.685073 + 12.339320 * ϕ)
Well 34/4-4			
	FSA1		10^(-2.581731 + 20.619210 * ϕ)
	FSA2		10^(-2.581731 + 20.619210 * ϕ)
Well 34/4-7			
	FSA2		
	FSA1		10^(-4.659332 + 28.679080 * ϕ)
	Alke Fm		

4.2.4 Grain density

From the conventional core analysis, four wells were tested for the grain density. The grain density can be a good indicator to lithology to identify good sands, clays and if there are heavy minerals present. The grain density is also direct input in calculating the total porosity. Sandstones and mudstones have many impurities/heterogeneity and vary both on micro and macro scale. Table 9 show how the different minerals in the reservoir vary in density, especially the carbonates and the iron oxide are heavy minerals. From the formation analysis, facies containing palaeosols or carbonate content such as carbonate clasts/carbonate nodules causes the grain density to increase and can applied to identify these types of rocks. No correlation between wells are possible due to large heterogeneity caused fluvial deposition and large distances between wells (1-3km).

Rock type	Minerals	Approximal grain density [g/cc]
Fluvial Sandstone		
	Quartz	2,64
	K-feldspar	2,52-2,59
	Plagioclase	2,59-2,74
	Kaolinte	2,41
	Mica	2,82-2,86
Carbonates		
	Calcite	2,71
	Dolomite	2,85
	Siderite	3,89
Clay minerals		
	Smectite	2,12
	Chlorite	2,76
	Illite	2,52
	Kaolinte	2,41
Iron oxide		
	Goethite	4,34
	Hematite	5,18

Table 8: Approximal grain density for reservoir minerals

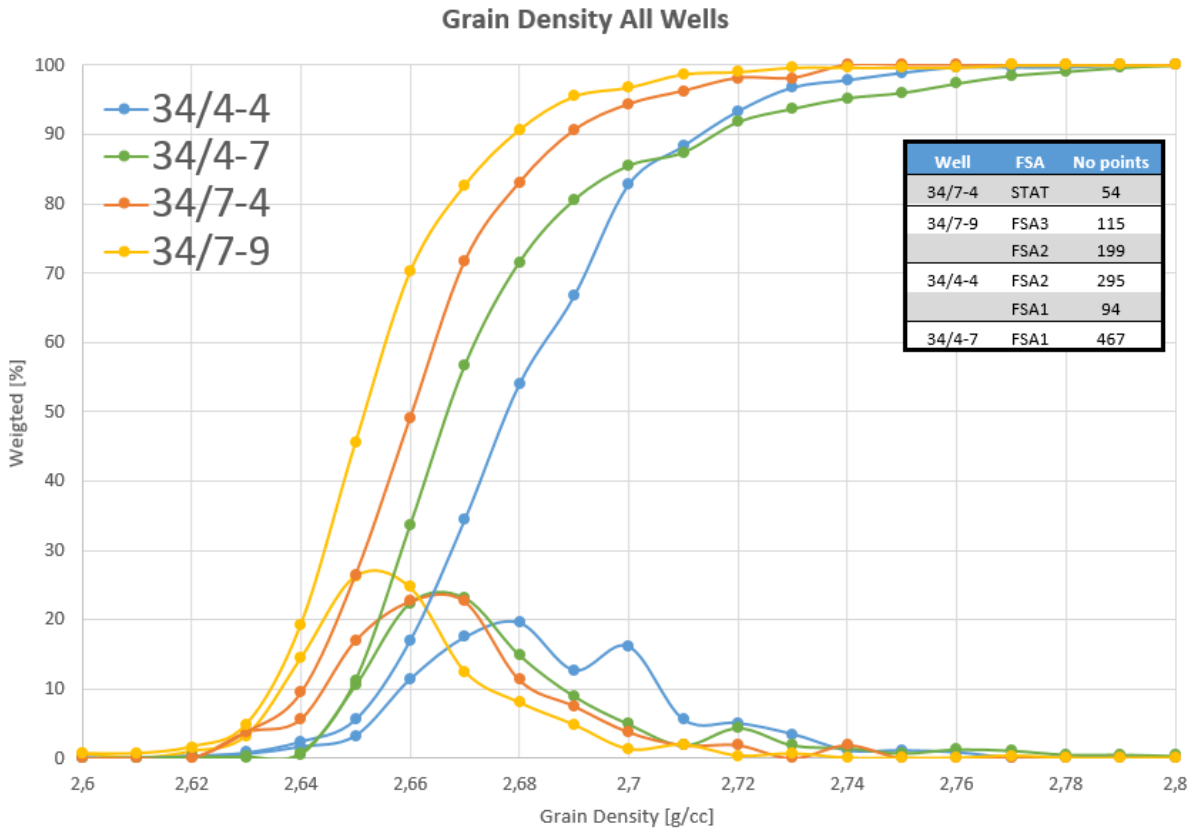

Figure 24: Grain density from well 34/4-4, 34/4-7, 34/7-4 and 34/7-9

In well 34/7-9 and well 34/4-4 the conventional data covers two fluvial assemblages and can be vertically evaluated. The core interval in well 34/4-4 represents almost the entire CMA2, Figure 26B. This assemblage has increasing content of hematite and illite, and decreasing in smectite. FSA1 compromises the lower of CMA2 and should have low content of hematite and illite and high of smectite. From the table smectite and illite has reasonable low densities and hematite has very high. The content of hematite may be as high as 40% in the upper CMA2 and this could be the reason for the big vertical separation between FSA2 and FSA1.

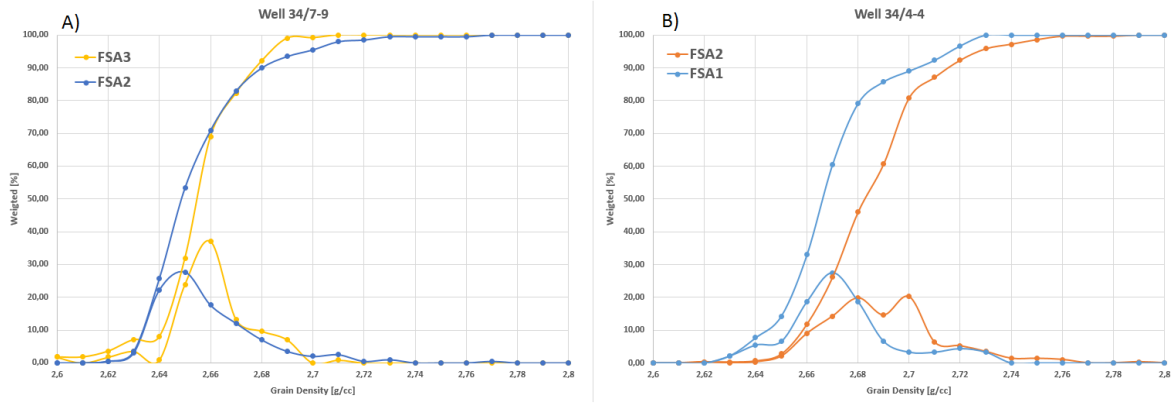

Figure 26: Vertical correlation of grain density in well 34/7-9 and 34/4-4

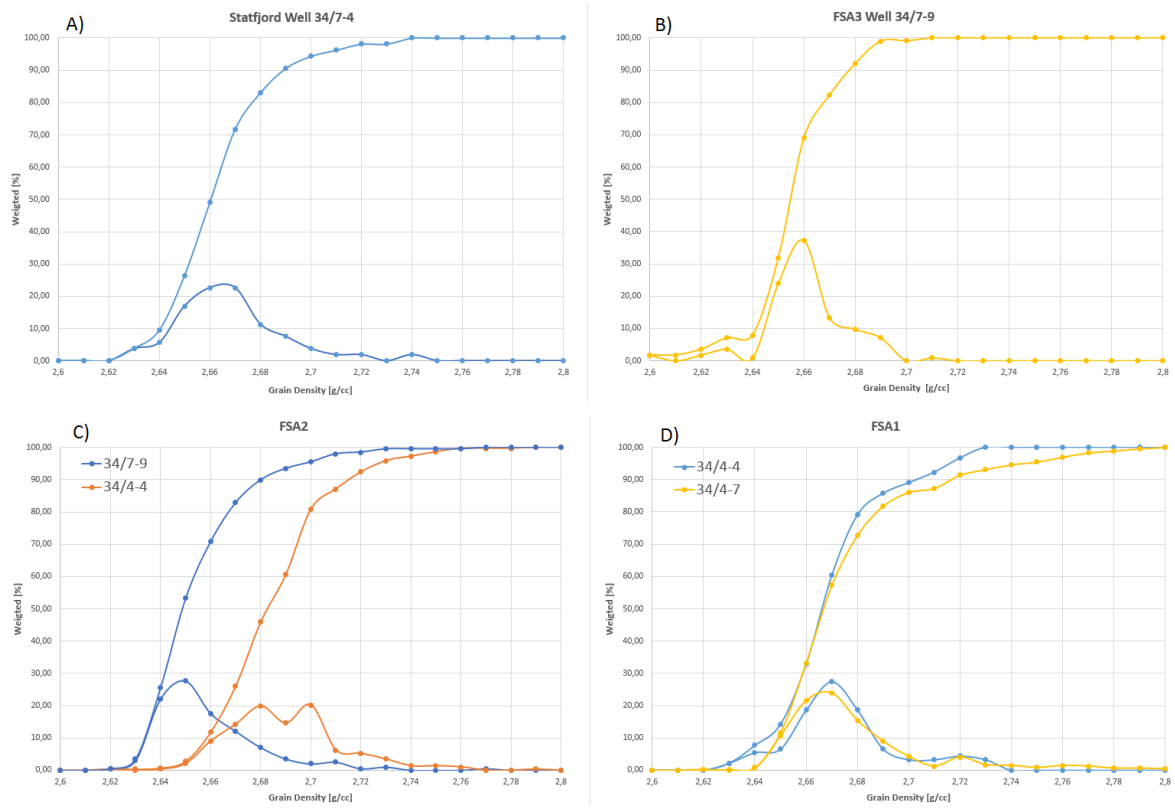

Figure 25: Correlation of grain density of the different fluvial assemblages

In well 34/7-9 the FSA are quite similar, the FSA2 has almost the same average but FSA3 seems more concentrated at 2.66 g/cm^3 (g/cc) compared to FSA2 between 2.64-2.66. FSA2 contain more heavy minerals than FSA3, above 2.7 g/cc. In this well the FSA2 does not contain as nearly as much heavy minerals as in well 34/4-4. This show how heterogeneity the reservoir is and can be very hard to make any clear correlation. Another reason is that well 34/7-9 contains very clean sandstones compared to 34/4-4 and therefor the grain density is much lower. FSA1 seems to have much better correlation than FSA2 between well 34/7-4 and well 34/4-4 from the graph with an average density around 2.7 g/cc. The content of heavy minerals seems higher in well 34/4-7 which contains measurements up to 2.79 g/cc compared to well 34/4-4.

The grain density (ρ_{ma}), as mentioned before under porosity calculation, are a direct input when calculating the total porosity and this varies from well to well. In the clean sandstone in well 34/7-9 the value is around 2.65 g/cm^3 and increasing to 2.66 – 2.68 g/cm^3 in the other wells. Due to the fact that the grain density varies so from well to well a standard value of 2.66 g/cm^3 is used.

4.3 Formation factor, saturation exponent and cementation factor

The formation factor is defined as the ratio of resistivity in a fully saturated brine and the known resistivity of the formation when it is 100% saturated with water

$$F = \frac{R_o}{R_w}$$

The formation factor is inversely related to the porosity, and also a function of pore structure and pore-size distribution. The Achie equation state that

$$F = \frac{a}{\phi^m}$$

Where a is the lithology factor and m is the cementation factor. By applying log on each side the equation can be rewritten to

$$\log F = \log a - m \log \phi$$

and be plotted as a straight line in a log-log plot, see Figure 27 (34/7-3). The line is forced to fit the standard value for a = 1. As mentioned above the formation is related to the pore geometry, and the formation factor should increase with decreasing permeability assuming the porosity stays constant.

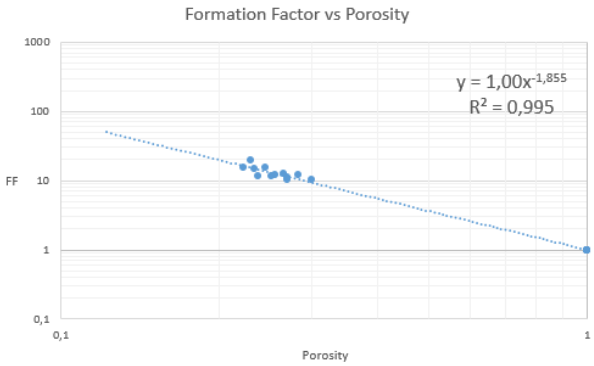

Figure 27: Formation factor plotted vs porosity to estimate the cementation factor m = 1.855 from trend line

The saturation exponent n is measured in a drainage test of the cores, by measuring the resistivity at the in- and outlet. The resistivity is plotted as the resistivity index

$$RI = \frac{R_t}{R_o} = S_w^{-n}$$

By applying log on each side the equation can be rewritten as

$$\log RI = -n \log S_w$$

The results from the SCAL reports are plotted in Figure 28. Well 34/7-9, which had the most points, indicating saturation value of around a value between 1.7 and 2.1 while the points from well 34/7-3 are a bit higher. Well 34/7-9 contains very little silt compared to well 34/7-3, and the water saturation should be higher in this well because of the properties to silt. Due to the size of silt, the smaller silt grains will fill the pore between the sand and may/or may not reduce porosity, but the permeability will decrease significantly with increasing

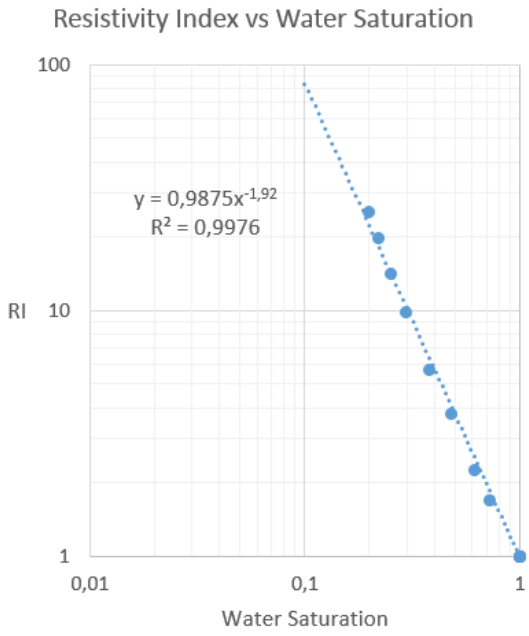

Figure 28: Resistivity index vs water saturation to estimate saturation factor n = 1.92

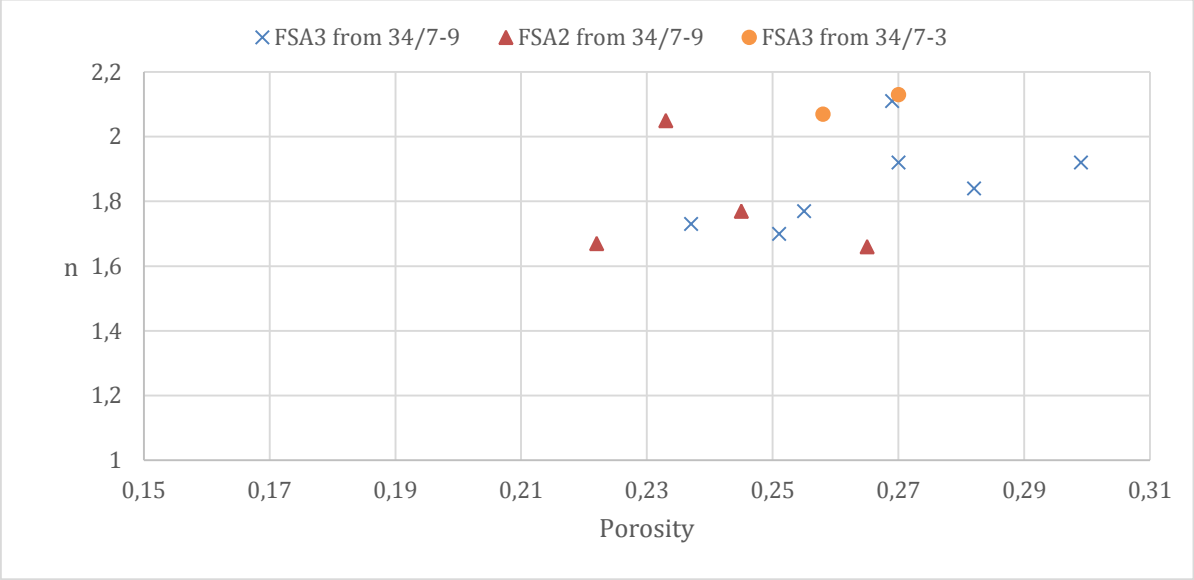

Figure 29: Results for the saturation factor plotted against porosity

silt content. The total surface area in the rock will increase and consequently the irreducible water saturation will increase. In addition, the reduction of pore throats will increase the capillary forces between the grains, resulting the energy need displaced or produce the oil will increase.

The values from the SCAL report are used to evaluate the rest of the wells in the reservoir. The cementation factor is changing significantly between the cores, and a value of 1.85 will be used in the rest of the reservoir for both Lunde and Statfjord. The saturation factor for Statfjord are not given in any of the SCAL reports, and a standard value of 2 is used. Considering that the standard value is 2 for both the cementation factor and for the saturation factor, the results from the Lunde formation is very good. With decreasing values the water saturation will increase, explained under water saturation.

Table 9: Summary of SCAL reports and evaluation of other wells

From SCAL: Property	34/7-3	34/7-6	34/7-9
a	1	1	1
m	1,86	1,82	1,86
n	2,1	-	1,83
For evaluation of other wells : Property	**Lunde**	**Statfjord**	
a	1	1	
m	1.85	1.85	
n	1.87	2	

4.4 Water saturation

Water saturation is one of the most important and challenging parameters to estimate for a petrophysics, and multiple methods can be applied leading to different results. These differences can lead to uncertainty when calculating the IOIP or IGIP, and must be evaluated carefully. In this section there are three different approaches, two electrical-properties; Indonesia and Waxman Smith method, and capillary pressure.

4.4.1 Indonesia equation

This model was developed by field observation in Indonesia and is used in formation with clay/shale content. This equation used the Archie exponents, the cementation factor m, saturation exponent n and the lithology factor a, the effective porosity, and the resistivity of the logs. This method is very easy to use and can be directly calculated from the "user formula" in IP

$$S_w = \left[\left(\left(\frac{V_{cl}^{2-V_{cl}}}{R_{cl}}\right)^{1/2} + \left(\frac{\phi_E^m}{aR_w}\right)^{1/2}\right) R_t\right]^{-\frac{1}{n}}$$

4.4.2 Waxman Smith Equation (SWE)

WSE related the resistivity of a shaly formations sand to the conductivity, and the cation exchange capacity (CEC), which is controlled by the clay content of the rock and controls the surface activity. In formation with high content of clay the CEC is higher due to larger surface areas where conduction can occur. In water bearing core the conductivity is expressed by

$$1.\ Clean\ sand:\ \ C_o = \frac{1}{F} C_w$$

$$2.\ Shaly\ sand:\ \ C_o = \frac{1}{F^*}(C_w + C_e)$$

where C_e=BQ_v, B=equivalent conductance of the counter-ions, Q_v= Concentration of clay exchange active cations per PV (pore volume). The relation between CEC and Q_v is

$$Q_v = \frac{CEC\ (1-\phi)GD}{100\ \phi}$$

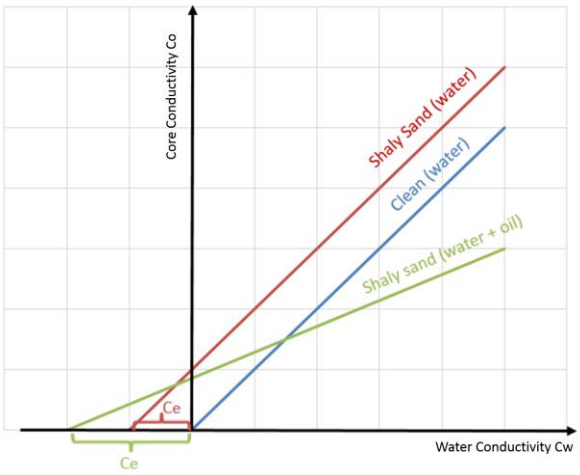

Figure 30: Illustration of the relationship between water conductivity and the core conductivity in clean sand (water), shaly sand (water) and shaly sand (oil and water)

Illustration of core conductivity and the water conductivity in clean sand and shaly sand saturated with water, and one shaly sand saturated with oil and water. For core saturated with oil the conductivity will be lower due to resistivity of the hydrocarbons being high and is expressed by

$$3.\ C_t = \frac{1}{G^*}(C_w + BQ_v') \overset{Q_v'=\frac{Q_v}{S_w}}{=} \frac{1}{G^*}\left(C_w + \frac{BQ_v}{S_w}\right)$$

Where C_t is the conductivity of a partially water saturated sand, G^* is a geometric factor; Function of porosity, water saturation and pore geometry, but independent of Q_v.
Combining the three equation for core conductivity the water saturation can be expressed as

$$S_{wT} = \frac{R_t}{F^*}\left(\frac{1}{R_w} + \frac{BQ_v}{S_{wT}}\right)^{-\frac{1}{n^*}}$$

where $F^* = \frac{a^*}{\phi^{m^*}}$, the porosity refers to the total porosity, hence the total water saturation S_{wT}. R_t is the resistivity of the formation. [9].

The Archie exponents are found from the lab and the Waxman-Smith exponents; n^*, m^* and a^* are defined as

$$a^* = a = 1$$
$$m^* = m + 0.1$$
$$n^* = n + 0.1$$

If there are good core data available the WSE is preferred compared to the Indonesia, and should give a better result. In Figure 28 from well 34/7-9 all the cores where tested for Q_v and the equation for Q_v is given in the figure. The same curve can be found from well 34/7-6 and the results are almost identical, see Table 10.
The Waxman Smith method did not give any reasonable good match with the Indonesia and capillary pressure. All of the cores from the SCAL report are taken from zones with porosity higher than 20%. This reason for the miss match can be that all the cores are taken from porosity above 20%, so that the trend line would look different if lower porosity were included.

Table 10: Result for Qv

Well	Qv [meq/PV]
34/7-6	0.0005*x**-3.401
34/7-9	0.0005*x**-4.326

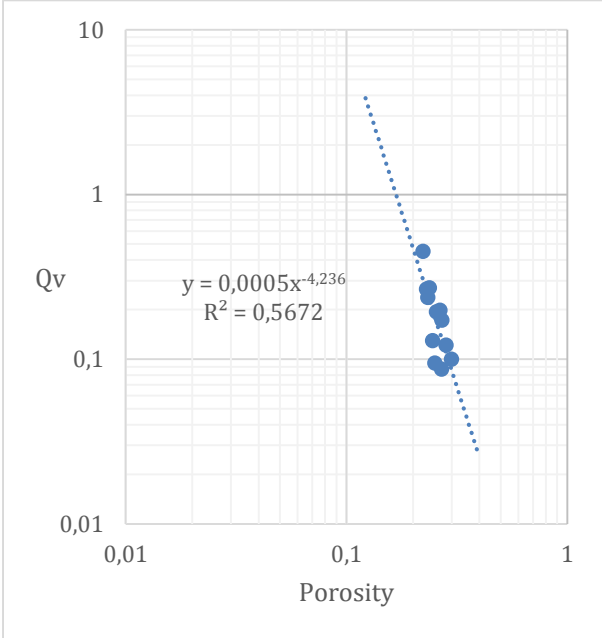

Figure 31: Qv vs porosity from SCAL report well 34/7-9

4.4.3 Capillary pressures

As the last method, the water saturation can be calculated from capillary pressure curves from the SCAL reports. The capillary pressure curves represent the drainage curves from the SCAL report and varies greatly in cores with different permeability. The porosity and permeability normally varies from 20% to 30% and 0.1 mD to 1-2 D in the cores.

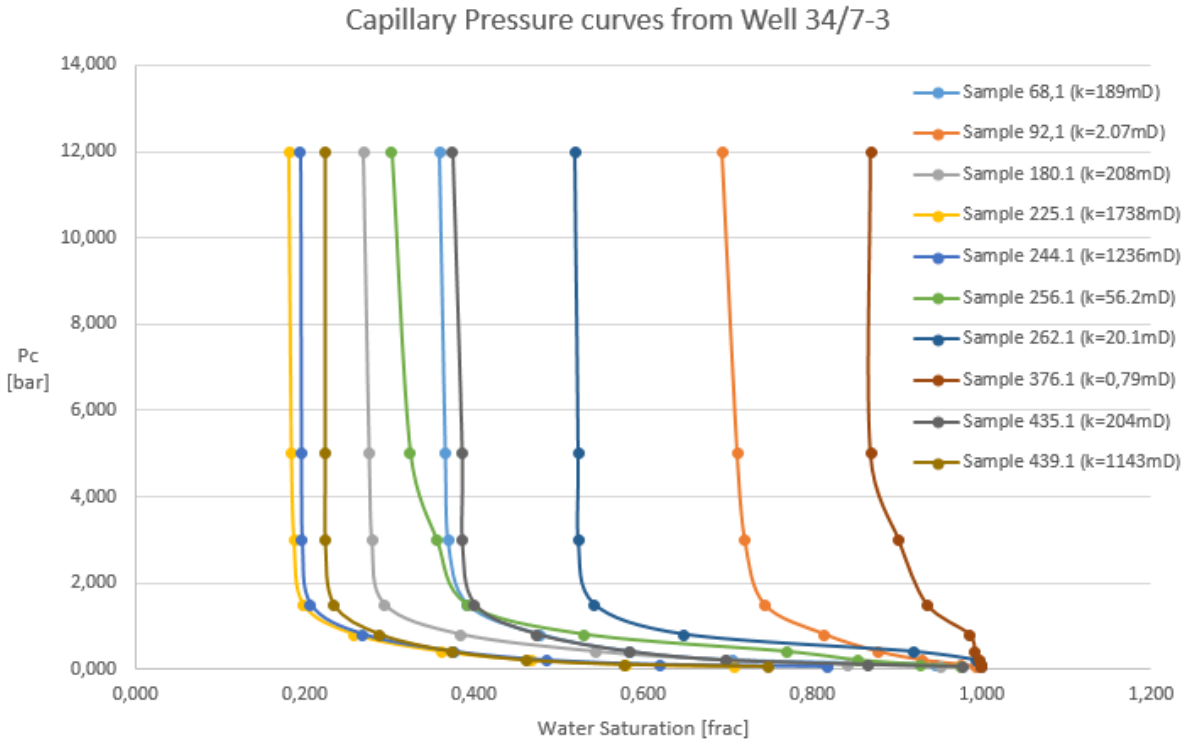

Figure 32: Capillary pressure curves from SCAL report well 34/7-3

The capillary pressure curves is normalized by

$$S_{wN} = \frac{S_{wJ} - S_{wIRR}}{1 - S_{wIRR}}$$

From normalized points from the zone, a power trend line is applied to get the normalized water saturation expressed as

$$Normal\ Power\ Function: \quad S_{wN} = aJ_{res}^{-b}$$

$$Shifted\ Power\ Function: \quad S_{wN} = a(J_{res} - b)^{-c}$$

Where J_{res} represent the reservoir properties at reservoir conditions and is expressed by

$$J_{res} = \frac{\Delta\rho\ g\ 3.141\ (FWL - depth)}{\sigma \cos\theta}\, a \sqrt{\frac{K}{\phi}}$$

Where K=permeability, ϕ=porosity, σ=interfacial tension oil/water, θ=contact angle oil/water, Δρ=density differences oil/water, g=gravitational constant, FWL=Free water level.

The software "CurveExpert Professional" was applied to extract different trend lines from all the zones for differnet permeability range, normally above and below 100mD, but also 10mD in one fluvial assemblage. Due to heterogeneity of the reservoir and the big differences in permeability,

the curves will be very different for high/low permeability and must be taken into account. The example in the Figure 33 below is from well 34/7-9, FSA2, for permeability below 100 mD.

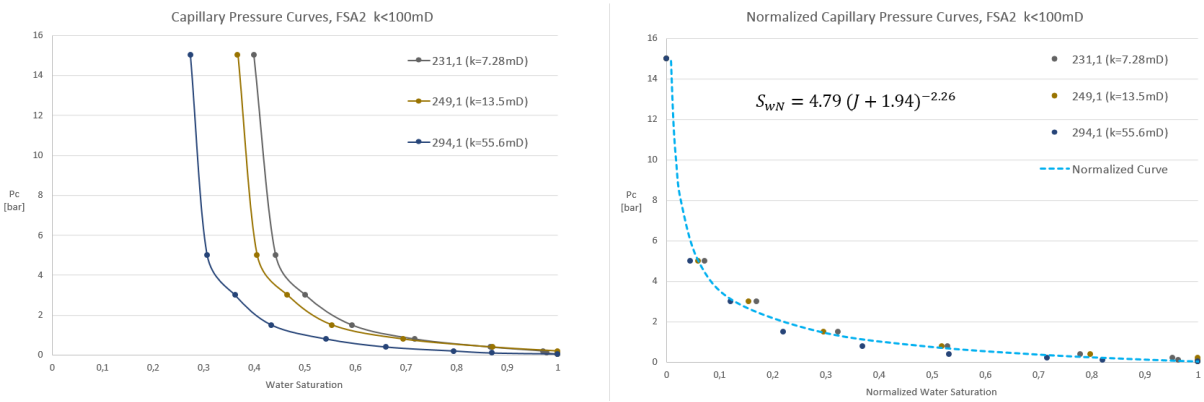

Figure 33: Illustration normalized capillary pressure for FSA2 below 100 mD

The irreducible water saturation curve can be found by plotting the irreducible water for each core vs the permeability in a semi-log plot, Figure 34. The trend line is of exponential form and has to be recalculated such that S_{wi} is a function of K. From the Figure 34 below, the following equation is found

$$S_{wirr} = 0{,}1890 \log(\mathrm{K}) + 0.7395$$

The curves is refered to as S_{wirr} and all the results can be found in Table 11.

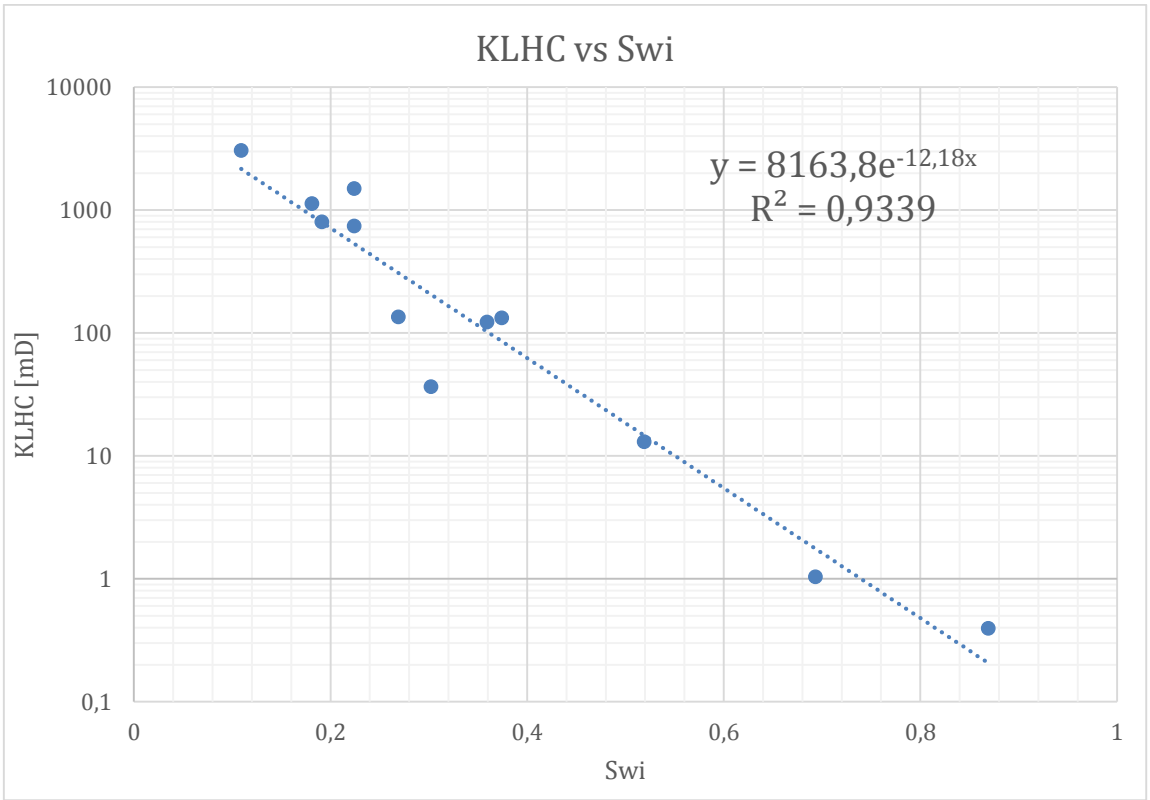

Figure 34: Irreducible water saturation vs permeability and trend line used to estimate formula for Swirr

The water saturation from capillary pressure can be found by the formula

$$S_{wJ} = S_{wN}(1 - S_{wirr}) + S_{wirr}$$

To be able to calculate the water saturation from capillary pressure the product of surface tension and contact angle has to be estimated. First the water saturation is calculated from Indoneisa and Waxman-Smith method, and then the water saturation curves is matched by changing the product such that the curves match sufficient. Example of the watersaturation for well 34/7-6 is given in Figure 35. The indonesia showed a more resonable water sauration than for the Waxman Smith and the capillary pressure was ajusted to match this curve. The final water saturation is always given by the capillary pressure. It represents the reservoir at reservoir conditions, it takes into account the interaction between oil and water, flow through the rock with respect to pore geometry. In Table 11 all of the equation and input values for calculation of water saturation based on capillary pressure are listed.

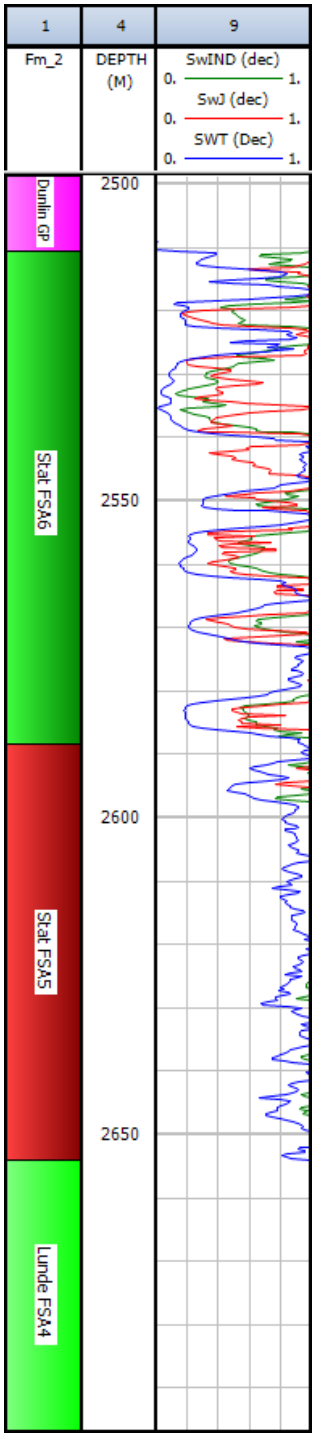

Figure 35: Results from water saturation using the Indonesia method (SwIND), Waxman Smith method (SWT) and capillary pressure (SwJ)

There are some core data that does not give very representative information, example well 34/7-3 sample 376.1 (k=0.79, ϕ=0.23), see Appendix A. Due to the permeability is so low and the high S_{wi} the curve is hard to fit anything, however it still gives the information that the reservoir below 1mD will produce poorly, eventhough the porosity is above 20%. The curves above 100mD tends to show similarity between well and formation, but below 100mD or 10mD the curves are very different and follows no certain pattern. See appendix A for all capillary pressure curves and tables.

The results is used to evaluate the rest of the wells in the Snorre field. The normalized capillary pressure curves above 100mD and 10 mD do not vary significantly, however for below 100mD/10mD the curves are very different. For example FSA3 below 100 and 10 mD the curves are very different, most likely the value for well 34/7-3 which only has one sample is not representable to use on other wells. Further there are no capillary pressure for FSA1, so the curves from FSA2 will be used since FSA1 and FSA2 are partly similar and have many common properties.

Table 11: Results of water saturation from capillary pressure method

Well	Fluvial Assemblage	K	Δρ [kg/m3]	σcosθ [10^5]	SwN	Swirr vs k	FWL [m]
34/7-9	FSA2	k<100mD	289	2000	4,791(J+1,94)**-2.26	-0.1491*log(K) + 0.5241	2601
		k>100mD	289	2000	0,171J**-0,9573	''	''
	FSA3	k<100mD	289		2,03(J+1,42)**-1,72	''	''
		k>100mD	289		0,175(J+0,0644)**-1,20	''	''
34/7-6	FSA4		289		0.405 (J+0.539)**-1.31	-0.3191*log(K) + 0.7444	2612
34/7-3	STAT	k<100mD	289	300	23,2(J+2,37)**-3,59	-0.1890* log(K) + 0.7395	2606
		k>100mD	289	300	0,174(J+0,376)**-1,83	''	''
	FSA3	k<10mD	289		9280(J+8,07)**-4,33	''	''
		k>10mD	289		0,117(J+0,225)**-1,5	''	''

The capillary pressure curves can directly indicate if the sample from the reservoir shows good reservoir flow properties. In Figure 36 there is marked between poor, moderate and good reservoir properties. The reservoir quality increases with increasing permeabilities together with decreasing irreducible water saturation.

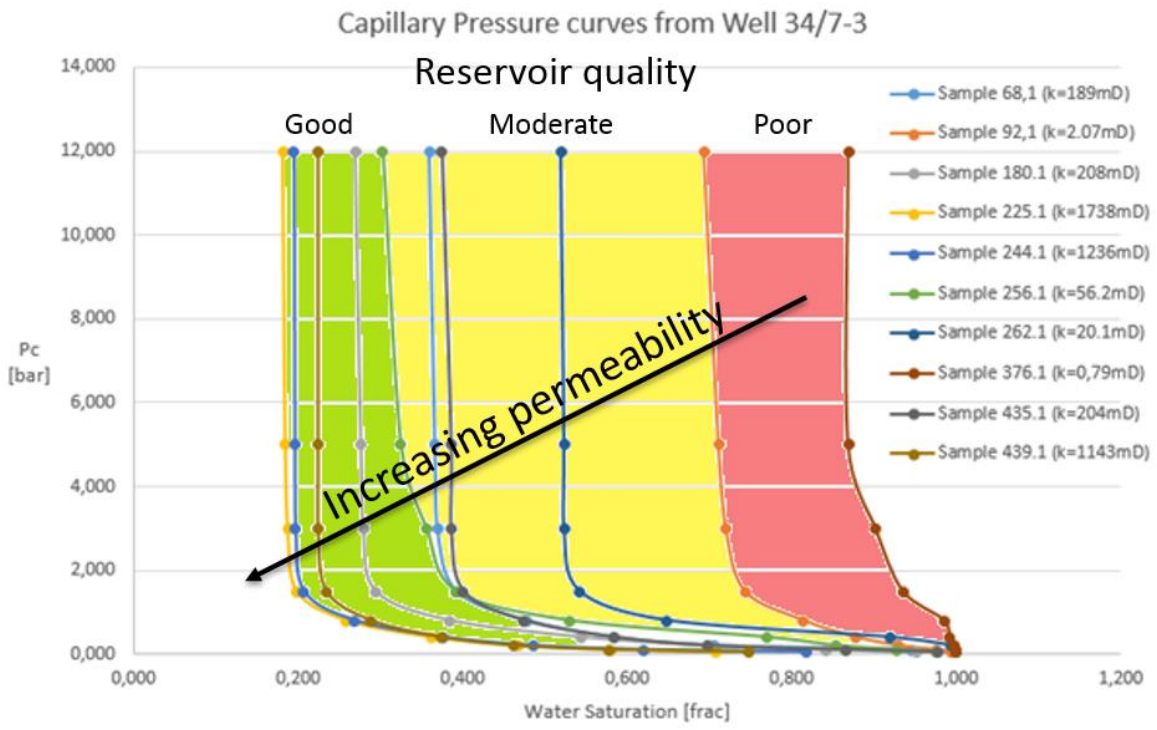

Figure 36: Capillary pressure related to reservoir quality and permeability

4.5 Grain size distribution from SCAL report

A total of 4 samples were cut to the length of 1 inch (2.54cm) and tested for grain size distribution, all in the Statfjord formation in well 34/7-3

1. 2417.10m
2. 2418.10m
3. 2418.95m
4. 2562.90m

The three first samples show that the reservoir are heterogeneous and changes over very short distances. Sample 1 and 3 looks similar, the log show some separation between the neutron and density and the majority of grains are coarse to very coarse. Sample 2 lies in the middle of sample 1 and 3 show almost no separation in the neutron/density log and have more fines grains than the two others, but still there is no silt content. Sample 2 have a better sorting than the other samples, around medium to fine. This may indicate that there was a calmer period during the sample 2 with less current in the river, and less energy to transport big particles down the river. There is also the same behaviour above and below the separation indicating cyclises of coarse sand and fine sand, related seasonal

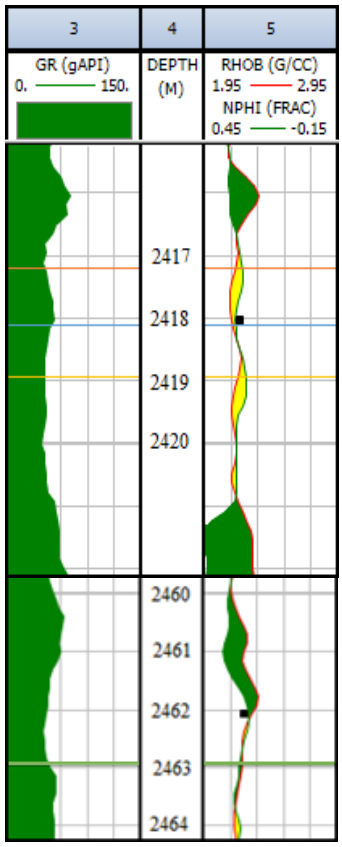

Figure 37: Location of samples from IP with gamma ray and neutron/density log

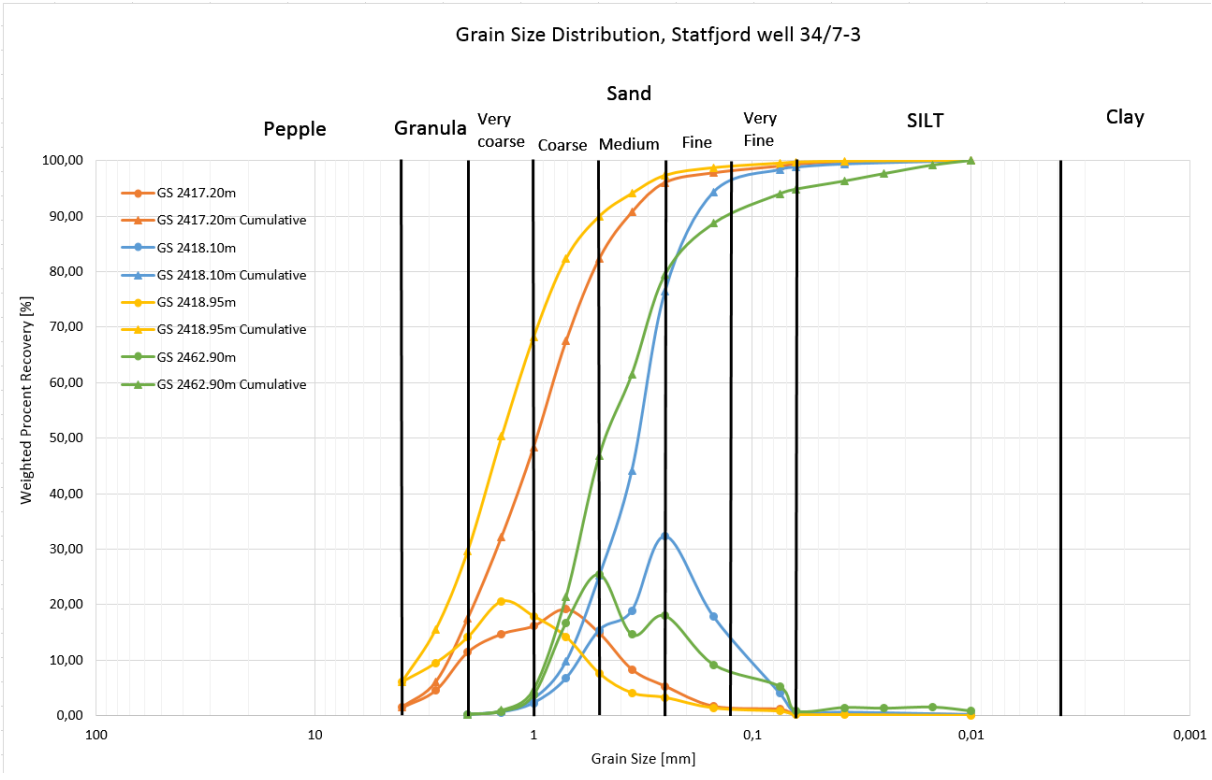

Figure 38: Grain size distribution from the Statfjord formation well 34/7-3 containing 4 samples

deposition. Another sample, about 150m deeper, from sandstone with negative separation between the neutron/density show silt content from the grain size distribution (Figure 38, Green curve). This sample has the majority of grain from medium to fine grains and around 5% silt content. Silt content in the sandstone it not good for the reservoir properties, it binds more water and increase S_{wirr}, reduces porosity/permeability. This example from the log and the grain size distribution is used to evaluate if there are silt content in the reservoir. The more negative separation in density/neutron and still having reasonable low GR, indicates higher silt content. Similar of the separation is becoming more positive (yellow) the sandstone is becoming more clean and coarse grained.

4.6 Mudlog

By comparing the fluvial assemblages in multi well cross sections, trends in the density/neutron logs identifies how the wells are differentiating by their content of mud, silt and sand. In Figure 38 the high content of silt is characterized by large negative separation in the neutron/density and are not good for reservoir properties. The following pages present the fluvial assemblages side by side with gamma ray and neutron/density for vertical and horizontal correlation. The silt content varies greatly through the reservoir and correlation between wells can be very difficult. The vertical correlation seems to be more apprehensible. A fluvial succession with clean sandstone is often followed by clean sandstone for a certain interval before it gradually becomes more silthy. All the assemblages show very heterogeneity and changes significantly from well to well. The silthy sandstones are deposited in streams where the current is slow enough such that the smaller particle is deposited. Good sandstones is deposited in a channel where all the small particles are carried on by the stream and coarse sand particle can be posited.

Figure 40-45 illustrates all the fluvial assemblages in a cross section view. The formation are interpreted as wide alluvial plains and to assume that the depositional system changes over distance is assumed, and can explain how neighbour wells are representing completely different results from the logs. For instance FSA1 in Figure 40; Even though the wells are only 1 km apart (short compared to others) the content of silt in 34/4-4 is significantly higher than in 34/4-7 which has many very good sandbodies.

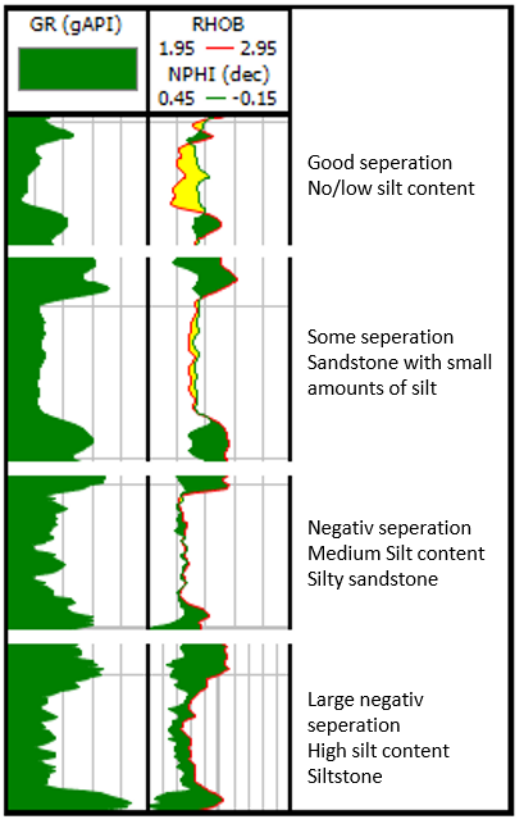

Figure 39: Generalization of silt content in the reservoir related to neutron/density and gamma ray

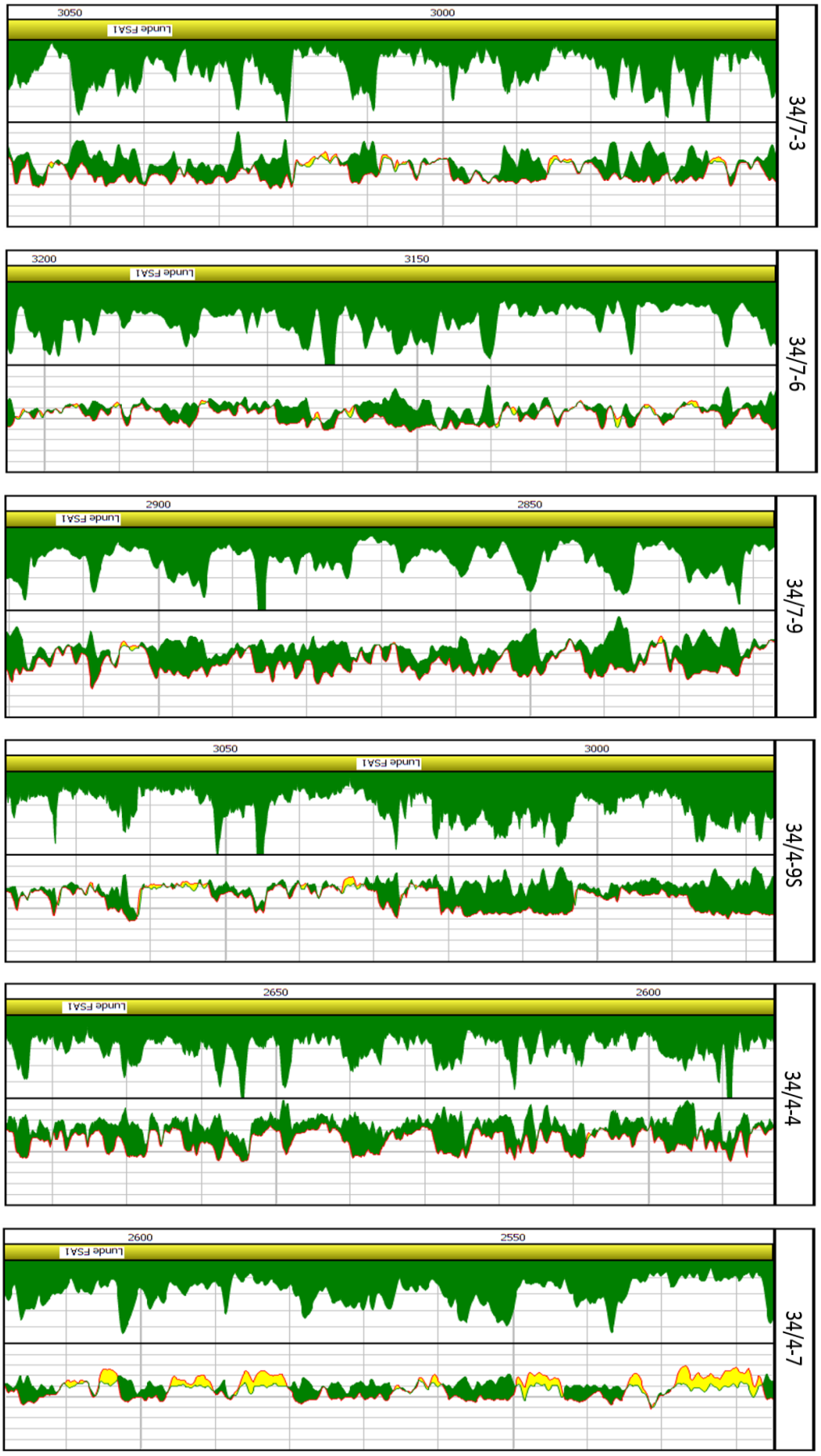

Figure 40: FSA1 mudlogs from wells: 34/7-3, 34/7-6, 34/7-9, 34/4-9S 34/4-4 and 34/4-7

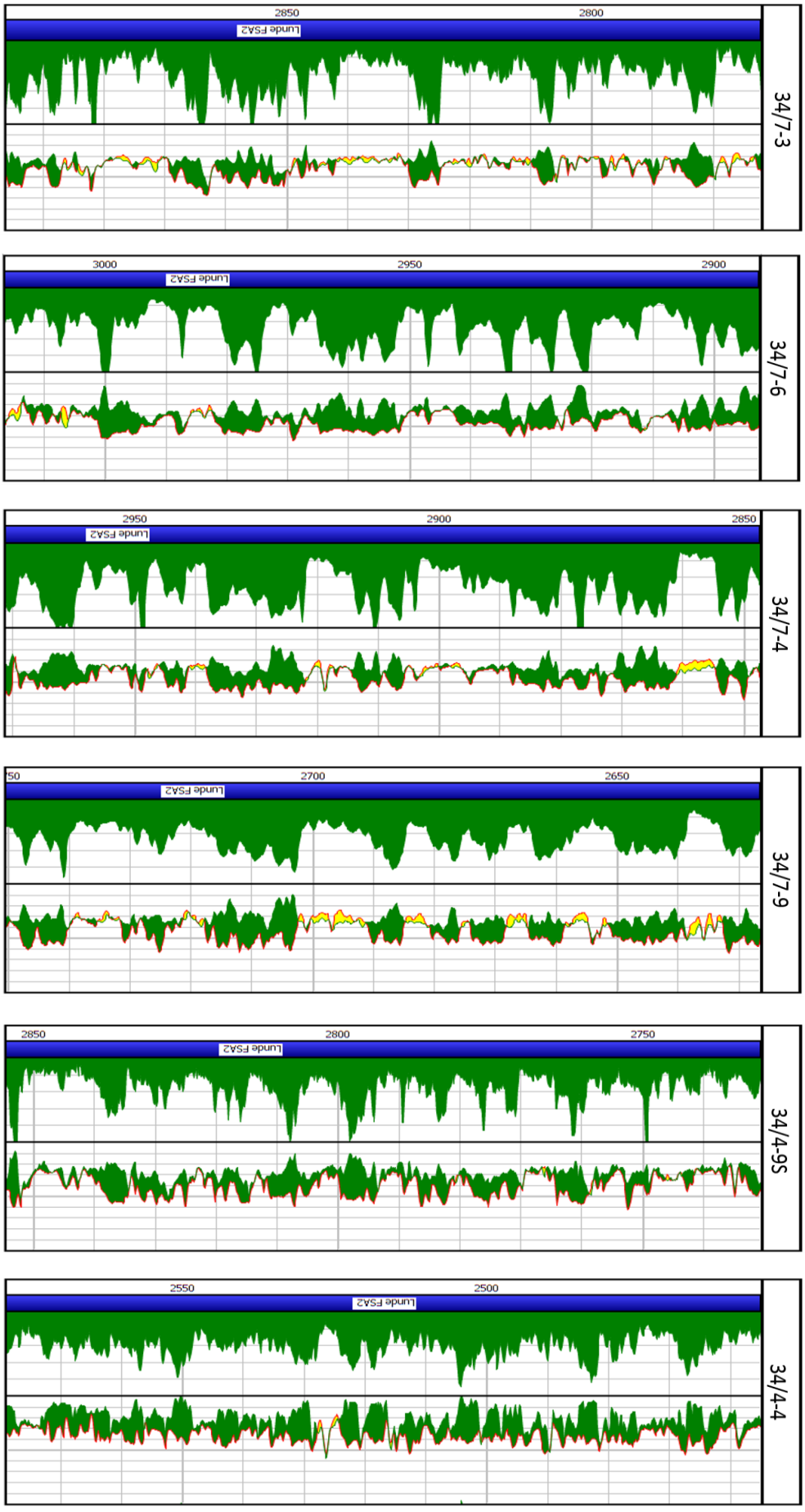

Figure 41: FSA2 mudlogs from wells: 34/7-3, 34/7-6, 34/7-9, 34/4-9S, 34/4-4 and 34/4-7

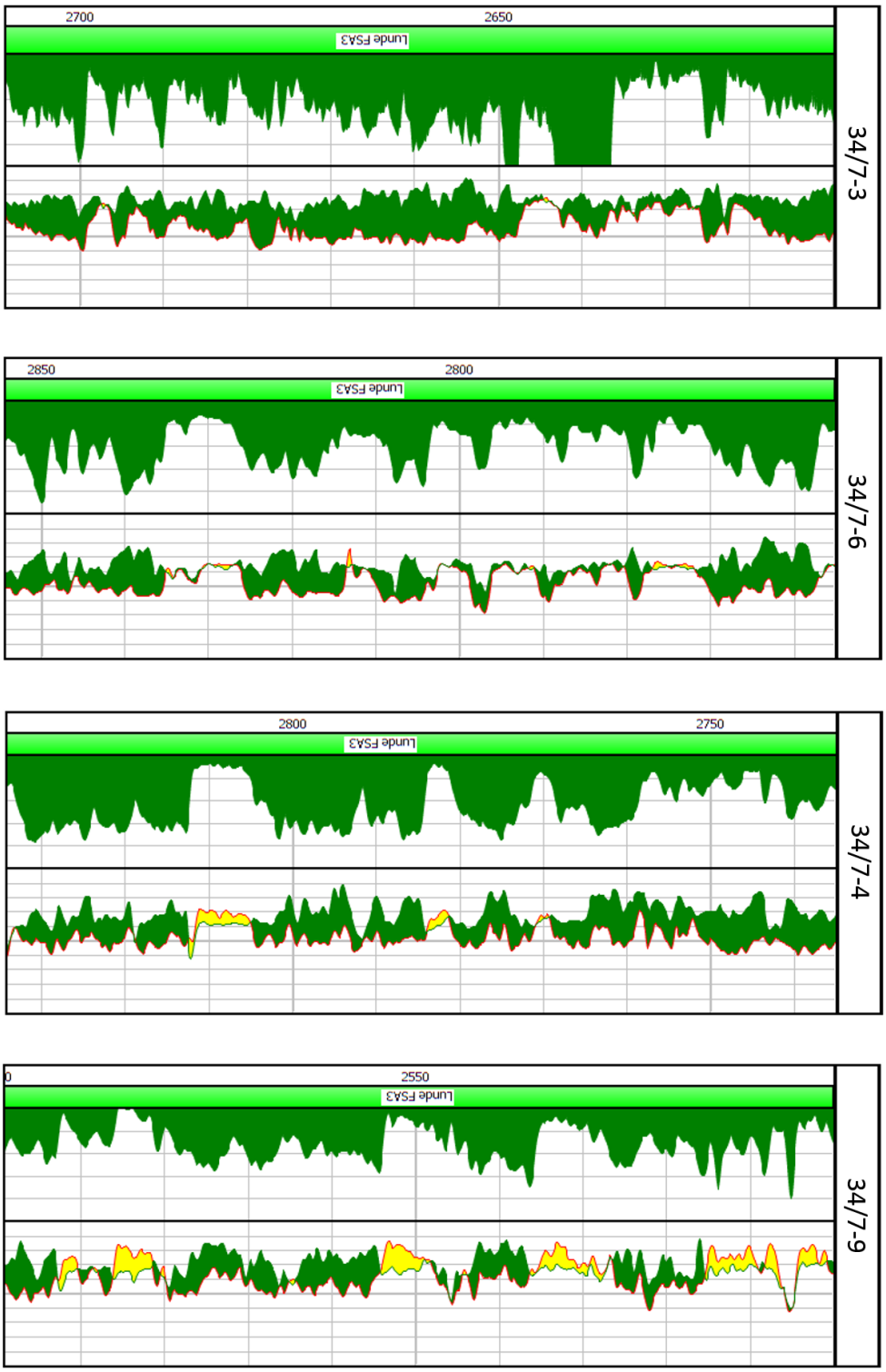

Figure 42: FSA3 mudlogs from wells: 34/7-3, 34/7-6, 34/7-4 and 34/7-9

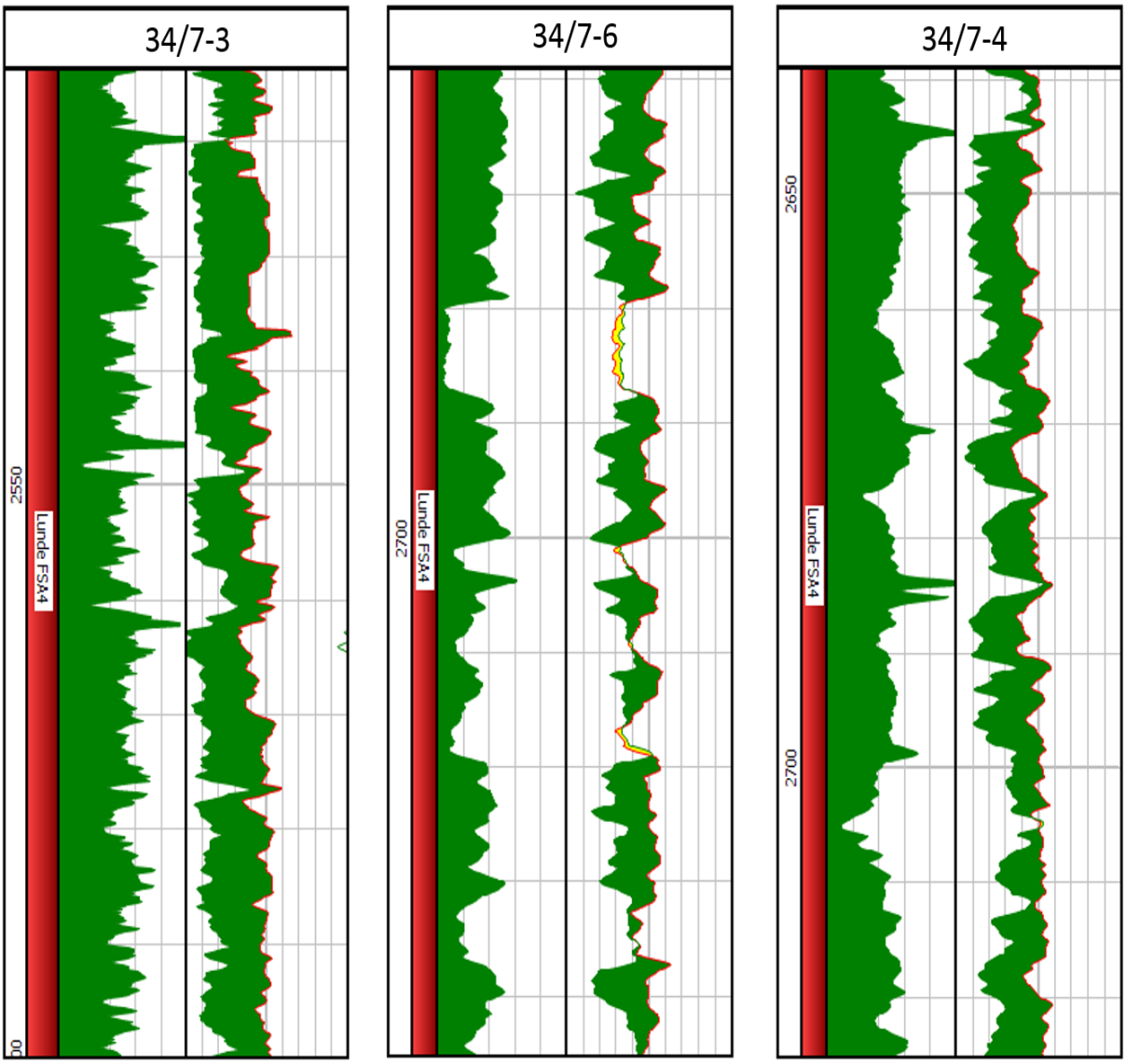

Figure 43: FSA4 mudlogs from wells: 34/7-3, 34/7-6 and 34/7-4

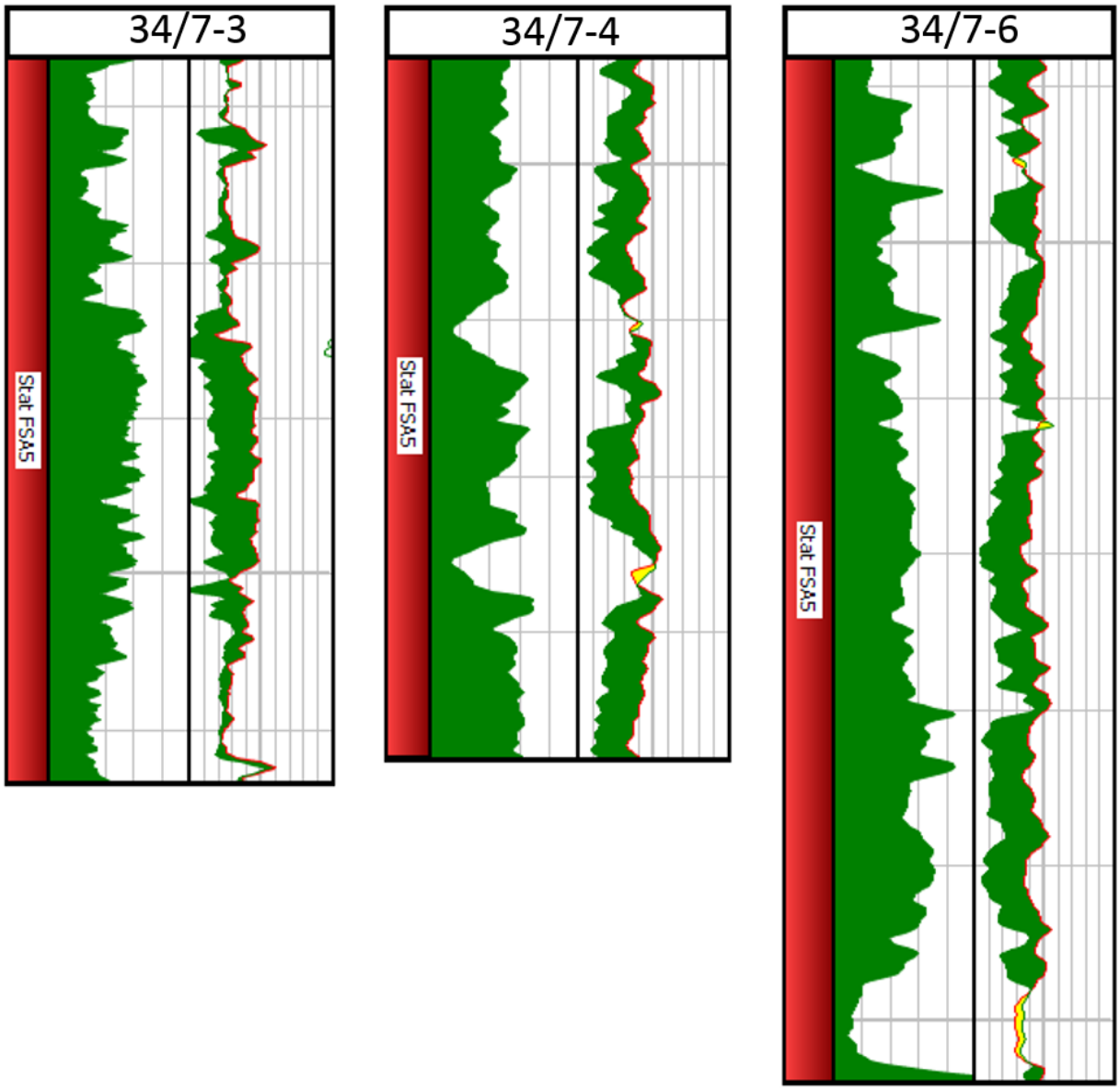

Figure 44: FSA5 mudlogs from wells: 34/7-3, 34/7-6 and 34/7-4

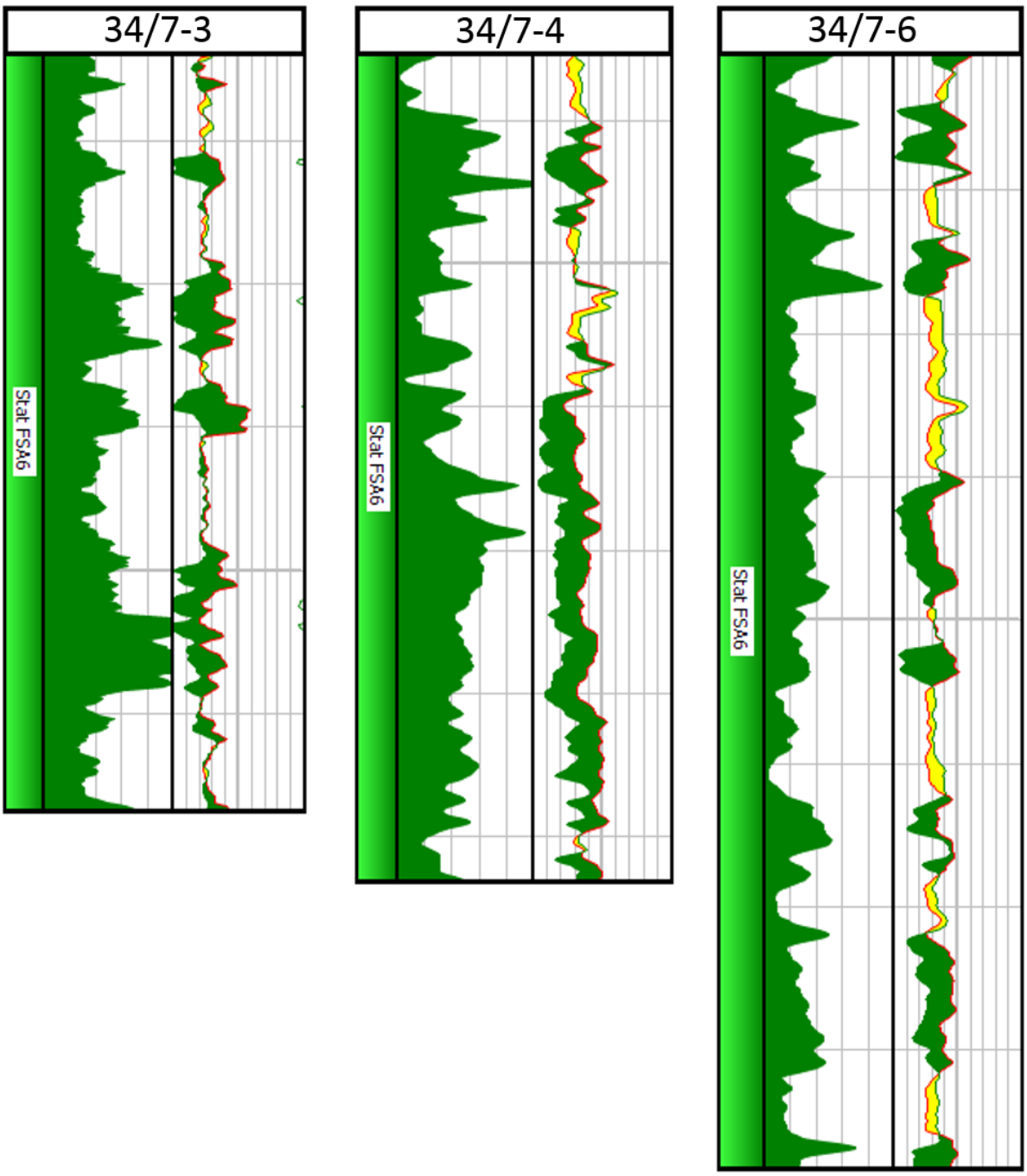

Figure 45: FSA6 mudlogs from wells: 34/7-3, 34/7-6 and 34/7-4

4.7 Reservoir properties

After the porosity, permeability and water saturation is complete the reservoir properties can be summarized and the net to gross (N/G) can be calculated based on a certain cut-off values. The cut-off values can vary from field to field, and a standard for the North Sea is $V_{cl} > 0.4$ and $K > 0.05$. In this evaluation the permeability cut-off is set to $V_{cl} > 0.4$ and $K > 0.1$. The N/G is simply the fraction the values in each reservoir unit that not satisfies the given cut-off value. On the next page is a field correlation with cross-section of 6 wells and their key reservoir properties. Entire reservoir results can be found in appendix C. The lower part of Lunde has an N/G of around 0.60 and decreasing into the middle of Lunde (FSA2) and reaches the lowest value in upper Lunde (FSA4). This unit consists of an N/G constant of below 0.10 all except for one well. Lower Statfjord has N/G from 0.25-0.50 compared to the upper that has the best N/G normally over 0.60 except for one well.

The reservoir properties such as porosity and permeability vary from greatly with the different fluvial assemblages and with depth and any correlation between wells is very hard. The average of the permeability is calculated geometric because of the reservoir has a fluvial depositional system. An arithmetic method are more appropriate in more homogeneous systems and would overestimate the permeability in this reservoir. The lower and middle Lunde, FSA1-FSA2, and showing similar permeability's just below 100 mD, compared to the upper Lunde, FSA3–FSA4, that has value from 0.1 and up to 50 at the highest. Statfjord has clearly the best permeability and ranges from below 100 and up to 400mD in the best well. The lower Statfjord has value from 2 to 70 mD.

Porosity varies from 0.18 to 0.28 in most of the fluvial assemblages. The whole Lunde formation has an average around 0.22, except for FSA4 that has constant below 0.20. The FSA3 show some exceptional high porosity in two of the wells, 34/7-9 and 34/4-9S with 0.25 and 0.26. Reason for this can be repeated successions of well sorted and coarse sandstone bodies. Upper Statfjord, FSA6, has average from 0.22 to 0.26 compared to the lower Statfjord, FSA5, which has an average from 0.18 to 0.23. The reservoir properties are varying through the whole reservoir and are closely related to the depositional system. The braided depositional system has far better reservoir properties than the meander on every point. However, in some wells meander stream can have some exceptionally good sandstone intervals.

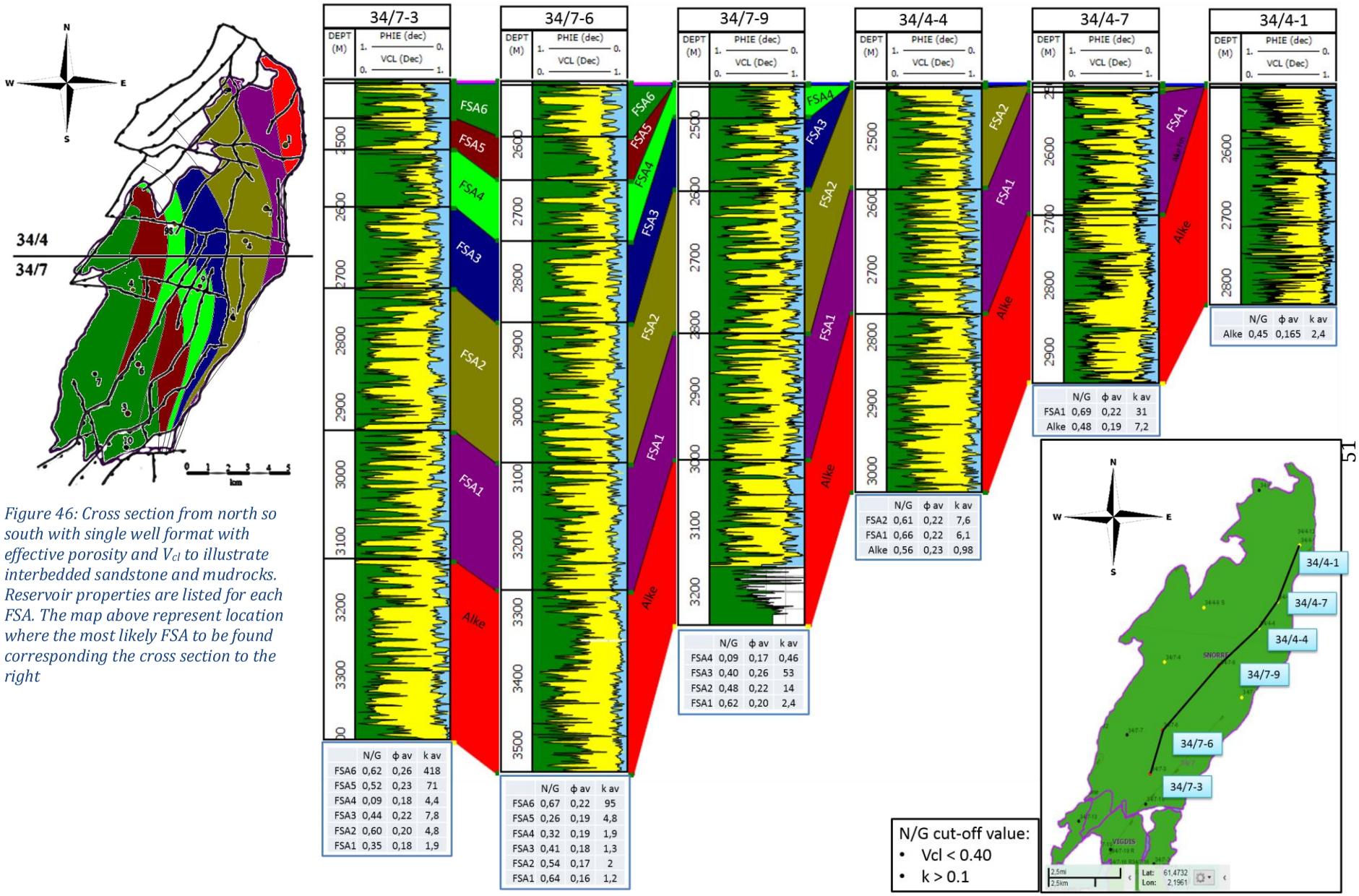

	N/G	ϕ av	k av
FSA6	0,62	0,26	418
FSA5	0,52	0,23	71
FSA4	0,09	0,18	4,4
FSA3	0,44	0,22	7,8
FSA2	0,60	0,20	4,8
FSA1	0,35	0,18	1,9

	N/G	ϕ av	k av
FSA6	0,67	0,22	95
FSA5	0,26	0,19	4,8
FSA4	0,32	0,19	1,9
FSA3	0,41	0,18	1,3
FSA2	0,54	0,17	2
FSA1	0,64	0,16	1,2

	N/G	ϕ av	k av
FSA4	0,09	0,17	0,46
FSA3	0,40	0,26	53
FSA2	0,48	0,22	14
FSA1	0,62	0,20	2,4

	N/G	ϕ av	k av
FSA2	0,61	0,22	7,6
FSA1	0,66	0,22	6,1
Alke	0,56	0,23	0,98

	N/G	ϕ av	k av
FSA1	0,69	0,22	31
Alke	0,48	0,19	7,2

	N/G	ϕ av	k av
Alke	0,45	0,165	2,4

Figure 46: Cross section from north so south with single well format with effective porosity and V_{cl} to illustrate interbedded sandstone and mudrocks. Reservoir properties are listed for each FSA. The map above represent location where the most likely FSA to be found corresponding the cross section to the right

4.8 CPI plots key wells

The CPI plot for the three key wells are listed in the following pages, the rest can be found in appendix B.

4.8.1 Well 34/7-3

Well 34/7-3 is located in the south and has a very long oil column of almost 200m, however the oil column does include mudstone dominated FSA4 that rarely has any good sandstone bodies, see Figure 47. This is the well that shows the best reservoir properties, and has porosity from cores reaching value of 28 to 30% in the good zones and the average of 26%. The geometric average permeability is 418 mD and decreasing down through the FSA5. The water saturation is decreasing through FSA5 as the reservoir properties are decreasing and in FSA4 the water saturation is practically 1. The separation between neutron/density is indicating an increase in silt content down from FSA6.

4.8.2 Well 34/7-6

This well looks similar to the well 34/7-3, but the top of Statfjord almost 100m deeper reducing the oil column by 100m, Figure 48. The porosity has an average of 22% and the average permeability around 100mD from the geometric average. The permeability is decreasing down the well as well as the water saturation. The sandstone bodies' show good separation between the neutron/density log indicating a clean sandstone and low content of silt. FSA5 has a low N/G and has only one good sandstone zone.

4.8.3 Well 34/7-9

In this well the Statfjord GP is eroded and a small part of the Lunde formation. The reservoir is completely from FSA3 and the porosity has an average of 26% reaches value up to 30% in the best zone. Opposite of the two previous wells, the permeability increases instead of decreasing downward. The sandstone in this FSA indicates a very good and clean sandstone with very low or no silt content and the water saturation is high throughout the column.

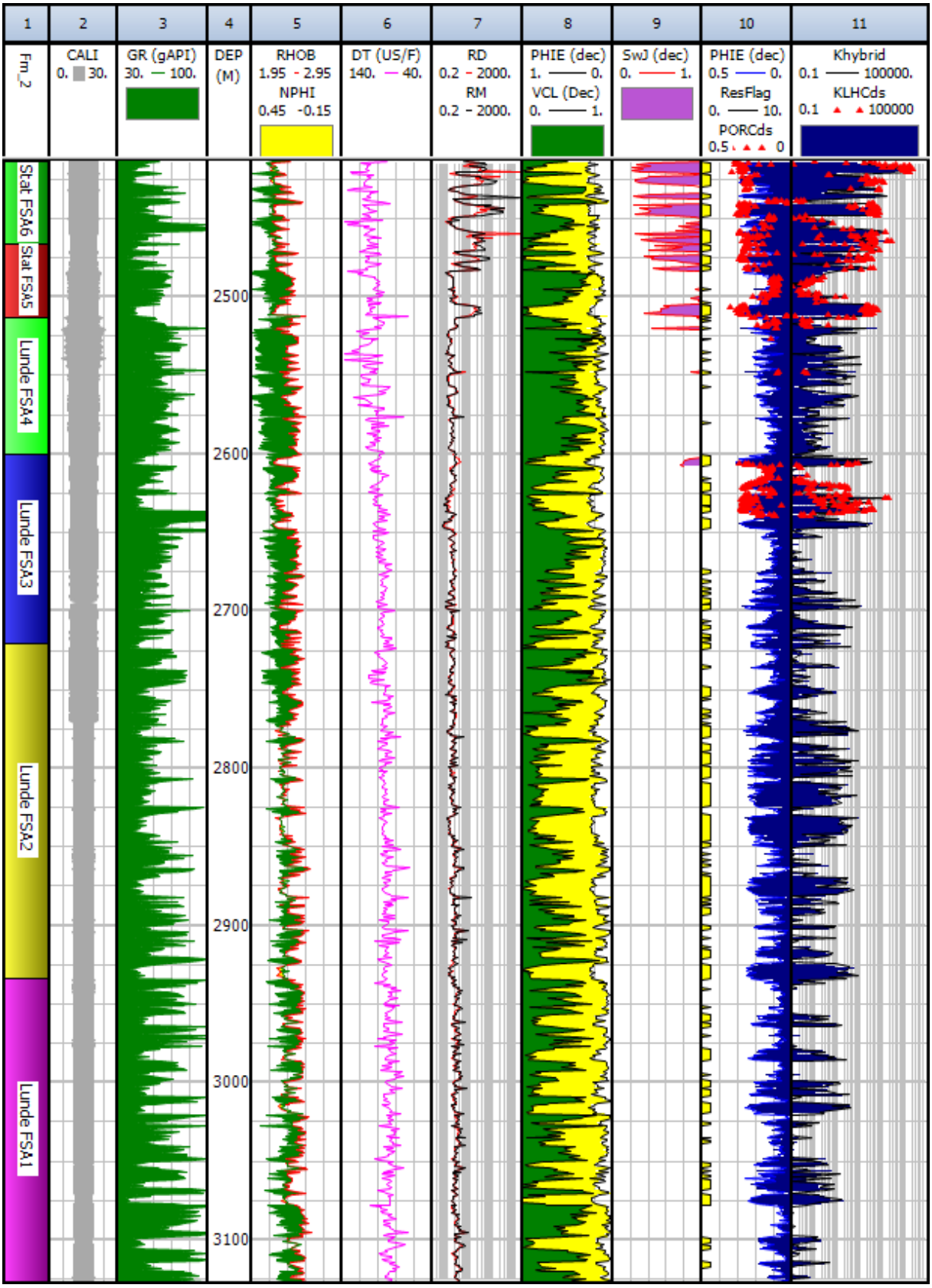

Figure 47: CPI plot well 34/7-3

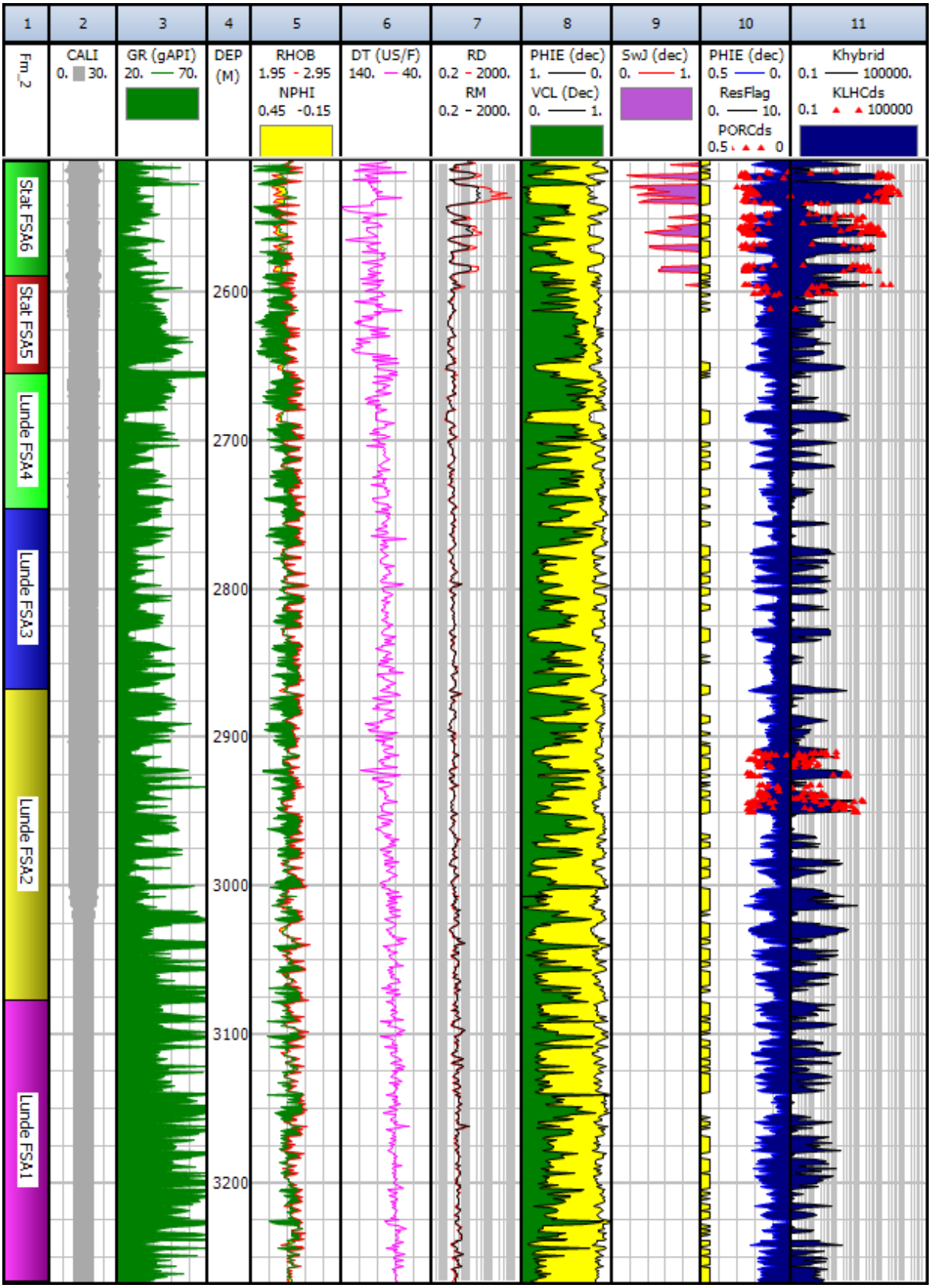

Figure 48: CPI plot well 34/7-6

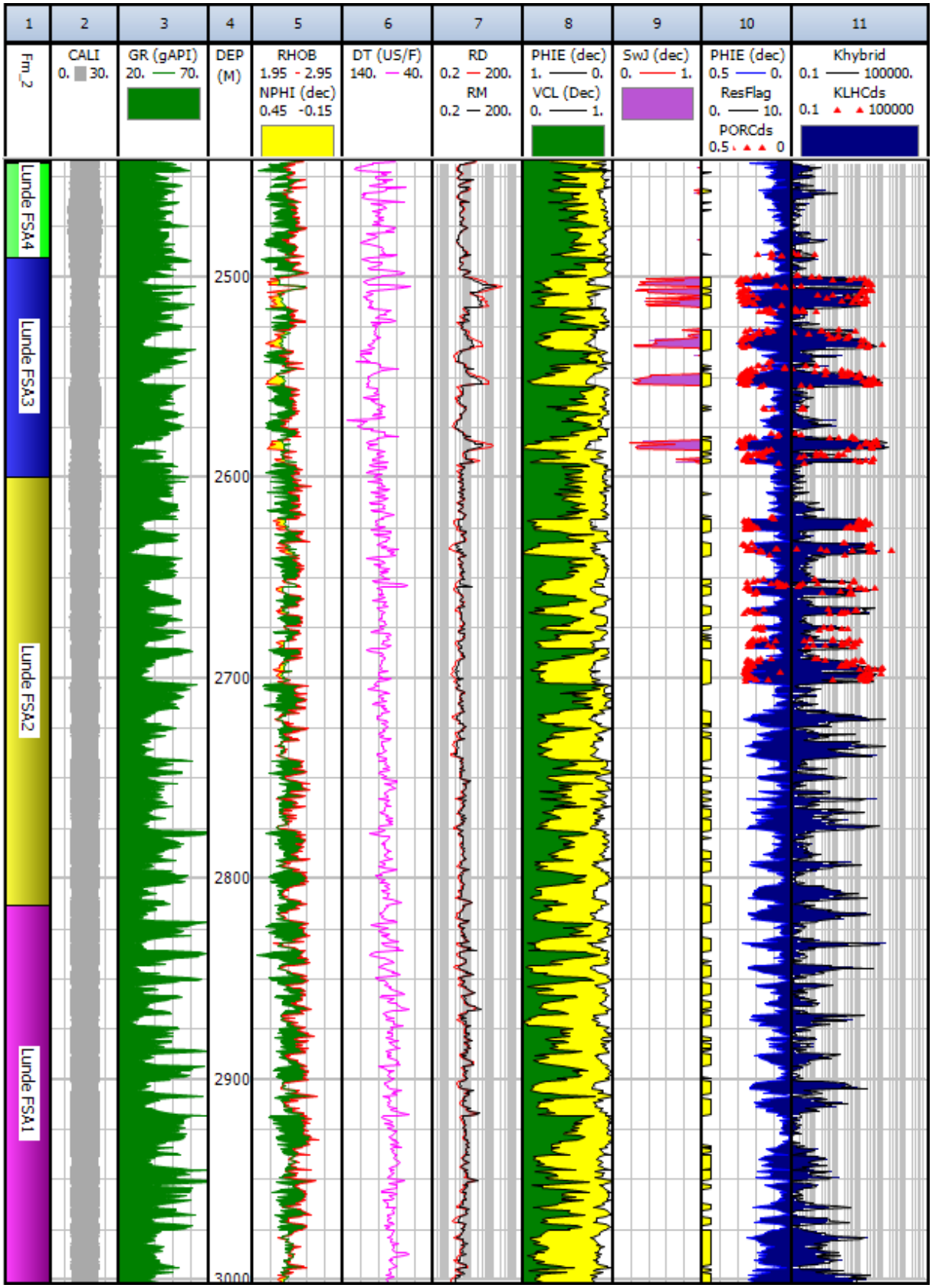

Figure 49: CPI plot well 34/7-9

5 Testing

5.1 Formation Pressure Evaluation

The formation pressure is tested with a Repeat Formation Tester (RFT) with a crystal gauge or with a strain gauge. The crystal gauge gives far better measurement and is preferred over the strain gauge. The oil and water have different densities and will therefore have different pressure gradients through the reservoir. The point where these gradients meet is called the oil water contact (OWC). The oil water contact varies from well to well and seems to be more elevated in the north, except for well 34/4-1. The reason for this can be non-communication in the faults or that migration of oil has come from the south filling up the southern part of the reservoir more than the north. This has to be evaluated with the fluid analysis to get a better understanding of why the OWC varies over 30m between the wells. The oil gradient changes from the south to the north indicating a change in composition of the fluid; it seems that the oil is becoming lighter in the north. More on this under the fluid analysis.

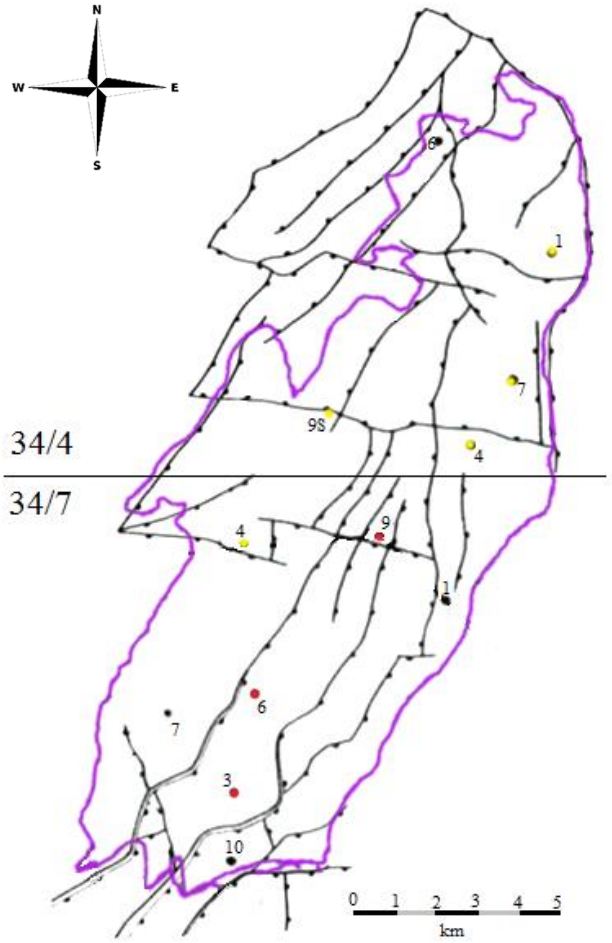

Figure 50: The Snorre field today (purple) and old fault map (black) from the original interpretation [8]

*Table 12: Results from RFT dat. * are only estimated OWC from NPD.*

Well	OWC [m]	Oil Gradient [bar/m]	Water Gradient [bar/m]	Method
34/7-10	2621	0,074	0,099	Crystal gauge
34/7-7	2589	0,071	0,098	Crystal gauge
34/7-3	2606	0,072	0,099	Crystal gauge
34/7-6	2612	0,078	0,101	Crystal gauge
34/7-9	2602	0,070	0,099	Stain gauge
34/7-1	2586	0,068	0,099	Both
34/4-4	2583	0,068	0,094	Unknown
34/4-7	2589	0,068	0,104	Crystal gauge
34/4-1	2618*			
34/4-6	2587	0,064	0,09900	Both

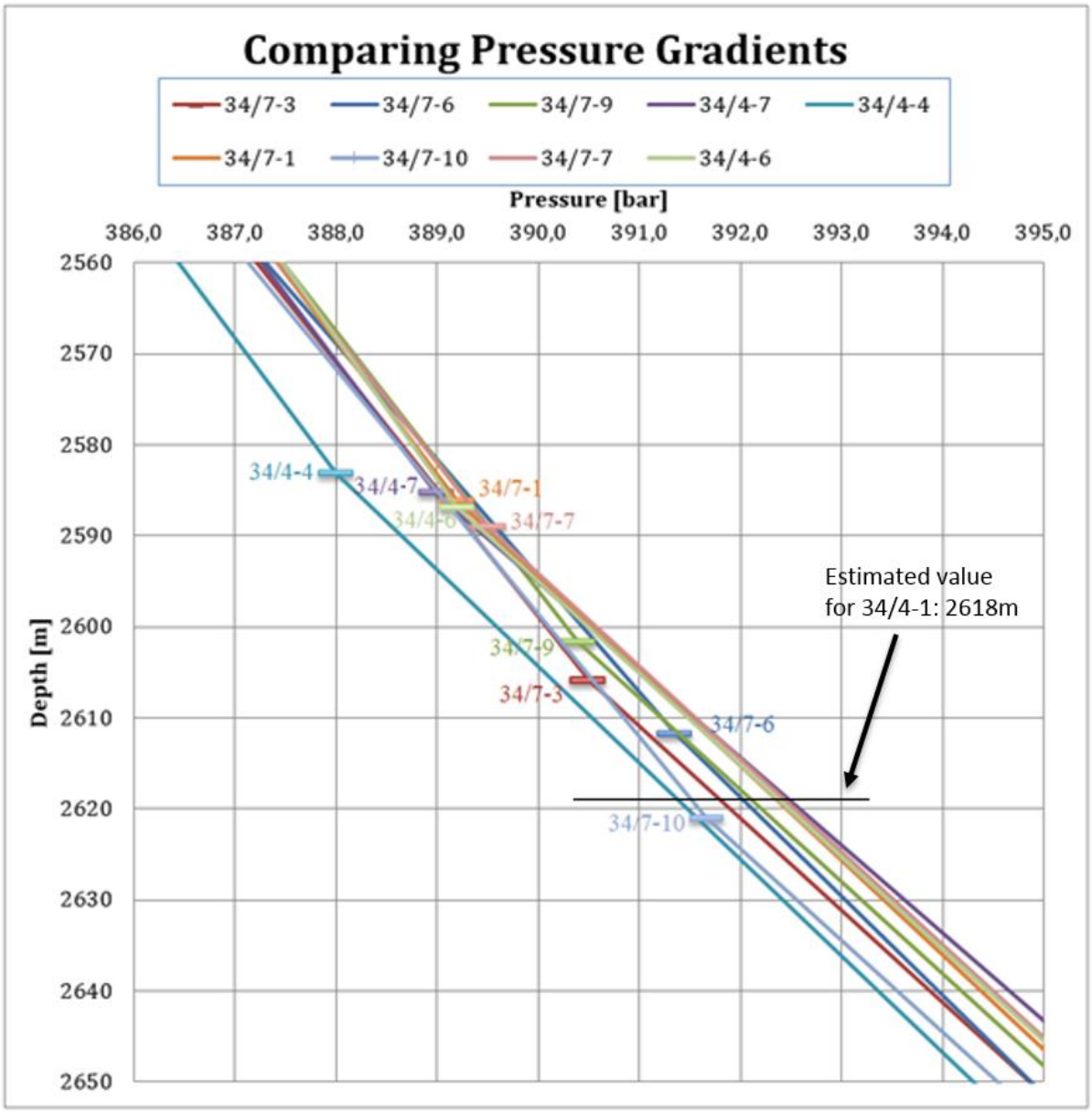

Figure 51: Pressure gradient for oil/water and the OWC

The pressure data can also be of help to evaluate barrier/segmentation in the reservoir, if the different zones are communication through a fault the OWC should be approximately the same. Figure 49 has the faults and the boundary of the Snorre field, shows how the faults are cutting through the reservoir. Faults dipping to the west represent the faults created during the Permian-Triassic rifting and the faults dipping to the east the late Jurassic rifting. From the pressure gradients the three key wells; 34/7-3, 34/7-6 and 34/7-9, seems to be in communication and the OWC doesn't differ that much but the oil gradient is a bit higher for well 34/7-6. This well was tested with strain gauge and result might not be accurate.
The OWC from well 34/7-7 and well 34/7-10, respectively 2589 and 2621 differs from well 34/7-6 and well 34/7-3 over reasonable short distances indicating that the two south-east

dipping fault might be sealing. Also in the middle of the field the OWC varies from18 and 21m from 34/7-9 compared to well 34/7-1 and 34/4-4. The faults around 34/7-9 are complex and there might be more than 1 fault causes different OWC.

In the east of the field, well 34/7-1, 34/4-4 and 34/4-7, the OWC remains the same, +/- 3m, and the oil gradient are exactly the same. However, the pressure in 34/4-4 seems to be lower than in the other two wells. There are no present faults between well 34/7-1 and 34/4-4 and communicating through the fault between 34/4-1 seems to be a reasonable assumption. It may also be old data that are not accurate that are causing this pressure difference. In the north of the field, well 34/4-1 has a OWC that is far lower than the surrounding wells, about 30m, indicating that there might be some barriers present surrounding this well or that the OWC is estimated wrong. One other explanation for the different OWC can be active fluid migration. If the fluid (oil) migrating into the reservoir, example in well 34/4-1, this might show a lower OWC and still have communication through the faults.

To evaluate pressure data and determine OWC in these types of reservoir is sometimes inconclusive or the found OWC can be wrong in sometimes. For an example in well 34/7-10 the oil water contact from the water and oil gradient crossed at 2600, however DST had tested the formation for oil down to 2615. So between the oil gradient and the water gradient there must be a vertical barrier causing the pressure to be slightly higher further down in the water zone.

5.2 Drill-stem tests (DST)

The main purpose of a DST is to test the reservoir properties, estimate reservoir pressure, and detect boundaries/heterogeneity in the reservoir and more depending on the reservoir. Back in the 80's conducting a DST was normal and was applied in each of the exploration wells. The pressure and rate data are imported into the program Saphire for evaluation.

5.2.1 Well 34/7-3

DST1

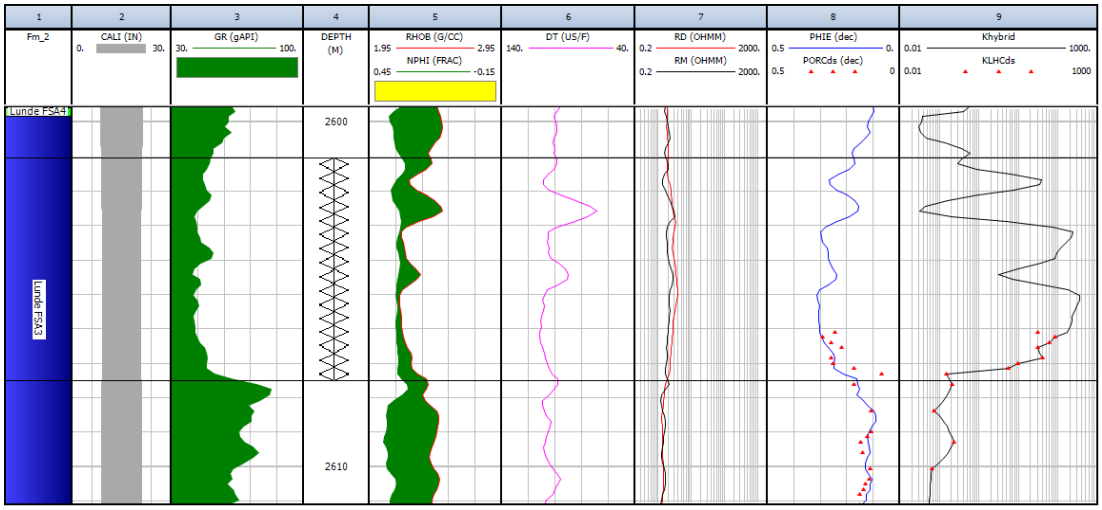

Figure 52: Log values and properties from the perforated zone in DST1 well 34/7-3 FSA3

The perforated section is 2601 – 2607.5m RBK and is part of FSA3. The well produced for 13 minutes and shut inn, followed by the main draw down and the main build up. The main draw down was open for six hours before the well was shut in for 40 minutes due to problems with the choke manifold. It reopened and flowed for 12.5 hours before the main build up.

The input data is listed in Table 13. The average porosity is taken from IP and the oil viscosity and compressibility is given as a standard value. The rest of the input is taken from the completion report from NPD. The model used for this DST is a standard model, constant wellbore storage, homogeneous reservoir and parallel faults as the boundary. In order to calculate the permeability from the zone a radial flow period is necessary. In the pressure data the effect of a nearby boundary is causing the pressure gradient to increase very fast and the radial flow may not be reached. Therefore the result from this test must be seen in context with other data, see summary of results.

Input data:		
Well radius	0.354	ft
Pay zone	21.3255	ft
Porosity	0.23	
Bo	1,23	Sm3/Sm3
μ	0.5	cP
Ct	5.0E-5	psi-1
Main results:		
Well and well bore parameters:		
C	0,00184	bbl/psi
S	0.254	
Reservoir and boundary:		
Pi	5760.28	psia
k.h	2190	md.ft
k	43	md
N - No Flow	117	ft
S - No Flow	125	ft

Table 13: Input data and results from DST1 well 34/7-3 FSA3

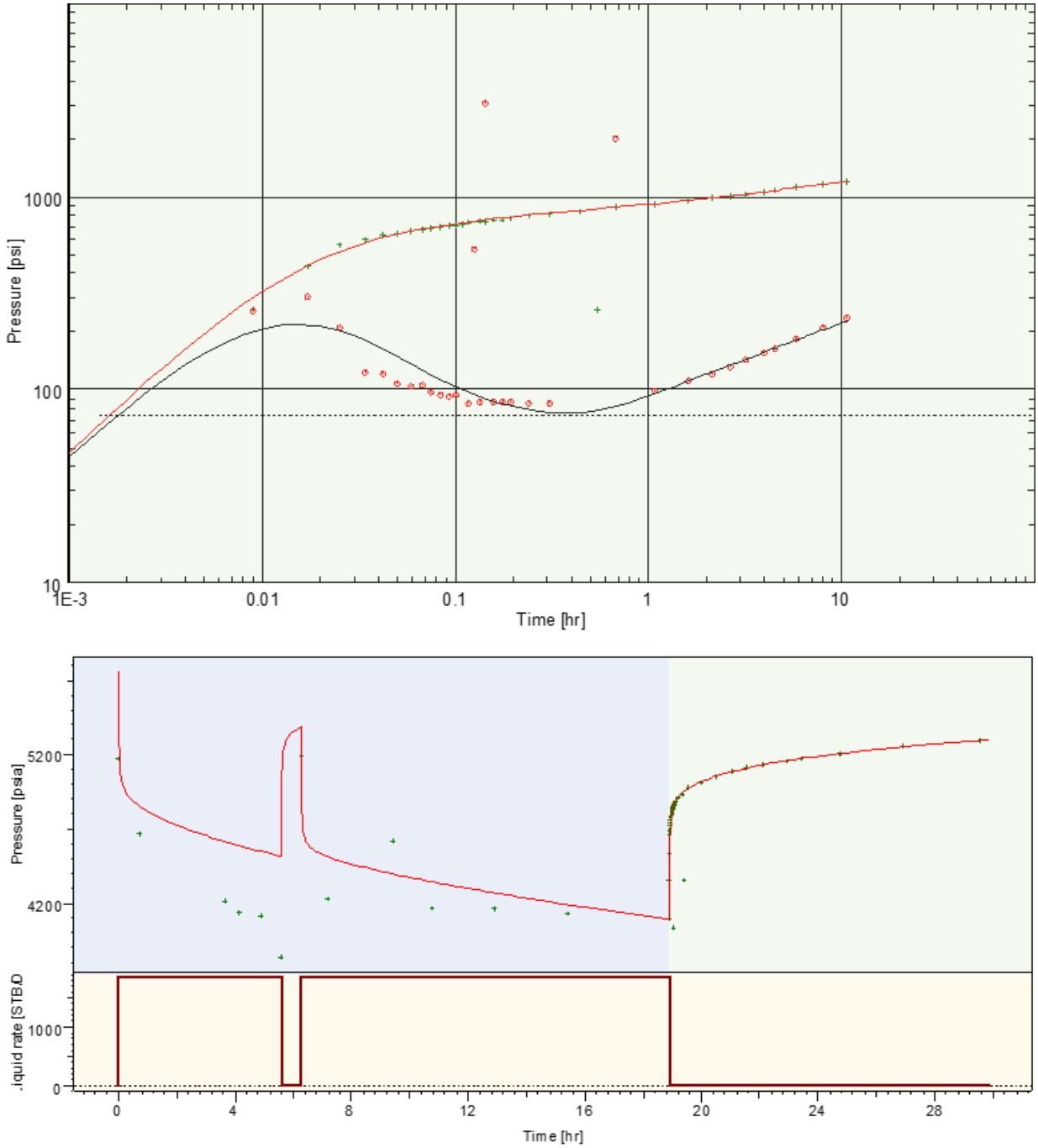

Figure 53: Top: Plots from Saphire DST1 well 34/7-3. Log-log plot of the main build-up period. Bottom: History plot

DST2

This DST is perforated 2505-2513 RKB in the FSA5 over the lowermost in Statfjord GP, Figure 54. After the initial flow period the well was opened for one hour before the well has to close due to excessive heat from the burners. This is the period in Figure 55 where the model doesn't match the history plot. The well was opened again for the main draw down followed by the main build up period.

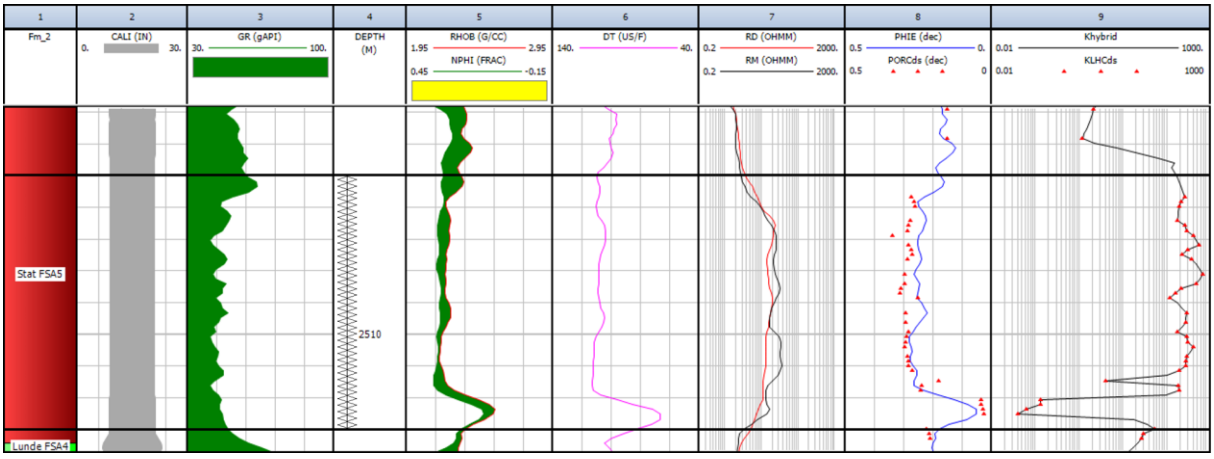

Figure 54: Log values and properties from the perforated zone in DST2 well 34/7-3 FSA5

The input data and results are listed in Table 14. The model that gave the best match for this data set was a radial composite model with N=4. The fault are intersecting creating an angle of 45° degrees (180/N). The well is located 117 and 125 ft from each fault. The model has a good match from the log-log plot of the main build-up. The history plot show a bad match and some problems before the main draw down. This can be related that the rates are not very accurate. However since the draw down is long, about 20 hours, and matches very well the results is expected to be valid. The skin is -1.5 and due to lack of information about the test this value cannot be explained. Normally a skin in such test are normally positive.

Input data:		
Well radius	0.354	ft
Pay zone	26.2467	ft
Porosity	0.23	
Bo	1,23	Sm3/Sm3
μ	0.5	cP
Ct	5.0E-5	psi-1
Main results:		
Well and well bore parameters:		
C	0.005	bbl/psi
S	-1.5	
Reservoir and boundary:		
Pi	5414.66	psia
k.h	5260	md.ft
k	200	md
L1 - No flow	117	ft
L2 - No flow	125	ft
N	4	

Table 14: Input data and results from DST2 well 34/7-3 FSA5

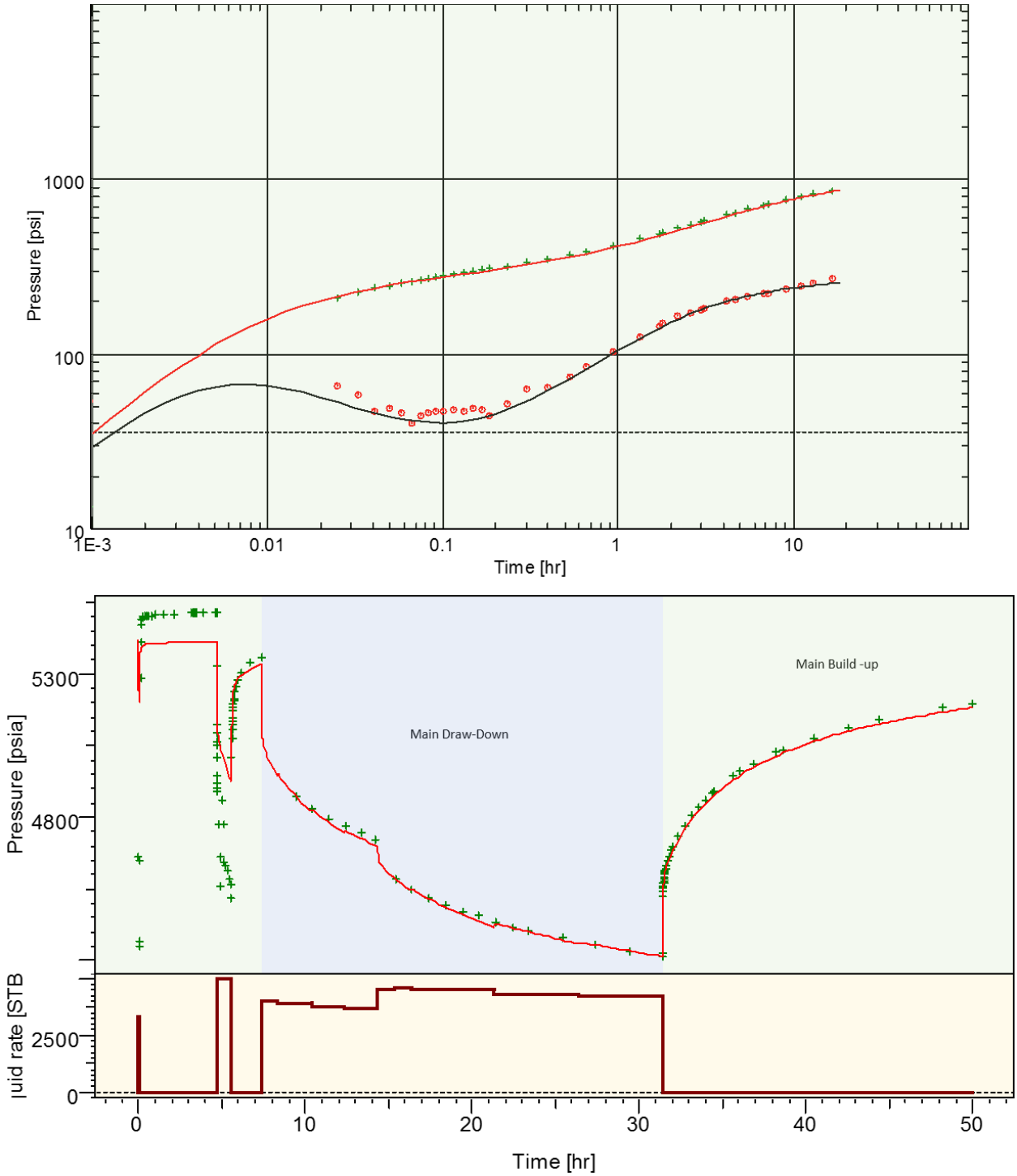

Figure 55: Top: Plots from Saphire DST2 well 34/7-3. Log-log plot of the main build-up period. Bottom: History plot

DST3

This DST was perforated 2440.5-2450 RKB in the upper Statfjord formation FSA6, Figure 56. The main draw down and build up lasted for 20 and 28 hours respectively.

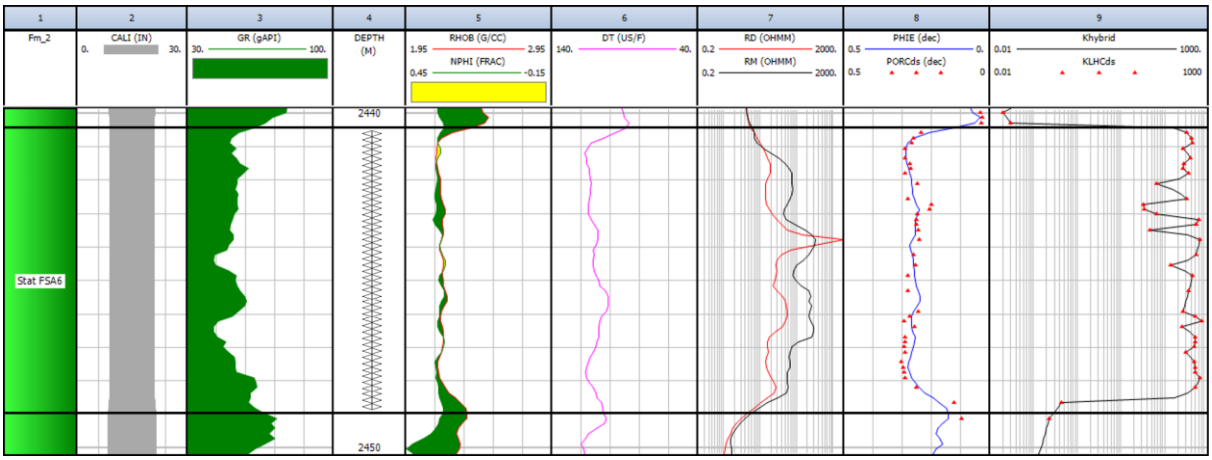

Figure 56: Log values and properties from the perforated zone in DST3 well 34/7-3 FSA6

Input and results are given in Table 15. The results from this model is very uncertain. The model is radial composite with infinite acting on the boundaries which give the best fit. With this model at Ri (radius of investigation) = 700ft the permeability are estimated to quadruple (M and D = 0.25) due to increased pressure drop after 1 hour. This is very uncertain as the data set are not very good, but it is the model that gives the best fit. However intuitively the permeability of this test are clearly much better that FSA5 or FSA3. When the well is closed for production the reservoir pressure are very quickly increased back up the initial pressure, indicating very good flow properties in the perforated zone. So the results are uncertain but not dismissible.

Input data:		
Well radius	0.354	ft
Pay zone	26.57	ft
Porosity	0.26	
Bo	1,23	Sm3/Sm3
μ	0.5	cP
Ct	5.0E-5	psi-1
Main results:		
Well and well bore parameters		
C	0.008	bbl/psi
S	3.65	
Reservoir and boundary:		
Pi	5455	psia
k.h	28100	md.ft
k	1060	md
Ri	700	ft
M	0.25	
D	0.25	

Table 15: Input data and results from DST3 well 34/7-3 FSA6

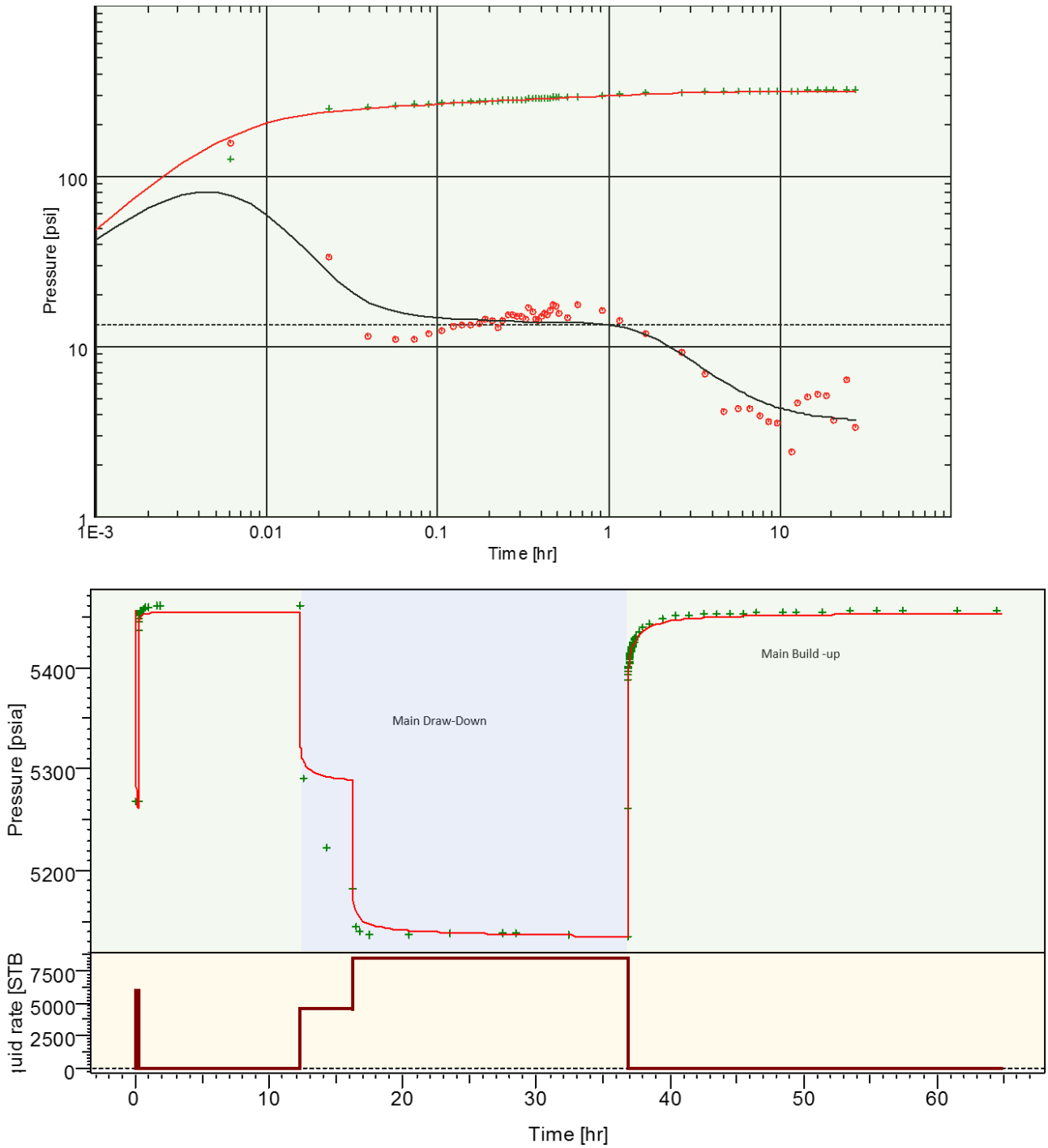

Figure 57: Top: Plots from Saphire DST3 well 34/7-3. Log-log plot of the main build-up period. Bottom: History plot

5.2.2 Well 34/7-9

This Drill Stem test from the Upper Lunde Formation, FSA3, consists of perforations in 4 different sandbodies in the following interval:

- 2501 – 2504 m RKB
- 2506 – 2515 m RKB
- 2527 – 2536 m RKB
- 2550 – 2553 m RKB

The total pay zone is 27.9m according to the NDP completion report.

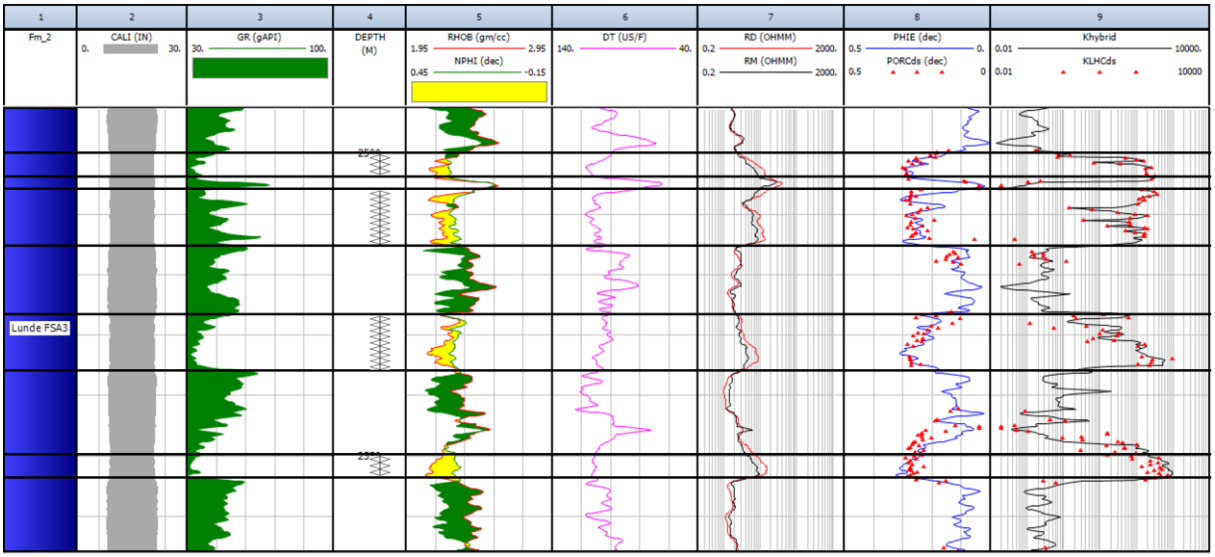

Figure 58: Log values and properties from the perforated zone in DST well 34/7-9

The lowest interval was perforated first, followed by a quick clean up. Reason for this was problems with the equipment and the charges didn't went off. Then the rest of the intervals were perforated followed by a clean-up flow and a pre-test flow and shut in. The main flow period lasted for 142.4 hours interrupted by some small shut in to preform PLT survey. The main build up lasted for 50.5 hours. The input data is from the NPD completion report, except the well radius and the compressibility, which were set to a standard value. The model used for this DST is a standard model, constant wellbore storage, homogeneous reservoir and rectangular faults as the boundary. Due to the long duration of this DST a model with a rectangle boundary was applied, see results in

Input data:		
Well radius	0.354	ft
Pay zone	93.53	ft
Porosity	0.26	
Bo	1,33	Sm3/Sm3
μ	0,48	cP
Ct	5.0E-5	psi-1
Main results:		
Well and well bore parameters:		
C	6.31E-9	bbl/psi
Skin	0.785	--
Reservoir and boundary:		
Pi	5448.59	psia
k.h	8610	md.ft
k	94.1	md
S - No flow	673	ft
E - No flow	63	ft
N - No flow	129	ft
W - No flow	2890	ft

Table 16: Input data and result for DST well 34/7-9 FSA3

the Table 16. The boundary effect is both very close and far away, and this makes sense considering complex faulting around this well. The long duration of test and the good history match enhances the validity of the test.

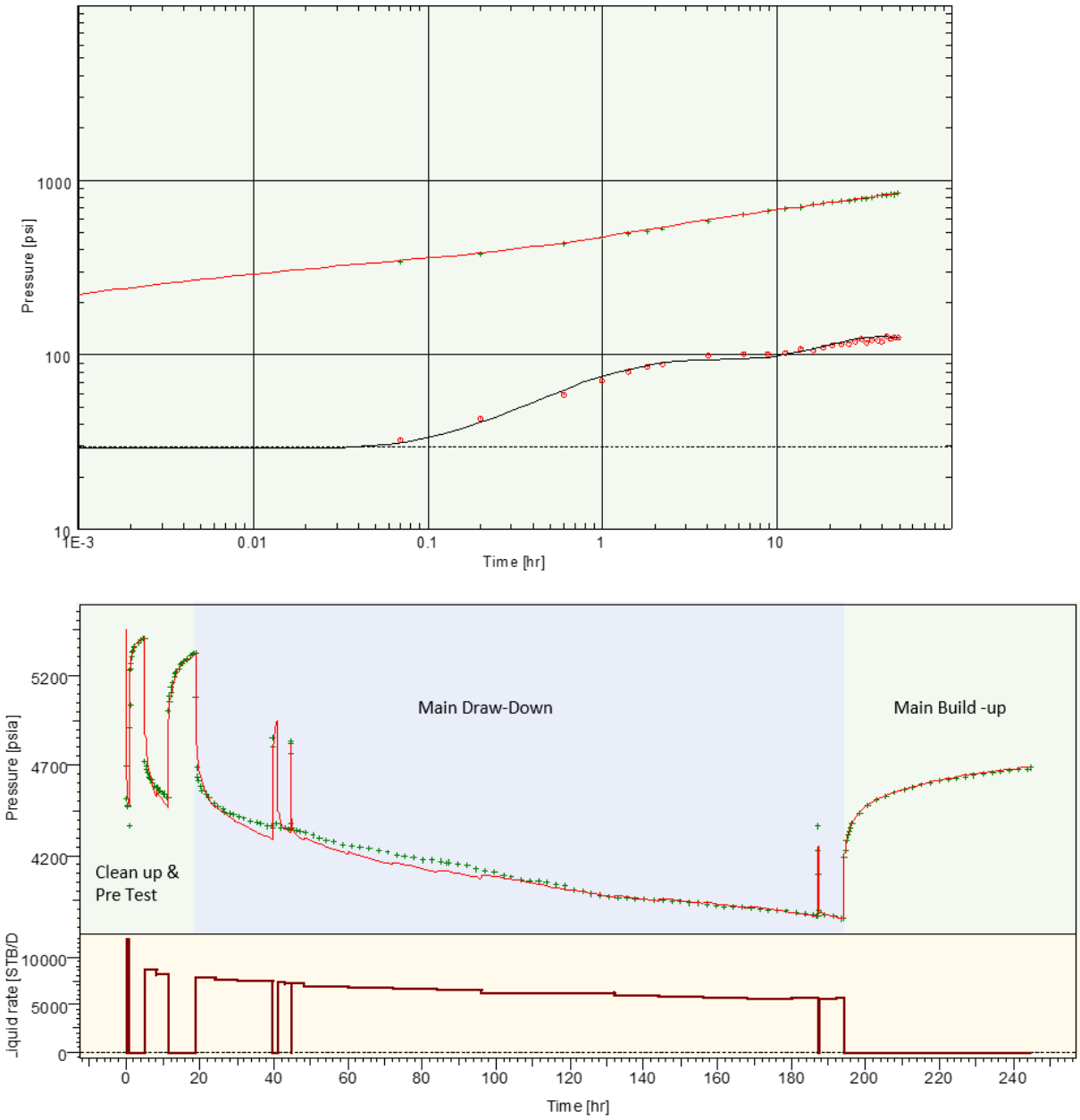

Figure 59: Plots from Saphire well 34/7-9. Top: Log-log plot of the main build-up period. Bottom: Production history plot

5.2.3 Summary DST results

The two DST are taken from FSA3 from two different wells and the results differs by 50 mD, see Table 17. Reason for this can be several, one that the test from 34/7-3 doesn't reach radial flow before the boundary effect and the calculated permeability from the slope is wrong. The other reason, that might be more likely, is that the sandstone bodies have different properties. The sandstone bodies from well 34/7-9 has much more clean and good sand compared to the one in 34/7-3 that is based on the neutron/density log has silt content. The porosity doesn't vary significantly, but the permeability is better in well 34/7-9.

Both cases suggest that zone permeability lies in the middle of the geometric and the arithmetic value, and clearly a use of arithmetic approach would overestimate the permeability. In most of the wells there is some silt content, and from the reservoir results FSA3 is best represented by the DST from well 34/7-3.

The two other DST from Statfjord GP show better zone permeability than FSA3 from Lunde. FSA5 test permeability lies in the middle of the geometric and the arithmetic average compared the upper Statfjord test, DST3, showing a test permeability high above both value calculated from IP. A permeability of 1D could be possible but it would take more testing to verify that the actually permeability is this high.

Table 17: Summary of DST results compared to petrophysical method

Well/DST	Interval	K DST [mD]	Fluvial Assemblage	K Arithmetic [mD]	K Geometric [mD]
34/7-3					
DST1	2601 – 2607.5	103	FSA3	92	23
DST2	2505 – 2513	200	FSA5	257	156
DST3	2440.5 – 2050	1060	FSA6	271	357
34/7-9					
DST1	2501 – 2504 2506 – 2515 2527 – 2536 2550 – 2553	94	FSA3	165 122 132 629	132 84 43 583

6 Fluid analysis

Fluid analysis is an important part of the reservoir characterization. It has impact on reserves calculation, reservoir fluid, flow capacity and knowledge of the fluids are elevated pressure and temperature are important factors. The factor controlling the properties of the fluid are

- Formation volume factor (B_o/FVF)
- Gas oil Ratio (GOR)
- Buddle point pressure (P_b)
- Viscosity (μ)
- Interfacial tension (σ)
- Density (ρ)
- Isothermal compressibility (C_t)

The formation volume factor and the GOR has a big impact on the reserves calculation. The Bubble point pressure is an important factor in the production phase. If pressure drops below the bubble point, gas will start to go out of the oil and there will be complication in the production. The viscosity and compressibility are input data for the analysis of the drill stem tests and directly in the calculation of the permeability. The density and the interfacial tension is input data when calculating the water saturation.

Table 18: Fluid properties

Well	GOR [Sm^3/Sm^3]	Density oil STO [kg/m^3]	Oil density res cond. [kg/m^3]	Pb [bar]	Bo [Sm/Sm]	Viscosity [cP]	C_t [bar^{-1}]
Well 34/7-10	71,2	827,8	717	114	1,25	0,57	
Well 34/7-3	61,2	833,0		90,0	1,26		
Well 34/7-6	85,0	839,0		118,5	1,3		
Well 34/7-9	104,8	825,8	711	155,0	1,33	0,48	
Well 34/7-4	73,5	840,0		60,8	1,27		
Well 34/7-1	133,0				1,4		
Well 34/7-7	70,6	836,2	764	90,2	1,9		8.37*10**-5
Well 34/4-4	162,6	840,0		169,6	1,42		
Well 34/4-7	164,6	834,6		178,9	1,42	0,401	
Well 34/4-6	91,3	824,5	700	135,5	1,32	0,656	
Well 34/4-1	155,0		654	220,0	1,5		

Table 18 have listed all of the available fluid data found on NPD and in articles published. The fluid data varies significantly and systematically through the reservoir. The GOR has its lowest value in the south, 61.2 in well 34/7-3, and increasing to the north-east and reaches it maximum 164.6 in well 34/7-4. The volume factor is showing a similar trend; Increasing from 1.19 in the south to 1.50 in the north (Figure 60). The bubble point pressure show a high correlation to FVF,

where high FVF values correspond to high bubble point pressures. The densities at reservoir conditions varies about 110 kg/m^3 from the lowest to the highest value, however the STO oil only varying between 820-840 kg/m^3. The viscosity has only 4 values and varying between 0.4 and 0.65, and seems to have no systematically variation pattern through the reservoir.

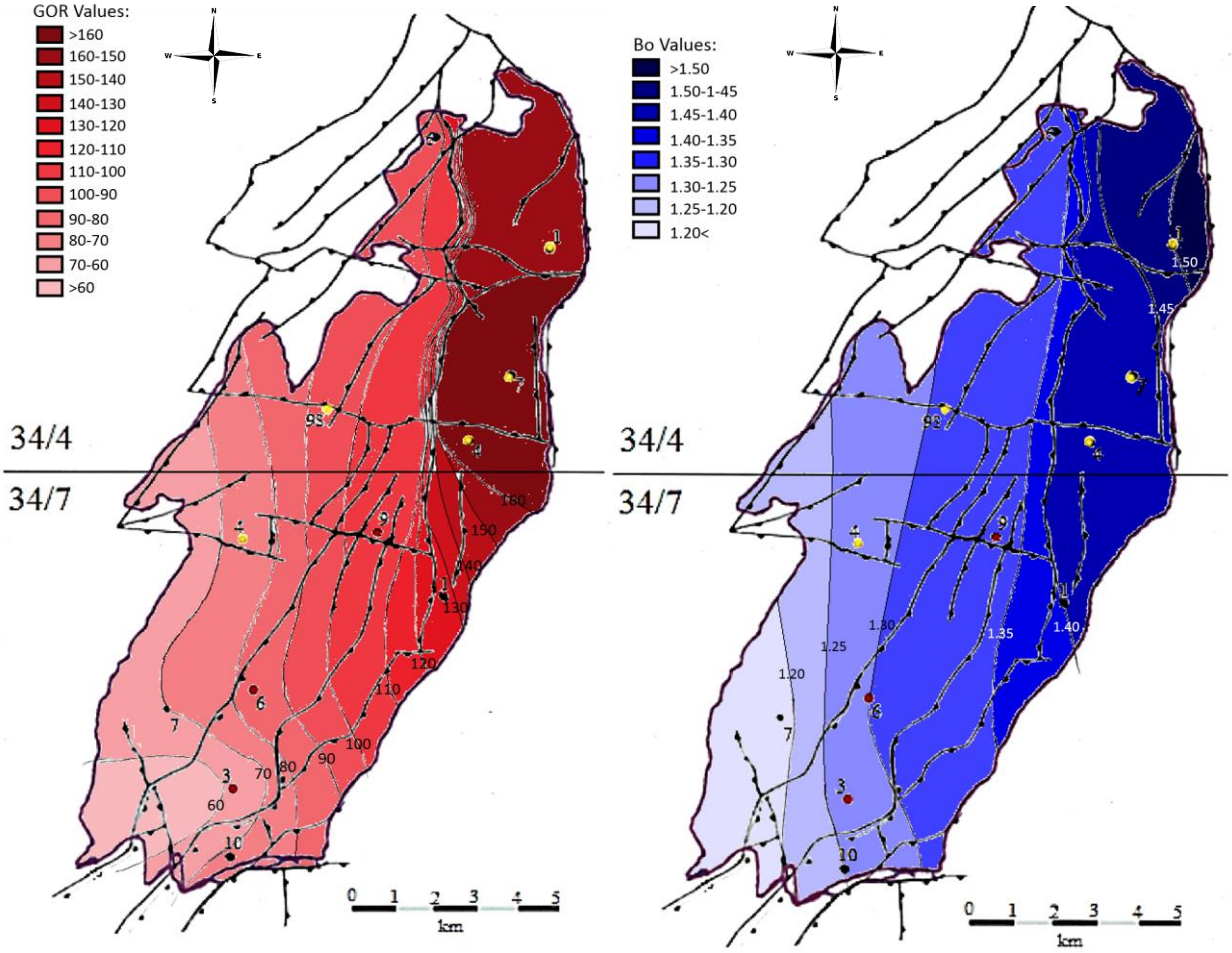

Figure 60: Distribution of GOR and Bo factor in the Snorre field [8]

Correlation between GOR, B_o and P_b factor are plotted in Figure 61. The correlation between points seem to be reasonable good, except some point on P_b has lower value that a trend line would suggest. Such graphs as this can be used to estimate values in wells where not all of the data are given or maybe correlation with other field or formations.

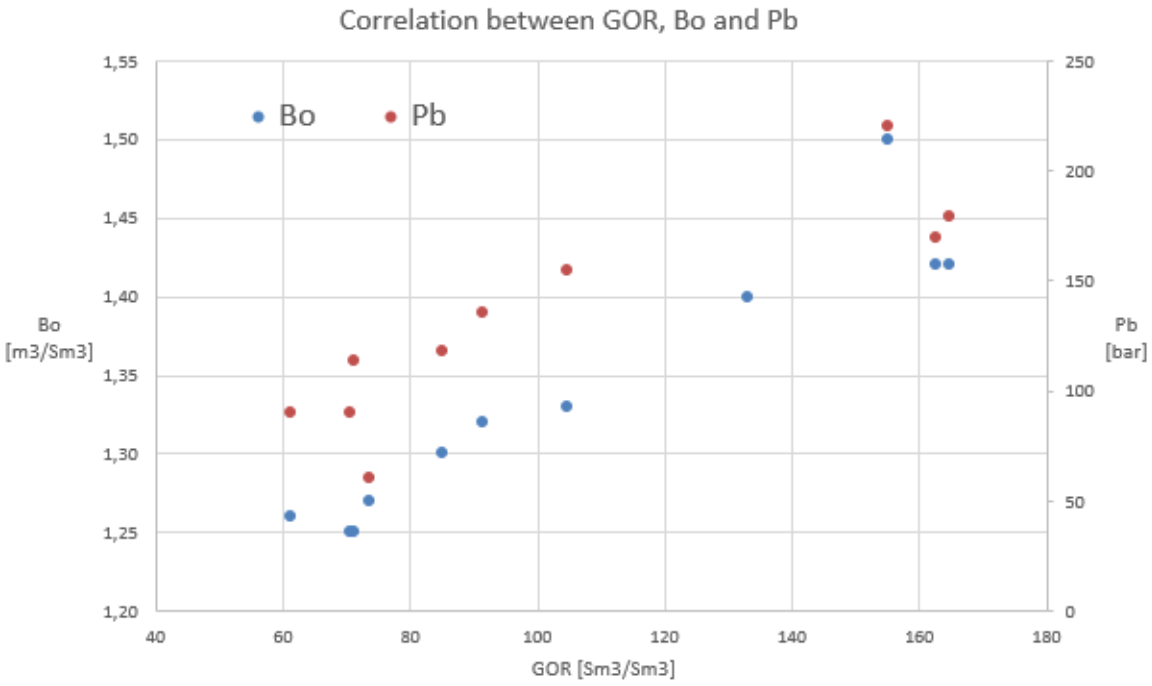

Figure 61: Relation between Bo, Pb and GOR

The compositional analysis of the reservoir fluid listed in Table 19 show some variation with regards to content of methane (C1), between 20 and 37% at the largest. There is no systematically variation of this through the reservoir, and the rest of the components are evenly distributed with a heavy end fraction variation from 25 to 32 mol%.

	Mol %							
	34/7-10	34/7-3	34/7-6	34/7-9	34/7-4	34/7-7	34/4-4	34/4-6
N2	0,24	1,13	1,3	0,21	0,24	1,08	1,06	1,86
CO2	1,06	0,15	0,23	1,26	0,4	0,29	0,24	0,16
C1	23,63	19,38	25,28	31,55	22,87	20,48	37,41	26,22
C2	6,85	5,33	7,14	8,07	6,35	5,74	9,02	8,48
C3	8,91	8,04	9,37	7,91	8,88	8,23	7,44	8,77
i-C4	1,33	1,44	1,33	1,2	1,33	1,27	1,25	1,34
n-C4	5,15	5,7	6,11	4,62	4,67	4,9	3,89	5,29
i-C5	1,87	2,3	2,03	1,63	1,94	1,62	1,26	1,71
n-C5	2,69	3,22	3,17	2,49	3,26	2,83	1,81	2,66
C6	3,51	4,33	3,43	3,3	3,89	3,49	2,34	3,22
C7	5,19	6,68	5,28	4,82	4,21	6	34,28	5,1
C8	5,11	6,56	5,04	4,71	4,44	5,25	(C7+)	5,02
C9	2,99	4,25	3,64	2,91	4,57	4,77		3,05
C10+	31,47	31,49	26,65	25,32	32,95	34,05		27,12

Table 19: Fluid composition (mol%)

7 Barriers and segmentation

There is no doubt that a reservoir the size of Snorre with two different faulting sequences has several barriers and a segmentation of the reservoir is needed to proper evaluate the reservoirs fully potential. The reservoir is segmented based on pressure data, DST, fluid analysis, fluvial assemblages and faulting history. The south reservoir can be divided into different segments based on the two major faults OF (Outer fault) and IF (Inner fault); W, C and E, see Figure 62. There are no eminent indications that these fault are sealed, communication through the fault is possible. However the DST has pressure response that suggests that there are boundaries or heterogeneity in the reservoir. The boundary effects from the DST vary from different fluvial assemblages and are mostly interpreted as heterogeneity in the reservoir. However around well 34/7-9 there are both close and far away boundaries response indicating complexity around the faults and further evaluation is needed.

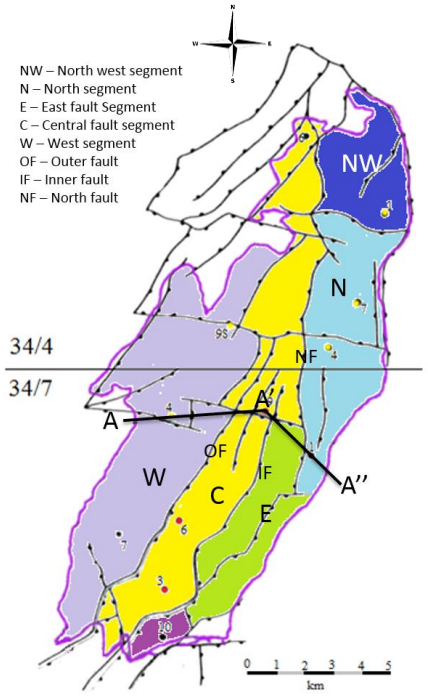

Figure 62: Example of segmentation, with different segments: W, C, E, N and NW. Boundaries: OF (outer fault), IF (inner fault) and NF (north fault) [8]

The three major faults, including the north fault (NF), typically have a throw between 100-200m in the south decreasing north (Karlsson, 1986). The reservoir is cut by a series of rotated blocks cut by a series of fault striking north-north-east. Figure 63 shows a cross section of the field and how the faults are dividing the reservoir into different segments. The scale of this figure is 1:4 and the rotated blocks have a dip of 8-10° (K. Jorde et al). The whole Lunde formation is interpreted to have the same thickness throughout the reservoir, compared to the Alke

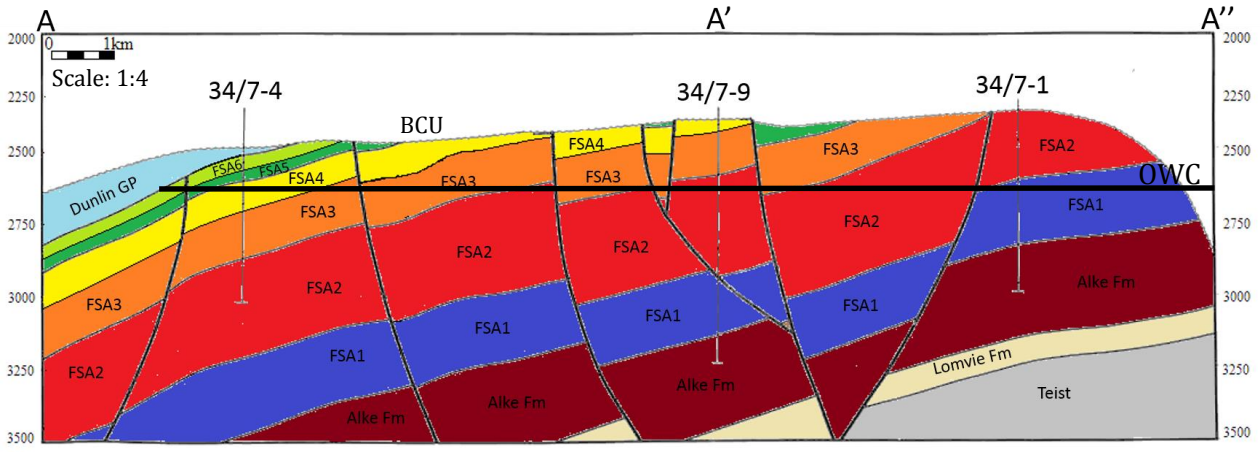

Figure 63: Cross section from A-A'-A'' from Figure 58 illustrating fault blocks and the base cretaceous unconformity (BCU). The figure illustrate all the fluvial assemblages and a general OWC at 2600 [8]

formation thickens to the North-west. Figure 62 show an example of how the reservoir can be segmented based on the fault, pressure data and fluid data. Another important factor in the Snorre field is erosion and must be taken into account when evaluating the reservoir. The reservoir was exposed to heavily erosion during the late Triassic and Jurassic time. At this time the Tampen spur was located at a topographic high causing erosion over the entire area, most in the north where the entire Lunde formation was eroded, see Figure 64. Based on old structural/fault maps, petrophysical evaluation of the logs and articles published of the structure of the Snorre field, a reservoir map where created where the most likely different fluvial assemblages would serve as oil bearing reservoir. In the south the oil-bearing reservoir is completely Statfjord, moving the north-west the erosion is becoming more eminent and in the north, well 34/4-1, the whole oil column is in the Alke formation. The bottom of Statfjord formation and top of the Lunde formation are very similar and represent a transition zone to the Statfjord formation. This transition is represented by almost completely mud plain with some single channelized sandstone. Net to gross are significantly low, especially in FSA4 and the entire region may be considered to non-reservoir due to the high content of mud plains.

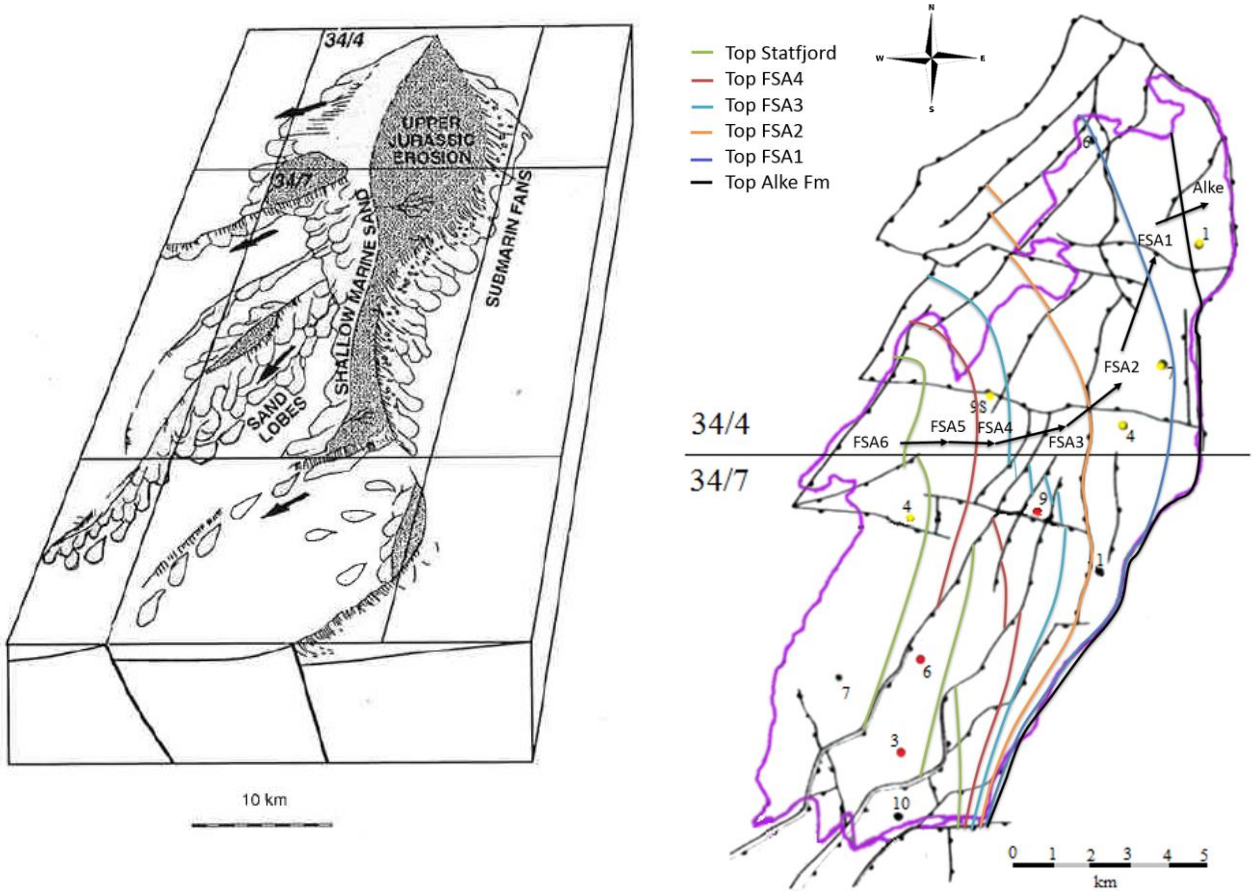

Figure 64: Left: map illustration erosion on the Tampen Spur area. Right: How the different reservoir fluvial sandstone assemblages are eroded in the Snorre field from south to north [8]

8 Summary of reservoir properties

The reservoir is composed of series of sandbodies in a mudstone matrix from the Statfjord group in the south and the Lunde formation to the east and north. Deposition from fluvial system is very heterogeneity, and the fluid properties vary significantly, but systematically on a bigger scale (kms). Comparing the reservoir in the north to the south, several big differences are noticed. The GOR varies of 164.6 Sm^3/Sm^3 in the north to 61.2 Sm^3/Sm^3 in the south. The bubble point pressure is higher in the north, 178.9 bar, compared to the south, 90 bar. Also the B_o factor drops from 1.5 in the north to 1.19 in the south. Lateral difference in the oil density is also observed at reservoir conditions, however the stock tank oil doesn't changed significantly through the reservoir. Temperature is not significantly affected, only by 2-3 degrees from east to west. Vertical differences also occur, but in a much smaller scale.

Table 20: Summary of depositional system and reservoir properties; N/G, porosity and permeability

Reservoir unit	Depositional environment	N/G	Porosity	Permeability [mD]
FSA6	Monsoonal braided streams	0,58	0,24	100-400 (1000mD)
FSA5	Single and narrow, low sinuosity or meandering streams	0,34	0,2	10-70
FSA4	Large meander/ straight sinuosity streams	0,10	0,17	0.1-4
FSA3	Small isolated meander streams	0,39	0,21	30-50
FSA2	Braided to meander streams	0,57	0,23	10-80
FSA1	Ephemeral braided streams	0,57	0,22	30-120

The permeability ranges from 1-120mD in the sandstone in the Lunde formation, with highest in the lower fluvial assemblages, FSA1 and FSA2, decreasing up to FSA3 and FSA4. The Statfjord formation lowermost FSA5 show a lower permeability compared to the upper FSA6 which has a significantly higher permeability and can reach several hundred mD. Drill stem tests from the reservoir may indicate higher permeability in the upper Statfjord. The porosity and N/G of the upper Statfjord and the lower Lunde formation seems to be similar compared to the lower Statfjord and upper Lunde which has generally lower values. FSA4 is dominated by mudstone and represent no acceptable reservoir, except for one well.

The Snorre reservoir has been through two rifting episodes, the perm-trias and the late Jurassic, and has two sets of faults dipping to the north-west and south-east and could reach a throw up to 150-200m in some areas. In addition to the rifting the Snorre area was exposed to heavily

erosion during the period of Jurassic caused the reservoir as it is today to be segmented into all the different fluvial assemblages described in this area.

Appendix A

Key data from SCAL reports:

Well 34/7-3							
Sample no.	Depth [m]	Porosity	Formation Factor	KLHC [mD]	Swi	n	FSA
68,10	2415,10	0,283	10,5	189	0,359		Stat
92,10	2423,30	0,14	29,9	2,07	0,693		Stat
180,10	2462,90	0,239	16,8	208	0,269		Stat
225,10	2478,10	0,267	13,2	1738	0,181		Stat
244,10	2510,90	0,291	11,3	1236	0,191		Stat
256,10	2514,10	0,203	16,6	56,2	0,302		Stat
262,10	2607,10	0,258	12,5	20,1	0,519	2,07	FSA3
376,10	2619,10	0,232	14,1	0,789	0,869	3,68	FSA3
435,10	2636,10	0,274	11,7	204	0,374		FSA3
439,10	2637,10	0,27	11,5	1143	0,224	2,13	FSA3

Well 34/7-9							
Sample no.	Depth [m]	Porosity	Formation Factor	KLHC [mD]	Swi	n	FSA
4	2588,16	0,246		126,1	0,09		FSA4
6	2588,19	0,242		109,2	0,09		FSA4
7	2588,25	0,259		79,3	0,12		FSA4
8	2588,25	0,259		79,3	0,15		FSA4

Well 34/7-9							
Sample no.	Depth [m]	Porosity	Formation Factor	KLHC [mD]	Swi	n	FSA
13,1	2504,1	0,251	11,8	116	0,199	1,7	FSA3
20,1	2506,15	0,299	10,2	253	0,2	1,92	FSA3
30,1	2509,1	0,269	11,1	439	0,174	2,11	FSA3
77,1	2532,1	0,255	11,9	17,9	0,345	1,77	FSA3
88,1	2537,1	0,282	12	224	0,238	1,84	FSA3
113,1	2552,1	0,27	10,4	44,4	0,314	1,92	FSA3
145,1	2583,1	0,237	11,7	12	0,379	1,73	FSA3
163,1	2590,1	0,23	19,2	4,79	0,501		FSA3
184,1	2625,1	0,265	12,4	360	0,206	1,66	FSA2
231,1	2659,1	0,233	14,5	7,28	0,399	2,05	FSA2
249,1	2672,1	0,222	15,1	13,5	0,367	1,67	FSA2
294,1	2698,1	0,245	15,5	55,6	0,274	1,77	FSA2

Capillary pressure curves the corresponding normalized capillary pressure curves:

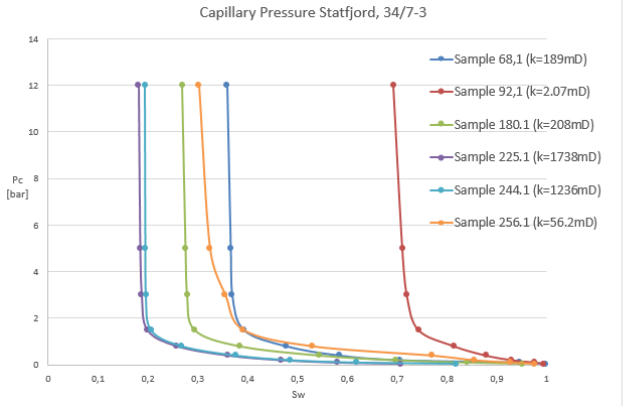

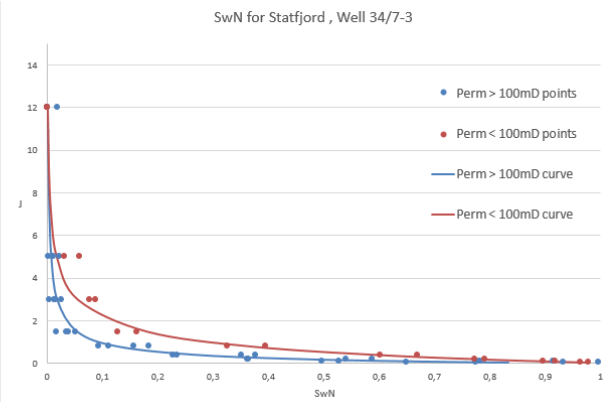

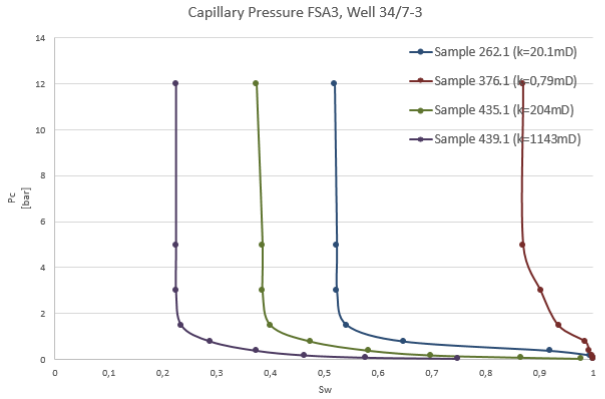

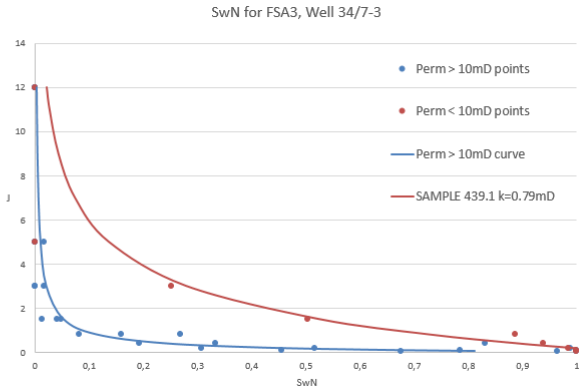

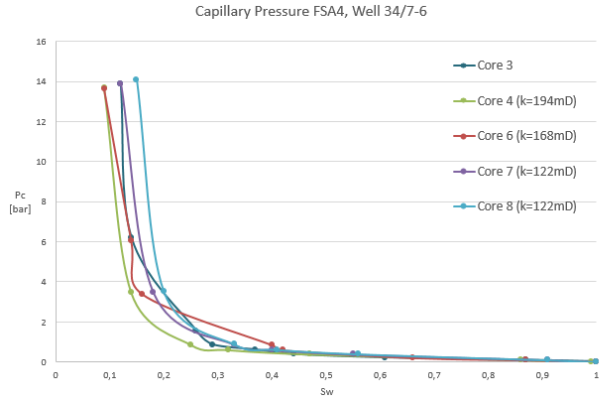

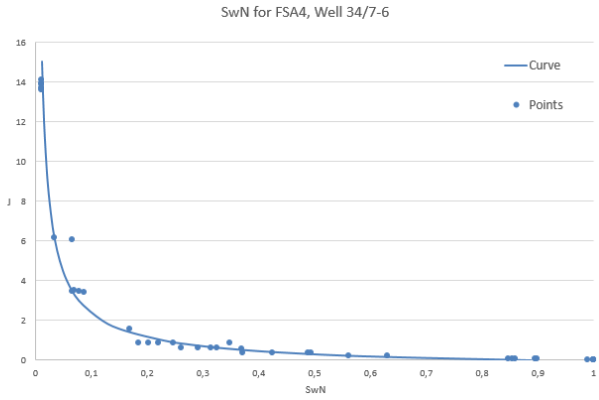

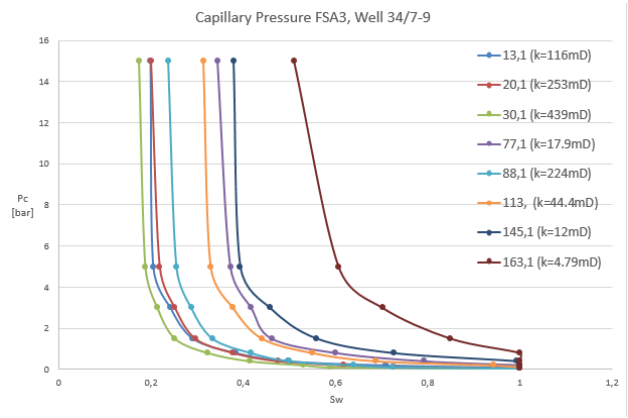
Capillary Pressure FSA3, Well 34/7-9
Pc [bar]
Sw
13,1 (k=116mD)
20,1 (k=253mD)
30,1 (k=439mD)
77,1 (k=17.9mD)
88,1 (k=224mD)
113, (k=44.4mD)
145,1 (k=12mD)
163,1 (k=4.79mD)

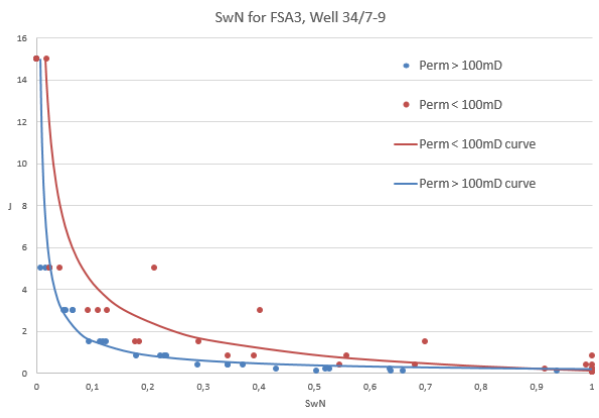
SwN for FSA3, Well 34/7-9
J
SwN
Perm > 100mD
Perm < 100mD
Perm < 100mD curve
Perm > 100mD curve

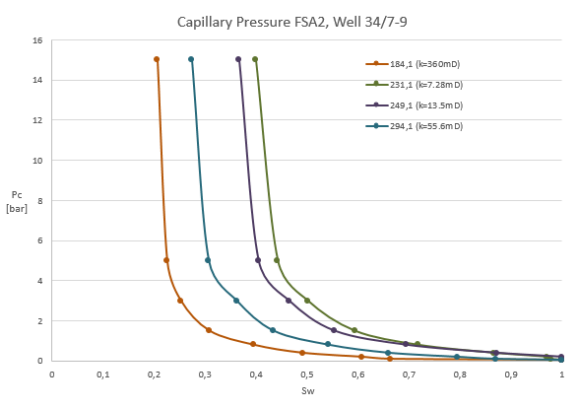
Capillary Pressure FSA2, Well 34/7-9
Pc [bar]
Sw
184,1 (k=360mD)
231,1 (k=7.28mD)
249,1 (k=13.5mD)
294,1 (k=55.6mD)

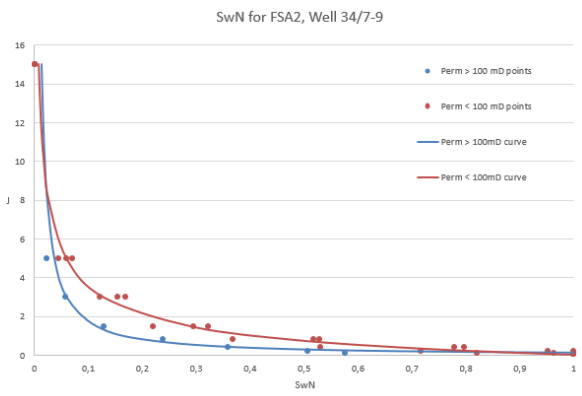
SwN for FSA2, Well 34/7-9
J
SwN
Perm > 100 mD points
Perm < 100 mD points
Perm > 100mD curve
Perm < 100mD curve

Appendix B

This appendix contain the CPI plots that are not part of the key wells

Well 34/7-4

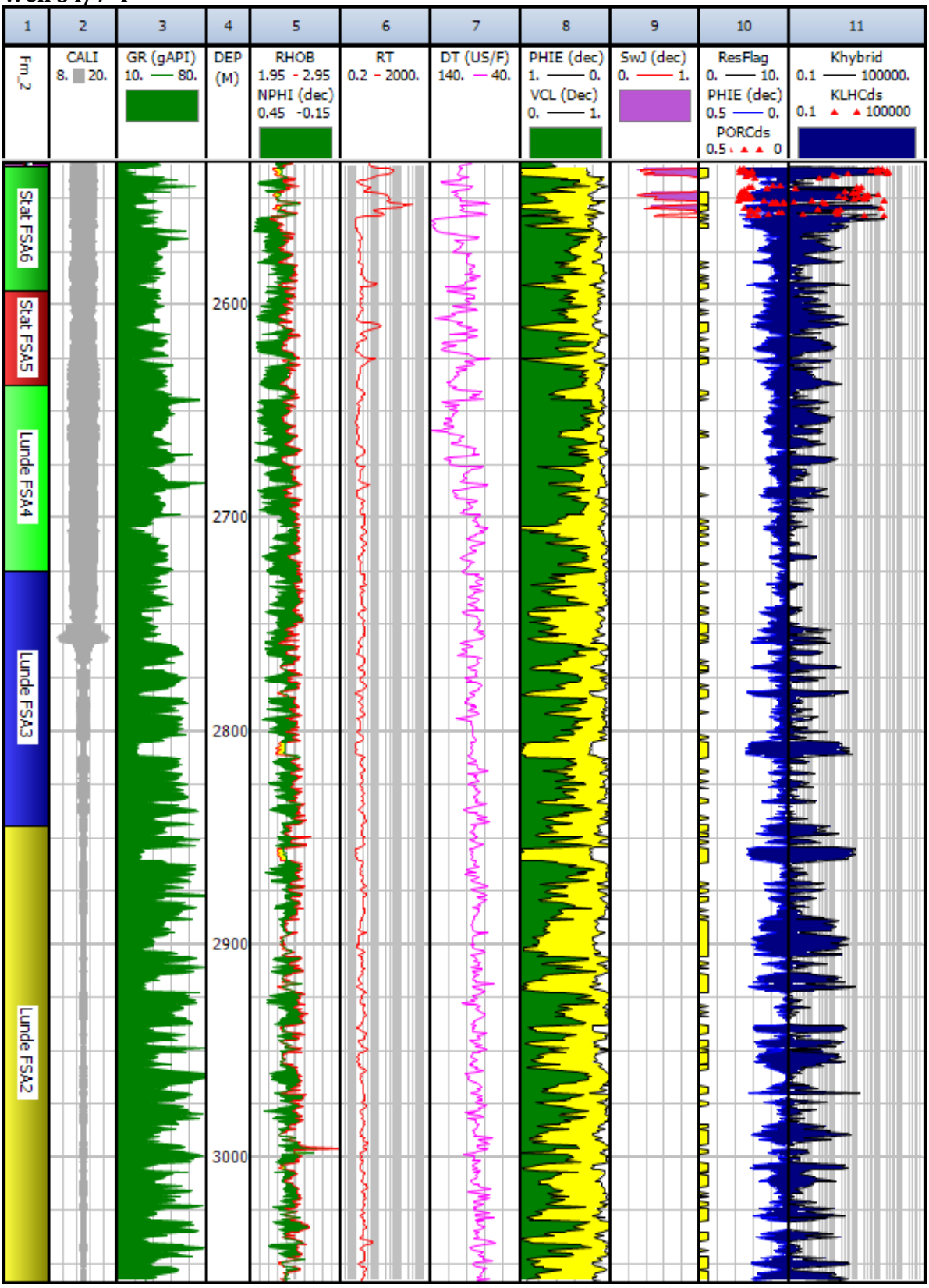

Well 34/4-9S:

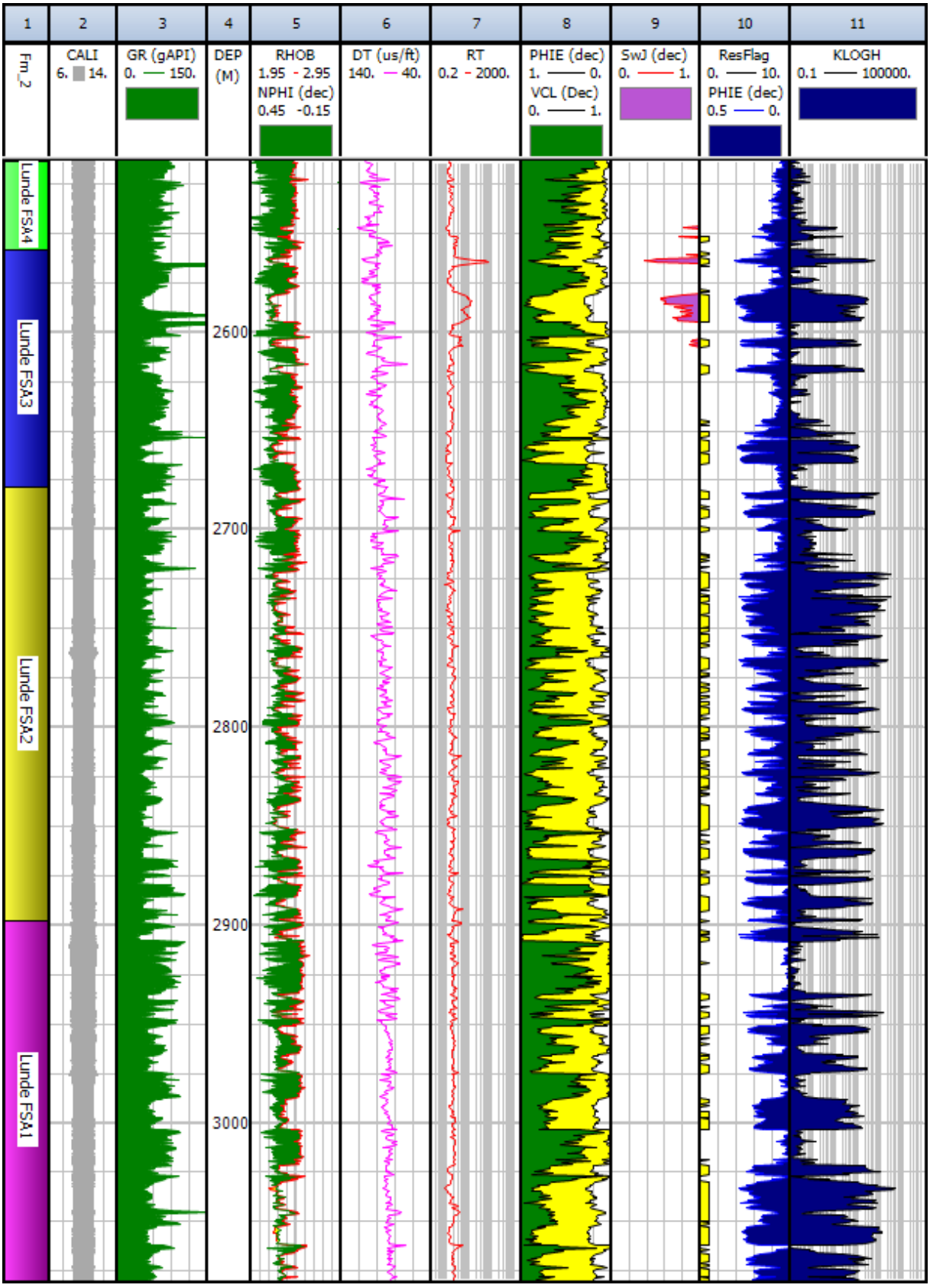
1
2
3
4
5
6
7
8
9
10
11
Fm_2
CALI
6. 14.
GR (gAPI)
0. 150.
DEP
(M)
RHOB
1.95 - 2.95
NPHI (dec)
0.45 -0.15
DT (us/ft)
140. 40.
RT
0.2 - 2000.
PHIE (dec)
1. 0.
VCL (Dec)
0. 1.
SwJ (dec)
0. 1.
ResFlag
0. 10.
PHIE (dec)
0.5 0.
KLOGH
0.1 100000.
Lunde FSA4
Lunde FSA3
Lunde FSA2
Lunde FSA1
2600
2700
2800
2900
3000

Well 34/4-4

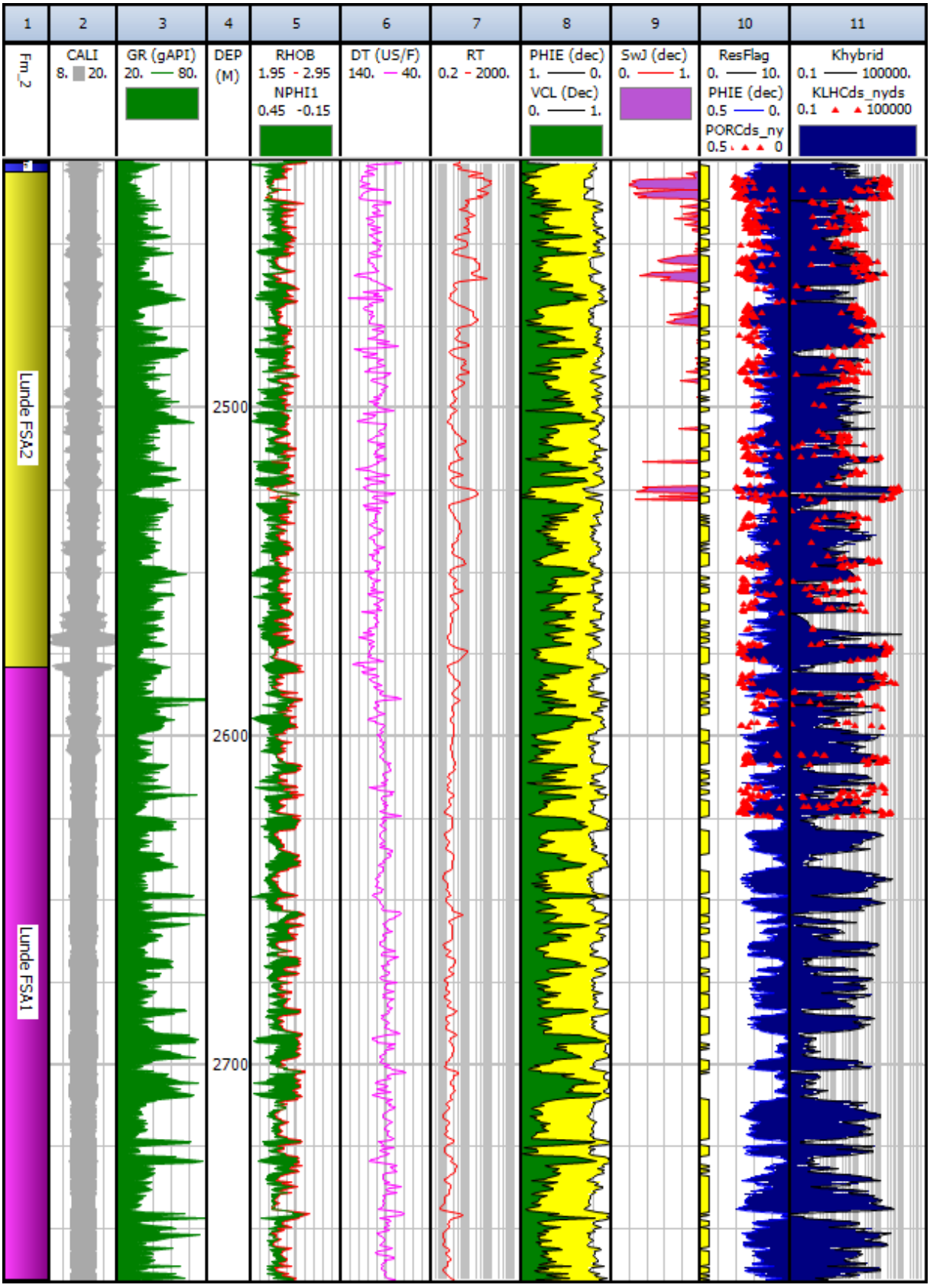
1
2
3
4
5
6
7
8
9
10
11
Fm_2
CALI
8. 20.
GR (gAPI)
20. 80.
DEP
(M)
RHOB
1.95 2.95
NPHI1
0.45 -0.15
DT (US/F)
140. 40.
RT
0.2 2000.
PHIE (dec)
1. 0.
VCL (Dec)
0. 1.
SwJ (dec)
0. 1.
ResFlag
0. 10.
PHIE (dec)
0.5 0.
PORCds_ny
0.5 0
Khybrid
0.1 100000.
KLHCds_nyds
0.1 100000
Lunde FSA2
Lunde FSA1
2500
2600
2700

Well 34/4-7:

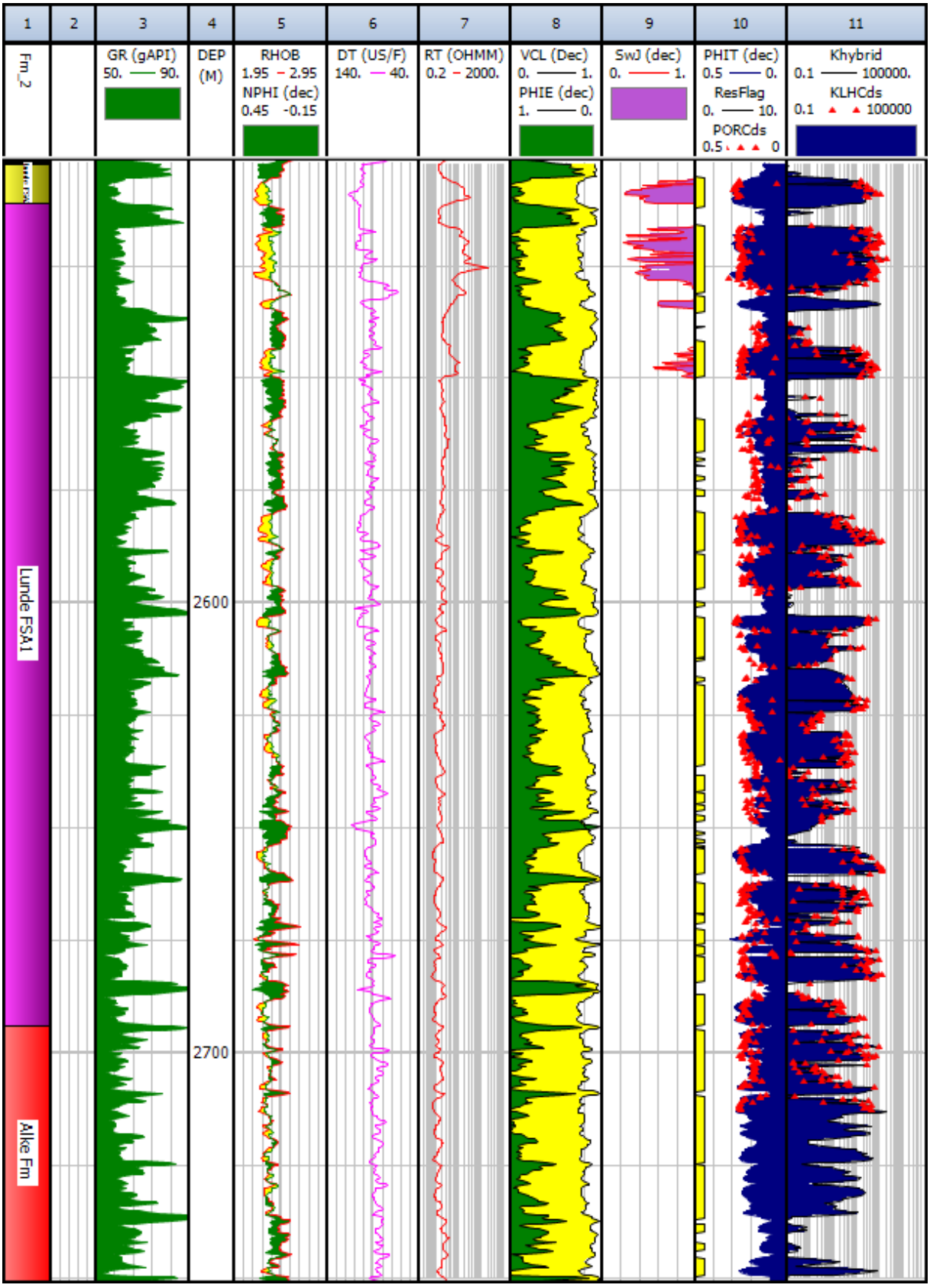
1
2
3
4
5
6
7
8
9
10
11
Fm_2
GR (gAPI)
50. 90.
DEP
(M)
RHOB
1.95 2.95
NPHI (dec)
0.45 -0.15
DT (US/F)
140. 40.
RT (OHMM)
0.2 2000.
VCL (Dec)
0. 1.
PHIE (dec)
1. 0.
SwJ (dec)
0. 1.
PHIT (dec)
0.5 0.
ResFlag
0. 10.
PORCds
0.5 0
Khybrid
0.1 100000.
KLHCds
0.1 100000
2600
2700
Lunde FSA1
Alke Fm

Well 34/4-1

Note that the water saturation in this well is very uncertain as the same value for Lunde is used on Alke formation and that the OWC only is an estimate, not from pressure points.

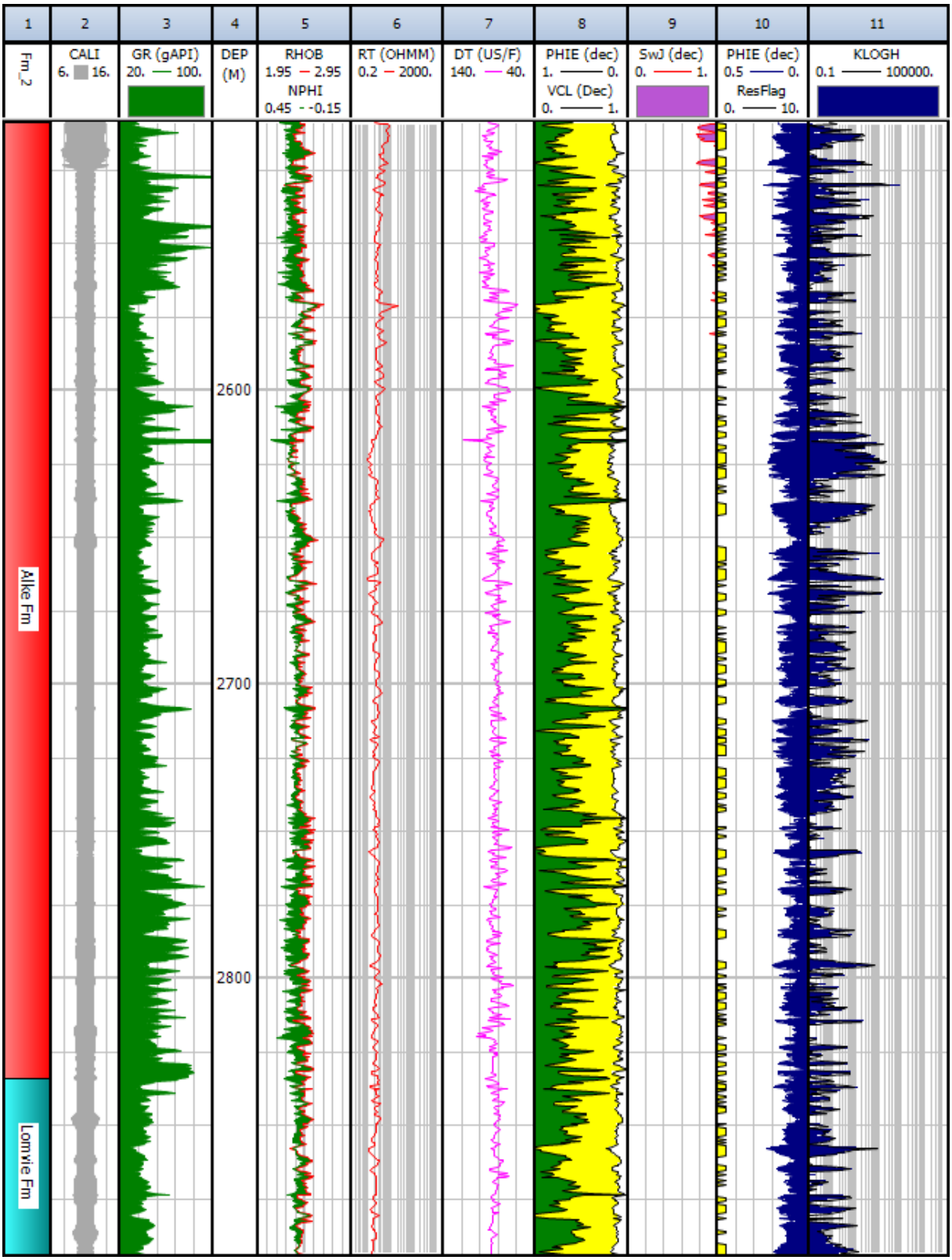

Appendix C

Complete list of reservoir results:

	34/7-3			k [mD]		34/7-6			k [mD]	
	Thickness	N/G	Phi	Geom	Arith	Thickness	N/G	Phi	Geom	Arith
STAT FSA6	53	0,62	0,26	418	1841	78	0,67	0,22	95	732
STAT FSA5	47	0,52	0,23	71	180	66	0,26	0,19	4,8	36
Lunde FSA4	86	0,09	0,18	4,4	44	91	0,32	0,19	1,9	7
Lunde FSA3	121	0,44	0,22	7,8	62	122	0,41	0,18	1,3	2,9
Lunde FSA2	213	0,60	0,20	4,8	13	210	0,54	0,17	2	7
Lunde FSA1	192	0,35	0,18	1,9	5,5	189	0,64	0,16	1,2	2,4
Alke										
	34/7-4			k [mD]		34/7-9			k [mD]	
	Thickness	N/G	Phi	Geom	Arith	Thickness	N/G	Phi	Geom	Arith
STAT FSA6	58	0,43	0,22	36	302					
STAT FSA5	44	0,25	0,18	2,3	6,4					
Lunde FSA4	87	0,09	0,13	0,2	0,4	47	0,09	0,17	0,46	0,8
Lunde FSA3	119	0,31	0,17	1,7	8,3	110	0,40	0,26	53	255
Lunde FSA2	214	0,55	0,17	3,5	11,6	213	0,48	0,22	14	102
Lunde FSA1						188	0,62	0,20	2,4	21
Alke										
	34/4-9S			k [mD]		34/4-4			k [mD]	
	Thickness	N/G	Phi	Geom	Arith	Thickness	N/G	Phi	Geom	Arith
STAT FSA6										
STAT FSA5										
Lunde FSA4	45	0,04	0,19	2	5,8					
Lunde FSA3	119	0,39	0,25	30	84,7					
Lunde FSA2	220	0,57	0,21	65	288	151	0,61	0,22	77	431,8
Lunde FSA1	182	0,47	0,22	78	294	187	0,66	0,22	118	365,5
Alke						267	0,56	0,23	5,4	32
	34/4-7			k [mD]		34/4-1			k [mD]	
	Thickness	N/G	Phi	Geom	Arith	Thickness	N/G	Phi	Geom	Arith
STAT FSA6										
STAT FSA5										
Lunde FSA4										
Lunde FSA3										
Lunde FSA2										
Lunde FSA1	187	0,69	0,22	31	149					
Alke	325	0,48	0,19	7,2	13,4	325	0,45	0,165	2,4	13,4

References:

1. Norwegian Petroleum Museum. “Oil and gas fields in Norway : Industrial heritage plan”, page: 185-188. 2011
2. N. Dahl and T. Solli. “The structural evolution of the Snorre field and surroundings areas” from the book “Geological Society. London. Petroleum Geology Conference series **1993.** v. 4”
3. K. Jorde and G. W. Diesen. “The Snorre Field – A Major Field in the Northern North sea” from the book “Giant Oil and Gas Fields of the Decade 1978-1988”
4. Johan P. Nystuen. Audun V. Kjemperud. Reidar Müller. Victoria Adestål and Edwin R. Schomacker. “Late Triassic to Early Jurassic climate change. northern North Sea region: impact on alluvial architecture. palaeosols and clay minerals” from the book “From Depositional Systems to Sedimentary Successions on the Norwegian Continental Margin”
5. www.statoil.no
    a. http://www.statoil.com/en/NewsAndMedia/News/2013/Pages/28Oct_Snorre2040.aspx
    b. http://www.statoil.com/en/TechnologyInnovation/OptimizingReservoirRecovery/Pages/2012_13Dec_Permanent_Reservoir_monitoring.aspx
6. Woodhouse, R. and Warner, H.R. 2005. Sw and Hydrocarbon Pore Volume Estimates in Shaly Sands - Routine Oil-Based-Mud Core Measurements Compared With Several Log Analysis Models. Presented at the SPE Annual Technical Conference and Exhibition, Dallas, Texas, 9-12 October 2005. SPE-96618-MS.
7. Lervik, Kjell-Sigve “Triassic lithostratigraphy of the Northern North Sea Basin”. April 2006
8. Johan P. Nystuen, Ragnar Knarud, Knut Jorde, Ken O. Stanley. ”Correlation of Triassic to Lower Jurassic sequences, Snorre Field and adjacent areas, northern North Sea”
9. Dr. Paul W.J. Glover “Petrophysics MSc PetroleumGeology”. Department of Geologyand Petroleum GeologyUniversity of AberdeenUK
    a. *Petrophysics MSc Course Notes on Clay/Shale Effects on Porosity and Resistivity Logs P 270-281*